# Hygrothermal Performance of Hempcrete Infill Wall Systems in Cold Climates

By

Mehdi Md Iftekharul Alam

A Thesis Submitted to the Faculty of Graduate Studies of

The University of Manitoba

in partial fulfillment of the requirements for the degree of

MASTER OF SCIENCE

Department of Civil Engineering

University of Manitoba

Winnipeg, Manitoba

*To Md Mosleh Uddin, Sharifa Islam*

*& Sharmin Sultana*

# Acknowledgments

First, I would like to express my sincere gratitude to my research supervisor, Dr. Miroslava Kavgic, for her invaluable instruction, excellent supervision, insight, and dedication throughout this research. Her knowledge guided me to overcome critical issues, and her direction encouraged me to deliver the highest quality work. Also, I would like to express my gratitude to my advisory committee members: Dr. Farhoud Delijani and Dr. Qiang Zhang. Their thoughtful comments and judgment were much appreciated and valued.

I want to express my gratitude to the officers and staff for their tremendous support in the experimental program conducted at W.R. McQuade Heavy Structure Laboratory, University of Manitoba.

My sincere gratitude also goes to the industrial partner and financial partner PLAINS HEMP® and software partner WUFI® for their indebted support in supplying materials and products to make the research successful.

Most importantly, the continuous support, love, and blessings from my parents and family make all this possible. This dissertation is dedicated to my beloved parents and my wife, having believed in me with constant love, support, and encouragement to all these years.

Finally, I would like to thank my colleague Mr. Asif Khan for his help and support in laboratory work. I want to honor the encouragement and support from all other friends during the last two years.

**ABSTRACT**

Hempcrete is a carbon-negative, non-toxic, breathable, and biodegradable building material. Nevertheless, the utilization of hempcrete in the construction industry remains low, mainly due to the high-variability of hemp-lime composites. Therefore, the development of locally available products, standards, and best practice guidelines requires comprehensive experimental tests and analysis to obtain reliable information about the material's thermophysical performance. The aim of this study was twofold: (1) development of hempcrete infill "wall" formula with excellent thermal properties using locally sourced materials; and (2) numerical investigation of the long-term hygro-thermal performance of hempcrete wall types that satisfy current National Energy Code of Canada for Buildings. The thermal properties of the hempcrete were obtained with heat flow meter Fox314, whereas the hygrothermal analysis of wall assemblies was performed using WUFI software. The densities of hempcrete samples produced in this study show excellent consistency, ranging from 298.55 $kg/m^3$ to 318.05 $kg/m^{3,}$ with the average density of all samples is 306.13 $kg/m^3$. Furthermore, the average thermal conductivities of all the samples range from 0.081 W/mK to 0.089 W/mK, with a standard deviation of 0.004–0.007 indicating consistency in the results. The results of the modeling analysis show that the average water contents in the mass percent of both wall assemblies under all four cases are significantly below the 20 mass-percent. Nevertheless, on average, the base wall has 36% to 54% higher water content than the multilayer wall throughout the simulation period. Moreover, RH profiles of both walls have regular patterns of seasonal fluctuation that gradually decrease over time, and especially of the multilayer wall, which under all scenarios, has lower RH compared to the base wall. The multilayer wall performs better and exhibits lower annual heat flow than the base

wall under all cases, and in particular, at the outside surface. The likely reason is the addition of the insulation layer that reduced heat losses at the external surface of the multilayer wall. Furthermore, due to the higher indoor air temperatures of cases II and IV than the other two, both walls have higher heat flow under II than I scenario and under IV than III scenario.

## TABLE OF CONTENTS

# List of Tables

# List of Figures

# Abbreviations and Acronyms

| Acronyms | Description |
|---|---|
| (GHG) | Green House Gas |
| (HDD) | Heating Degree Days |
| (WUFI) | Wärme und Feuchte Instationär (Heat and Humidity Transference) |
| (RH) | Relative Humidity |
| ($CO_2$) | Carbon-Di-Oxide |
| (HVAC) | Heating, ventilation and air conditioning |
| (LMK) | Lime-Metakaolin |
| (LCA) | Life Cycle Analysis |
| (AAC) | Autoclave Aerated Concrete |
| (HCB) | Hemp Concrete Brick |
| (IAQ) | Indoor Air Quality |
| (NECB) | National Energy Code of Canada for Buildings |
| (ASTM) | American Society for Testing and Materials |
| (CSA) | Canadian Standards Association |
| (DIN) | Deutsches Institut für Normung (German Institute for Standards) |
| (CSH) | Calcium Silica Hydrates |
| (HFMA) | Heat Flow Meter Apparatus |
| (GGBS) | Ground Granulated Blast furnace Slag |

# List of Symbols

| Symbol | Description |
|---|---|
| $T$ | Temperature |
| $\mu$ | Water vapor diffusion resistance factor |
| *R-value* | Thermal resistance |
| $CO_{2e}$ | Carbon-Di-Oxide equivalent |
| $Ca(OH)_2$ | Calcium Hydroxide |
| $\Delta T$ | Temperature gradient |
| $q$ | Heat flow |
| $S$ | Heat flow meter calibration factor |
| $L$ | Sample thickness |
| $k$ | Thermal conductivity |
| $Q$ | Output signal |
| $M\%$ | Mass percent |

# 1 Introduction

## 1.1 Problem Statement

Buildings typically account for around 30% of total global final energy use, 20% of energy-related greenhouse gas emissions (IPCC, 2014). In Canada, the residential and commercial building sector is the third-largest greenhouse gas (GHG) emitting industry, accounting for 12% of total national emission (Environment and Climate Change, Canada, 2019). Thus, buildings are playing a vital role in addressing global warming issues in Canada's sustainable development plan. In efforts to reduce the carbon intensity of the building stock, all jurisdictions in Canada will have to adopt codes for construction of "net-zero energy ready" buildings by 2030 (CaGBC, 2018). The introduction of net-zero energy codes will result in a drastic reduction in buildings operational loads. Higher energy performance of buildings will prompt innovation to decrease the buildings' embodied energy.

Currently, conventional building materials such as Portland cement have high embodied energy due to energy and carbon-intensive production. For example, in the production phase of each ton cement, approximately one ton of $CO_2$ emitted to the atmosphere (Florentin et al., 2017; Gibbs et al., 2000). A possible strategy to considerably diminish the embodied energy of building materials could be the use of natural or bio-based materials as they undergo fewer industrial operations compared to the conventional building materials, and they contain plaint based aggregates (Meliá et al., 2014). In this regard, new biocomposite materials could reduce the embodied energy related to the construction of buildings in two distinctive ways (Florentin et al., 2017;  Amziane & Arnaud, 2013). First, during their lifetime, they absorb atmospheric carbon dioxide through photosynthesis and lock it into the material that forms the product for building construction. Second, biocomposite materials can often be recycled or composted, reducing their waste impact after demolition. A mixture of hemp hurd, binder, and water, called “hempcrete” is especially promising biocomposite material.

Advantages of hempcrete are numerous, and some of them include high thermal and heat storage properties (Walker & Pavia, 2014; Elfordy et al., 2008); high acoustic performance (Arnaud & Gourlay, 2012); the excellent level of airtightness (Bevan & Woolley, 2008); high moisture buffering (De Bruijn & Johansson, 2013; Latif et al., 2015); good fire resistance (Gregor, 2014); high durability and carbon sequestration (Walker et al., 2014; Jami et al., 2019). Furthermore, hempcrete can be used to form external and internal walls, as well as insulating floor slab or roof insulation (Magwood, 2016). Consequently, the entire building’s envelope can be made of hempcrete.

However, hempcrete properties and performance much depend on ingredient amounts and the type of used binder. Thus, due to the much lower thermal conductivity of hemp hurd than the binder, an increase in the hurd content increases insulation properties and reduces strength, hardness, and thermal mass of hempcrete. Consequently, different hempcrete formulas will be applicable to building elements that are under different thermal and mechanical loads. For instance, higher insulation properties are desirable for roof and walls, whereas strength and acoustic properties are essential for floors (Shea et al., 2012; Arnaud & Gourlay, 2012).

Therefore, the commercial application of hempcrete in the construction industry and the development of codes and standards require comprehensive experimental tests and analysis to obtain reliable information about the thermophysical properties of different hempcrete formulas. Furthermore, the construction of buildings from hempcrete requires design solutions for envelope elements (e.g., walls, roof) that meet current construction practices. For instance, modern external walls tend to be relatively thin due to the high population density and high price per square meter in urban areas.

Due to its superior characteristics such as high thermal, heat storage, airtightness, acoustic, and moisture buffering capacity, hempcrete is gaining in popularity worldwide. Although Canada is one of the leading producers and exporters of hemp, production and commercial application of hempcrete in Canada have yet to be realized. Consequently, there is a need for the development and production of hempcrete mixes designed for Canadian climates using local resources. Furthermore, there is a limited number of studies that investigated different design options for the external walls filled with hempcrete that exposed to the extreme continental weather such as Winnipeg, where temperatures vary from -35 $^0$C in the winter to +35 $^0$C in the summer. In particular, there is a lack of studies focused on the development of design solutions that meet both the construction trends of maximizing floor area with thin external walls and the current National Energy Code of Canada for Buildings (NECB, 2015).

## 1.2 Objectives and Scopes

The main objective of this thesis has been twofold: (1) development hempcrete infill “wall” formula with excellent thermal properties using locally sourced materials; and (2) numerical investigation of the long-term hygro-thermal performance of hempcrete wall types that satisfy current National Energy Code of Canada for Buildings. The multiple steps that have been carried out to meet this objective are as follows:

1. To measure the physical properties of locally sourced hemp hurd, including bulk density, moisture content, and particle size distribution, as well as to compare obtained data to the results of previous studies.

2. To develop a hempcrete infill “wall” formula with excellent thermal properties using locally sourced materials, including hemp hurd, hydrated lime, and metakaolin. Four different hempcrete mixes with varying concentrations of metakaolin were developed. The main goal was maximizing the hemp hurd ratio within the hempcrete mixture to improve its thermal properties while reducing its carbon footprint and price.

3. To develop two wall type designs with different complexity and construction method that meet the current National Energy Code of Canada for Buildings. The first design type primarily relies on a hempcrete wall with plaster finishes on both sides (i.e., internal and external). The second design type reduces the hempcrete

section thickness up to the width of the standard frame size by including an additional insulating layer, thus developing a multi-layer wall system.

4. To investigate the hygrothermal performance of the developed wall designs over five consecutive years using the WUFI®2D finite element modeling tool.

5. To investigate the performance of the developed hempcrete wall types under different indoor and outdoor environmental conditions. Four distinct design boundary conditions were developed based on the available climatic scenarios in WUFI®2D.

## 1.3 Contribution to the Field

The main contributions of the thesis are as follows:

- In contrast to the majority of previous research studies that applied higher binder content for wall formulas, this research focuses on the maximizing hemp hurd ratio within the "wall" infill hempcrete mixtures to improve their thermal performance while reducing embodied energy and expenditure.
- There is a limited number of Canadian studies that developed hempcrete formulas only from locally sourced materials. Therefore, this research study advances the current knowledge by developing hempcrete mixes using locally sourced materials, including hemp hurd and eco-friendly pozzolan such as metakaolin. Furthermore, it is anticipated that the results and findings from this increase the affordability and availability of the hempcrete "wall" formulas in Canada, and especially Manitoba, while reducing their embodied energy as ingredients will not be shipped from abroad.
- There is a limited number of studies that investigated the design strategies for hempcrete wall systems that meet the current National Energy Code of Canada for Buildings. In particular, there is a lack of studies focused on hempcrete infill multi-layer wall systems that satisfy Canadian energy code and investigation of their long-term hygro-thermal performance under various interior and exterior conditions. Consequently, the results of this study are likely to be of interest to audiences in academia and industry.

- Finally, yet importantly, the majority of earlier studies focused on the development of hempcrete wall envelop systems exposed to temperate, semi moderate, or hot climates, and only a few focused on cold climates. Therefore, this study provides new knowledge and information about the potential for the application of hempcrete under Canadian weather conditions.

## 1.4 Thesis Structure

**Chapter 2**

This chapter provides a comprehensive review of literature focused on hempcrete and its application in building envelope systems. Therefore it gives a detailed description of hemp hurd and hempcrete formulation. Then hygrothermal properties of hempcrete, including thermal conductivity, heat capacity, porosity, and vapor diffusion resistance factor, are discussed concerning the effects on the hempcrete properties for different relative proportions of binders and density of the mixes. This chapter also discusses the development of hempcrete infill wall systems and its application as a regulator of indoor hygrothermal comfort.

**Chapter 3**

This chapter provides the research methodology. It starts with a detailed description of hemp hurds, including the methods of calculating bulk density, moisture content, and particle size distributions. Then it describes the hempcrete preparation method for wall applications using lime along with metakaolin in varying relative proportions. Subsequently, it explains the process of testing the hygrothermal properties of hempcrete, including thermal conductivity and dry density. Finally, it describes the numerical model development of a hempcrete infill wall that was used for comparison of long-term hygrothermal performance of hempcrete infill multi-layer wall systems that satisfy the National Energy Code of Canada for Buildings.

**Chapter 4**

This chapter provides the results and findings of the experimental and modeling analysis. It starts with a description and comparison of physical properties, such as bulk density, moisture content, and particle size distributions of hemp hurd. Then it describes the dry density of hempcrete samples. Further, the chapter provides the thermal conductivity test results of hempcrete. Next, it gives the hygrothermal results, including water content, relative humidity, temperature, and mold growth of the developed wall models. Finally, it provides the results of the heat flow analysis of the developed wall models.

**Chapter 5**

This chapter outlines the key findings of the work undertaken within this thesis. It also summarises the limitations and future recommendations for further research.

# 2 Literature Review

## 2.1 Introduction

Hempcrete is a light-weight mixture of hemp hurd and a lime binder with water that has a mass of around one-seventh to one-eighth of the concrete’s mass (Bedliva & Isaacs, 2014). Hempcrete has the potential to significantly reduce the embodied energy related to the construction of buildings while improving their indoor air quality (Tran Le et al., 2010; Ingrao et al., 2015). The advantages of hempcrete are numerous, and some of them are as follows. For example, hempcrete is a carbon-negative material that absorbs more $CO_2$ than emitting (Walker, 2006; Ip & Miller, 2012). In addition, hempcrete is a recyclable material that can be ground up and spread on farmers' fields as well as used to make new hempcrete.

Furthermore, because of its breathable and highly alkaline properties, hempcrete is a mold-resistant material. Also, due to its porous structure, hempcrete has a considerable hygroscopic capability, effectively behaving as a phase change material in thermal control and humidity regulations. In this regard, hempcrete can improve thermal comfort through passive regulation of indoor temperature and provide control of relative humidity through a constant exchange of water vapor between indoor and outdoor environments (Amziane & Arnaud, 2013). Some other advantages of hempcrete over conventional materials (e.g., fiberglass insulation) include better airtightness, high durability under stress, high adaptability with absorbance, low fractures, longevity, reduced thermal bridging, renewable, reusable, and vapor permeability (Amziane & Arnaud, 2013; Dhakal, 2016; Jami et al., 2019; Sutton et al., 2011).

Although hempcrete is non-structural material used with a load-bearing frame, it offers a beneficial compromise between thermal conductivity and thermal inertia, thus enabling a passive control of the indoor building environment.

Considering that other natural fiber-based composites (e.g., straw bale) belong to a high contribution to fire classes E and F (Motori et al., 2012), hempcrete is one of the most fire-resistant bio-based insulation materials. Hempcrete walls can also meet building code requirements and could be used in frame construction (Magwood, 2016). Moreover, hempcrete can be used to form external and internal walls, as well as insulating floor slab or roof insulation. Consequently, the entire building's envelope above grade can be made of hempcrete.

Due to its superior characteristics, hempcrete is gaining in popularity worldwide. Although Western Canada is one of the leading producers and exporters of hemp, the commercial application of biocomposite materials in Canada has yet to be realized. The utilization of hempcrete in the construction industry is low due to the various obstacles, including a lack of locally available products, standards, and best practice application guidelines.

## 2.2 Hemp Hurd and Binders

Hemp hurd is a biocomposite, made from the inner woody core of the hemp plant. Industrially, hemp hurd is processed by stripping the fiber from outside of the hemp stalk, leaving the hurd as a by-product. It is a mechanical process where the separation of the fibers from the hurds results in chopped pieces of hurds (Cazacu et al., 2016; Magwood, 2016). Hemp hurd is highly absorbent to water. In this regard, in 24 hours, it absorbs 325% water of its weight. Walker & Pavía (2014) found that the hydration and carbonation process utilizes most of its absorbed water in reacting with binders. The bulk density of hemp hurds is 110 ~ 162 $kg/m^3$ (Arnaud & Gourlay, 2012; Dhakal, 2016; Evrard, 2008; Hirst, 2013) and it varies depending upon the size distributions and origin. The specific gravity of the hurd is approximately 1.5 $g/mm^3$, the moisture absorption rate is 9.40 ≈ 9.90%, and the water absorption rate ranges from 85 to 105% (Arnaud & Gourlay, 2012; Dhakal, 2016).

Currently, there are no standards that define procedures for the particle size distribution of plant aggregates. Two approaches mostly used in the literature are mechanical sieve analysis (Pinkos, 2011; Nguyen et al., 2009; Hirst, 2013; Sinka et al., 2015; Page et al., 2017) and image analysis (Nguyen et al., 2009; Picandet, 2013; Page et al., 2017; Williams et al., 2018). However, both methods have their weaknesses. In this regard, the irregular shape of hemp hurd particles could generate inaccuracies. For example, previous studies reported that longer particles could pass through smaller openings (Nguyen, 2010; Page et al., 2017). Therefore, a percentage error of 15% is appropriate when using sieve analysis (Amziane 2013). On the other hand, the presence of small particles and fibers is difficult to detect in the image analysis, hindering the findings (Nozahic et al., 2012; Dinh, 2014). Furthermore, Nguyen et al. (2009) reported that it is rather challenging to classify fibered aggregates combining both methods (i.e., mechanical and image analysis).

Binders play an essential role as they impact building material in several aspects. For instance, binders affect the material's durability (Mukherjee, 2012), physical properties (Page et al., 2017; Tronet et al., 2016), environmental impact (Ingrao et al., 2015) and affordability (Jami et al., 2019; Ruggieri et al., 2017). While the review of the literature shows a wide variation in binder types and proportions within the hempcrete formulas, some binder types are particularly suitable for the development of hemp-concretes. In this regard, hydrated lime or slaked lime, which is an inorganic compound prepared from mixing Calcium Oxide (CaO) with water hence forming Calcium hydroxide ($Ca(OH)_2$), has been the most utilized binder in biocomposite building materials, including the hempcrete (Nguyen, 2010).

Previous research reported that hydrated lime is especially appropriate for hempcrete mixes because it allows hempcrete to breathe (Bedliva & Isaacs, 2014). Furthermore, hydrated lime has low thermal conductivity, high durability, good workability, low-maintenance, and autogenous healing properties. Hydrated lime prevents mold growth and pest infestation in hempcrete (Walker et al. 2014, Walker & Pavia 2010). The carbonation of lime also allows the absorption of carbon dioxide released during the calcination of lime (Hirst, 2013). Moreover, because hydrated lime is obtained by calcination between 800 °C and 1200 °C as opposed to 1450 °C for the production of Portland cement, the carbon emissions of the lime production are approximately 20% less than of cement (Amziane & Arnaud, 2013).

The pozzolans are often a vital component of the lime-based binders because they can improve the hempcrete's mechanical and thermal properties while reducing hempcrete's negative impact on the environment (Dinh, 2014; Magniont, 2010; Nozahic, 2012). Metakaolin is a calcined kaolin clay that reacts with lime and forms hydrates: calcium silica hydrate (CSH) and calcium aluminosilicates. Metakaolin is especially suitable pozzolan for hempcrete mixes because of its fast setting, high reactivity, and the ability to increase the compressive strength of the hydrated lime (Walker and Pavia, 2010; Sheridan et al. 2017). Furthermore, metakaolin is eco-friendly material due to the significantly less energy-intensive production process compared to cement (Sabir et al. 2001, Oliveira et al. 2005). For instance, metakaolin is obtained through calcination between 650 °C and 800 °C. As a result, its carbon emissions are approximately 55% less than that of Portland cement (Amziane & Arnaud, 2013). Consequently, mixing metakaolin with hydrated lime could be economical and sustainable binder solution for hempcrete.

## 2.3 Mix Proportions

Ingredient amounts significantly impact the overall performance of hempcrete, including hygrothermal, mechanical, and acoustical properties. Therefore, different hempcrete formulas will be applicable to building elements that are under different thermal and mechanical loads. For instance, higher insulation properties are desirable for roof and walls, whereas strength and acoustic properties are essential for floors (Magwood, 2016). The majority of the existing studies used ratio 1:1 combined with the density of 200-250 kg/m³ for loose-fill insulation in roof applications (Amziane & Arnaud, 2013), 1:1 to 1:4 combined with the density of 300-600 kg/m³ for wall purpose (Walker & Pavía, 2014; Pretot. et al., 2014; Dhakal et al., 2017), whereas 1:4 and higher binder contents with the density of 500-700 kg/m³ for floor utilization (Page et al., 2017; Shea et al., 2012).

For example, Dhakal et al., (2017) developed three hempcrete design mixes of 233 kg/m³, 317 kg/m³, and 388 kg/m³ using hemp hurd to binder ratio 1:1, 1:1.5, and 1:2, respectively. An imported Natural Hydraulic Lime's (St. Astier), pre-formulated hemp construction product composed of hydrated lime, a small portion of pozzolanic, and 2-30% Portland cement was used as a binder in the hempcrete mixtures. Furthermore, the study performed a hygro-thermal numerical WUFI analysis of two wall assemblies with a ratio of 1:2 over three consecutive years using one climatic condition. Although both wall assemblies behaved well, considering the hygrothermal parameters, construction with rain screen system had lower water content, dried faster, and reached a dynamic steady state earlier compared to the wall without air layer.

Williams et al. (2018) prepared five mixtures of hempcrete using different hemp hurd types and ratios. Thus three of them contained 16% hemp (fine, medium and coarse), 36% lime binder, and 48% water by mass. The remaining two mixtures contained medium graded hemp where one blend has 17%, 32%, and 51%, and the other 15%, 39%, and 46% of hemp hurd, binder, and water, respectively by mass ratios. The study concluded that thermal conductivity, compressive, and flexural strength increased with increasing binder ratios. It further explained that uniform hemp particle influenced the mechanical properties of the hempcrete.

Further, Rahim et al. (2016) produced hempcrete using 16% hemp, 36% lime, and 48% water by mass. They explained that hempcrete had interesting hygric properties, including high porosity, high absorption, and high vapor diffusion. Also, Oumeziane et al. (2014) developed two hempcrete design mixes of 450 kg/m$^3$ and 396 kg/m$^3$ using one hemp to binder mass ratio 2/3 (1:1.5). The study experimentally and numerically showed that the developed hempcrete mixes had excellent hygric properties.

Ip & Miller, (2012) made a non-load bearing hempcrete wall of 275 kg/m$^3$ using 30 kg hemp, 50 kg lime-binder, and 75 kg water to investigate the impact of hempcrete on climate change. They concluded that lime-binder is a prime contributor to GHG emissions. Similarly, Pretot. et al. (2014) produced a hempcrete wall by spraying including, wood framework, indoor, and outdoor coatings using hemp to binder mass ratio 1:2 (22 kg hemp for 44 kg lime-binder). The study found that the hempcrete wall has significantly lower embodied energy -1.5 kg $CO_{2eq.}$, compared to the conventional wall 28 to 32 kg $CO_{2eq.}$, making it environment-friendly building material. The study concluded that the hempcrete wall could be further improved by reducing the negative binder impact.

## 2.4 Hygrothermal Parameters

### 2.4.1 Thermal Conductivity

The insulation material has a significant impact on the building, including thermal performance, indoor air temperature, and energy consumption. The use of hemp hurd as a composite building material has been extensively investigated by several studies owing to its low thermal conductivity (Sassoni et al., 2014; Zampori et al., 2013; Zach et al., 2013; Motori et al., 2012; Dinh, 2014). They found that the dry thermal conductivity of hemp hurd typically ranges between 0.048 W/mK and 0.058 W/mK.

Due to the low thermal conductivity of hemp hurd, the conductivity of produced hempcrete is competitive to conventional building insulation materials such as fiberglass and Rockwool (Collet & Pretot, 2014; Evrard, 2008). However, the thermal conductivity of hempcrete depends on various factors. Some of the critical parameters include the dry density (Cerezo, 2005), hemp hurd to binder ratio (Page et al., 2017), binder type (Dinh, 2014), and water amounts (Rahim et al., 2016).

The literature reported that the thermal conductivity of hempcrete has a linear relationship with its density and increases with an increase in the dry density and decreases with a decrease in the dry density (Cerezo, 2005; Hussain et al., 2019; Walker & Pavía, 2014). For example, the thermal conductivity of hempcrete with the dry densities ranging from 220 kg/m$^3$ to 627 kg/m$^3$ varies from 0.06 W/mK to 0.14 W/mK (Evrard and Herde, 2005; Evrard, 2008).

Further, Williams et al. (2018) developed five design mixtures of hempcrete using various hemp hurds, and mass ratios to investigate the impact of mix proportions of hempcrete on its thermal conductivity. The study concluded that the increase of hemp to binder ratio from 1:1.8 to 1:2.6, increased thermal conductivity from 0.11 W/mK to 0.13 W/mK. Similarly, Page et al., (2017) produced hempcrete of 245 kg/m$^3$ and 400 kg/m$^3$ that had conductivity 0.057 W/mK and 0.086 W/mK, respectively. Similarly, Shea et al. (2012) developed hempcrete mixtures of density ranging from 330 kg/m$^3$ to 440 kg/m$^3$ with thermal conductivity ranging from 0.09 W/mK to 0.115 W/mK. Furthermore, Tran Le et al. (2010) constructed a hempcrete wall using hemp to binder mass ratio 1:2 combined with the density of 413 kg/m$^3$ to achieve thermal conductivity of 0.10 W/mK.

Water absorption of hempcrete also influences its thermal conductivity. For instance, Rahim et al. (2016), developed a hempcrete mix design using a 1:2.25 ratio by mass and found that the thermal conductivity ranged from 0.123 W/mK to 0.128 W/mK. Their study showed that under similar conditions and temperature differences, an increase of 8% (kg/kg) in water content increases approximately 10% thermal conductivity (0.131 W/mK to 0.146 W/mK).

Previous research studies have used the pozzolan (metakaolin, slag, etc.) alongside lime as binders to obtain low thermal conductivity hempcrete (Amziane & Arnaud, 2013; Dinh, 2014; Walker & Pavía, 2014). For example, hempcrete produced using 50% to 80% metakaolin by weight in composition had thermal conductivity ranging from 0.101 W/mK to

0.106 W/mK (Dinh, 2014). Furthermore, Walker & Pavía, (2014) developed two types of hempcrete using two pozzolans, metakaolin and Ground Granulated Blast furnace Slag (GGBS), to investigate an impact of different pozzolans in mix proportion on hempcrete's thermal conductivity. Thus, one hempcrete produced using metakaolin had conductivity of 0.117 W/mK to 0.123 W/mK, and another one produced using Ground Granulated Blast furnace Slag (GGBS) had conductivity of 0.126 W/mK to 0.129 W/mK. Consequently, hempcrete made of metakaolin tends to have lower thermal conductivity than hempcrete composed of GGBS. Moreover, Arnaud & Gourlay, (2012) used formulated lime (consisting of 75% hydrated lime, 10% hydraulic lime, and 15 % pozzolanic lime) as a binder to produce hempcrete mixes with thermal conductivity ranging from 0.06 W/mK to 0.12 W/mK.

Fluctuations in the relative humidity (RH) also cause changes in the thermal conductivity of hempcrete samples. In this regard, variations in RH from 15% to 65% results in changes in thermal conductivity in the range of 0.094 W/mK to 0.1 W/mK for hemp hurd to binder ratio 1:1 and the range of 0.105 W/mK to 0.116 W/mK for hemp hurd to binder ratio of $1{:}1\frac{2}{3}$ (De Bruijn & Johansson, 2013).

Heat capacity and thermal diffusivity also have a significant impact on physical properties of hempcrete. Therefore, the specific heat capacity of hempcrete with densities ranging from 381 kg/m³ to 627 kg/m³ ranges from 1000 J/kg K to 1590 J/kg K (Evrard and Herde 2005, Evrard 2008). Also, according to the literature, the specific heat capacity of hempcrete is higher for the lower thermal diffusivity hempcrete (De Bruijn & Johansson, 2013b;

Latif, Lawrence, et al., 2015). Furthermore, Hussain et al. (2019) prepared hempcrete mixes with the dry density ranging from175 kg/m$^3$ to 240 kg/m$^3$ that had a specific heat capacity ranging from 760 J/kg K to 1050 J/kg K and thermal diffusivity ranging from 0.28 m$^2$/s to 0.35 m$^2$/s.

### 2.4.2 Porosity and Water Vapor Diffusion Resistance Factor

The porosity of hempcrete influences the hygrothermal properties of hempcrete. The porosity of hempcrete depends on various factors, including ingredients used in proportion mix, the technique applied for producing hempcrete, water absorption, and density (Collet at el., 2013, Oumeziane et al., 2014). For example, three different hempcrete: precast hempcrete (PHC), sprayed hempcrete (SHC) and molded hempcrete (MHC) of densities ranging between 430 to 460 kg/m$^3$ had porosity of 68%, 66%, and 77%, respectively (Collet et al., 2013). The study explained that all three hempcrete mixes were highly porous because of open and interconnected porosity. Further, Oumeziane et al. (2014) produced two hempcrete mixes of 450 kg/m$^3$ and 396 kg/m$^3$ using the same ratios, which had a porosity of 67.6% and 71.5%, respectively. This study also showed that high-density hempcrete tends to have low porosity. Similarly, a four-year study of a hempcrete wall constructed by spraying within the timber frame reported a porosity of 68% (Moujalled et al., 2018).

The water vapor diffusion resistance factor ($\mu$) also influences the hygrothermal properties of hempcrete, and it varies depending on the testing method, application purpose, and density (Moujalled et al., 2018; Latif et al., 2015; Evrard, 2008). For instance, Colinart et al. (2016) developed a multilayered hempcrete wall of 450 kg/m$^3$ and used dry cup tests (ISO

12572) to determine the vapor diffusion resistance factor of 5.0. Also, Evrard (2008) produced hempcrete's combined with a density of 440 $kg/m^3$ and used dry cup tests (ISO 12572) to determine the vapor diffusion resistance factor of 4.85±0.24. Similarly, Latif et al. (2015) developed a hempcrete wall to determine the water vapor diffusion resistance factor following dry and wet cup tests described in the British standard BS EN 12086. According to the dry cup and wet cup tests, the water vapor diffusion resistance factor was 2.9 and 1.8, respectively. Furthermore, based on the experimental analysis of a hempcrete wall constructed by spraying within a timber frame, Moujalled et al. (2018) reported water vapor diffusion resistance factor ranging between 2.8 and 3.0. Due to the differences of testing chamber, the solution used in dry cup tests and RH conditions the vapor diffusion resistance factor varies between 2.9 to 5.0. For example, Evrard (2008) used silica gel in the dry cup tests and placed the samples in a climate chamber at 50% RH level that resulted in a high (4.85) vapor diffusion resistance factor. Whereas Latif et al. (2015) used salt solutions in dry cup tests and placed the samples in glass dishes at 0% inside and 50 (±3)% outside RH level that resulted in low (2.9) vapor diffusion resistance factor.

## 2.5 Hempcrete Integrated Wall System

Different designs and configurations of the hempcrete walls have a significant influence on the overall hygrothermal performance of a building. The majority of the existing studies focused on hempcrete infill wall systems investigated their hygrothermal behavior, including water content (Dhakal, 2016), distribution of relative humidity (Collet & Pretot, 2014), and temperature variations (Costantine et al., 2018).

Table 1 summarizes the different types of hempcrete wall systems, including varying indoor, outdoor, and hempcrete section thickness found in the literature. It can be seen that a typical hempcrete wall assembly is a "both sides coated single hempcrete layer" of thickness ranging from 300 mm to 360 mm (Evrard & Herde, 2010; Dhakal, 2016; Collet & Pretot, 2014, Costantine et al., 2018; Maalouf et al., 2018). For example, Dhakal (2016) developed a numerical model of two hempcrete walls that explained how the layers and thickness influenced the water content distribution on the wall. Thus, one hempcrete wall of 335 mm (base wall) combined with 300 mm of hempcrete section had total water content ranged from 7.78 $kg/m^3$ to 17.57 $kg/m^3$, and another hempcrete wall of 355 mm combined with 300 mm of hempcrete section had entire water content ranged from 5.13 $kg/m^3$ to 11.08 $kg/m^3$. The study concluded that the water content was below 15% in each layer for both walls where no long term accumulation of water content (i.e. condensation risk) was observed. Further, Collet & Pretot (2014) developed two hempcrete walls of a total thickness of 300 mm using precast blocks to investigate the impact of coating on relative humidity and temperature distributions. The study showed that an uncoated hempcrete wall had a quick response to changes in temperature and moisture, which reduced after adding 10 mm lime coating on either side of the second wall.

Table 1: Hempcrete infill wall system from the literature

| Literature | | Indoor surface | Hempcrete section | Outdoor surface | Total thickness |
|---|---|---|---|---|---|
| Dhakal, 2016 | Wall 1 | 20 mm lime render | 300 mm | 15 mm lime plaster | 335 mm |
| | Wall 2 | 20 mm wood cladding + 20 mm air space | 300 mm | 15 mm lime plaster | 355 mm |
| Collet & Pretot, (2014) | Wall 1 | uncoated | 300 mm | uncoated | 300 mm |
| | Wall 2 | 10 mm lime coating | 300 mm | 10 mm lime coating | 320 mm |
| Costantine et al., (2018) | | 15 mm gypsum plaster + 200 mm Optibric PV3+ brick | 130 mm | 20 mm lime sand plaster | 365 mm |
| Maalouf et al., (2018) | Wall 1 | 15 mm gypsum plaster + 200 mm Optibric PV3+ brick | 200 mm | 20 mm lime sand plaster | 435 mm |
| | Wall 2 | 10 mm hemp-lime plaster + 10 mm lime-sand plaster | 360 mm | 10 mm lime-sand plaster | 390 mm |
| Pretot et al. (2014) | | 10 mm sand-lime coating + 10 mm hemp-lime coating | 240 mm | 20 mm outdoor coating | 280 mm |

The hempcrete infill wall can also improve the energy performance of the building and reduce its carbon footprint under different climatic conditions. For instance, Maalouf et al. (2018) developed two hempcrete walls with two façade systems to investigate their energy performance and embodied energy. Therefore, one hempcrete multilayer wall of 435 mm was composed of a 15 mm inside gypsum plaster, 200 mm brick façade, 200 mm sprayed hempcrete, and 20 mm outside lime-sand plaster. The other hempcrete wall was a single-layered hempcrete wall of 390 mm made of 10 mm inside hemp-lime plaster, 10 mm lime-sand plaster, 360 mm sprayed hempcrete, and 10 mm outside lime-sand plaster. The study reported that the multilayer wall exhibited similar energy and carbon performances to the single-layered hempcrete wall.

Further, Pretot et al. (2014) tested a hempcrete wall following French thermal regulations to investigate the influence of thickness on the life cycle assessment of the hempcrete wall. Thus, a 280 mm thickness hempcrete wall combined with 20 mm outdoor coating, 240 mm hempcrete, and 20 mm indoor coating layer showed satisfactory performance, and an increase in hempcrete thickness improves indoor climatic conditions.

Moreover, Evrard & Herde (2010) performed a numerical analysis of two selected hempcrete walls, a 335 mm hempcrete wall made of a 300 mm hempcrete section, and a 341 mm hempcrete wall composed of a 284 mm hempcrete section, to investigate their hygrothermal and transient performances. The study concluded that hempcrete walls have a strong ability to improve indoor comfort (Evrard & Herde, 2010). Similarly, Costantine et al. (2018) developed a multilayer wall of thickness of 365 mm combined with a 130 mm external hempcrete layer. The results from their study show that the designed hempcrete wall provides an acceptable indoor thermal comfort (below 21 °C in winter and 26 °C in summer) and dampens the outdoor temperature variations.

## 2.6 Hygrothermal Performance

Hempcrete has high moisture transfer and storage capacity, and as such, it is as excellent (or nearly excellent) regulators of humidity. In this regard, Tran-le et al. (2019) reported that hempcrete is naturally hygroscopic because it releases and absorbs water vapor depending upon the air conditions to keep the indoor relative humidity within the acceptable comfort range. As a result, hempcrete walls can improve the indoor hygrothermal performance of a building (Tran-le et al., 2019; Piot et al., 2017; Moujalled et al., 2018).

Several studies numerically and experimentally investigated the hygrothermal performance of the hempcrete walls and its impact on the indoor conditions. For example, Dhakal et al. (2017) numerically investigated the hygrothermal performance of the two hempcrete walls, a face-sealed and vented rain screen, using finite element software WUFI. The findings of the study suggest that both walls perform well without any hygrothermal risks, including condensation, frost, and salt damage. Furthermore, Bejat et al. (2015) developed two hempcrete test cells using precast blocks to investigate the effect of external coating on the indoor relative humidity level. The study reported that uncoated hempcrete blocks had a 30% higher relative humidity compared to the externally coated hempcrete blocks.

Moreover, Marceau et al. (2017) developed a hempcrete design mixes using hemp to binder mass ratio 1:2 to investigate the influences of relative humidity and temperature on mold growth. They tested the hempcrete samples in a climatic chamber set at $30^{0}$C and 95% RH for 100 days. The study reported a mold growth after a satisfactory pH level dropped by 10% to 15% at the end of the inoculation period. Furthermore, it concluded that prime conditions for mold growth are relative humidity above 98% and the binder surface pH level below 10, as the high relative humidity close to saturation and drop of pH level enhances bacterial growth on hempcrete surface with aging. In comparison, a numerical analysis of mold growth and decay formations showed that relative humidity above 95% is responsible for mold growth on wood-based building materials (Viitanen, 2003).

## 2.7 Identifying Research Gap

The majority of existing studies focused on higher hemp hurd to binder rations for hempcrete wall mixes (i.e., 1:2 to 1:4), and there is a limited number of studies focused on the lower hemp hurd to binder ratios (e.g., 1:1). Thus, more research is required focusing on the maximization of hemp hurd ratio within the hempcrete “wall” mixtures to improve their thermal performance while reducing embodied energy.

Furthermore, because hempcrete’s characteristics and behavior depend on different parameters, studies carried out elsewhere can serve as a useful guideline for research and comparison of the results. However, their findings cannot be directly transferred to the local building codes and standards. As a result, there is a great need for research that will focus on the development and production of hempcrete mixes and materials using local, Canadian resources.

Moreover, there is a limited number of Canadian studies that developed hempcrete formulas only from locally sourced materials. Therefore, further research should focus on the design of the hempcrete wall system in the Canadian context. In particular, there is a need for the development of hempcrete wall configurations that meet the Canadian building regulations. Consequently, more research is required to study the standard thickness and design of the hempcrete integrated wall system according to national energy codes and guidelines.

Finally, yet importantly, the majority of earlier studies focused on the development of hempcrete wall envelop systems exposed to temperate, semi moderate, or hot climates, and only a few focused on cold climates. Therefore, there is a need for research about the potential for the application of hempcrete under Canadian weather conditions.

# 3 Experimental Program

This chapter provides the materials and methods used in this study. It starts with a description of hemp hurds, including the techniques of measuring bulk density, moisture content, and particle size distributions. Then it describes the hempcrete preparation method for application in walls using lime along with metakaolin in varying relative proportions. Subsequently, it explains the process of testing the hygrothermal properties of hempcrete, including thermal conductivity and dry density. Finally, it describes the numerical model development of a hempcrete infill wall that was used for comparison of long-term hygrothermal performance of hempcrete infill multi-layer wall systems that satisfy the National Energy Code of Canada for Buildings.

## 3.1 Raw Materials

### 3.1.1 Hemp Aggregate

Hemp hurd used as aggregate in this study is processed industrially from the soft inner core of the plant stem, chopped in medium size, and supplied in 33lb compressed plastic bags by the manufacturer Plains Hemp®, Gilbert Plains, Manitoba. According to the manufacturer, the hurd is highly absorbent and rich in cellulose (~45%), hemicellulose (~25%), and lignin (~25%) (Plainshemp.ca).

The bulk density of hemp hurd depends on several factors, such as particle grading and orientation, fiber/dust, moisture content, compaction applied, and biological composition depending upon the growing locations (Hirst, 2013). The bulk densities of the hemp hurds were measured following the ASTM C29 before oven drying and after oven drying for 24 hours at 105 ˚C that was carried out to remove the absorbed moisture from hemp particles (ASTM C29, 2007). Measurement bucket with dimensions 100 mm x 100 mm was filled with hemp by means of scoope where the height of the fall of hemps was below 5 cm from the top of bucket. The bulk density was measured after calculating the mass of the hemp, as presented in Figure 1 (a). Figure 1 (b) shows the oven drying of hemp hurds in laboratory storage. The accuracy of weighing machine used for calculating the bulk density is ±0.005 kg. The bulk density of hemp hurd obtained before oven drying was 114.6 kg/$m^3$. These results support the previous finding about the average bulk density ranging from 110 kg/$m^3$ to 162 kg/$m^3$ (Arnaud & Gourlay, 2012; Dhakal, 2016; Evrard, 2008; Hirst, 2013).


Figure 1: (a) Measurement of bulk density and (b) oven drying of hemp hurd

As illustrated in Figure 2, hemp hurd used in this research has frequent percentage of fiber content, and the particle sizes measured were roughly range from 1 mm to 25 mm in length, 1 mm to 15 mm in width, and 0.5 mm to 1 mm in thickness. Particle analysis was performed following the ASTM C136 standard sieve analysis testing method that determines the size of particles and the distribution of fine and coarse aggregates (ASTM C136, 2006). Amziane & Arnaud (2013) recommended applying a percentage error of 15% to the results of sieve analysis due to the variation in the geometry of hemp hurd particles.

Figure 2: Hemp hurds showing particles and fiber contents

The sieve analysis testing method included a stopwatch, mechanical sieves, and a shaker machine. The sizes of sieves presented in Figure 3 (a) were 2.36 mm, 4.75 mm, 6.3 mm, 9.5 mm, 12.5 mm, 16.0 mm, 19.0 mm, and 25 mm. Sample sizes of 100 grams and 200 grams of hemp hurds previously dried at the laboratory climatic conditions (24 Hours, $105^{0}$C) were measured separately. The scale accurate to 0.01 gram was used for measuring the samples. Further, Figure 3 (b) shows the test setup of the sieve shaker machine. The sieve shaker was run for approximately 8 to 10 minutes for the 100-gram sample and 18-20 minutes for 200-gram samples. After completion of the shaking cycle, hurd retained in every sieve was measured for masses. Obtain information was further used for plotting the particle size distribution curve using the cumulative method of sieve analysis. The findings of the sieve analysis are presented in the chapter 4.

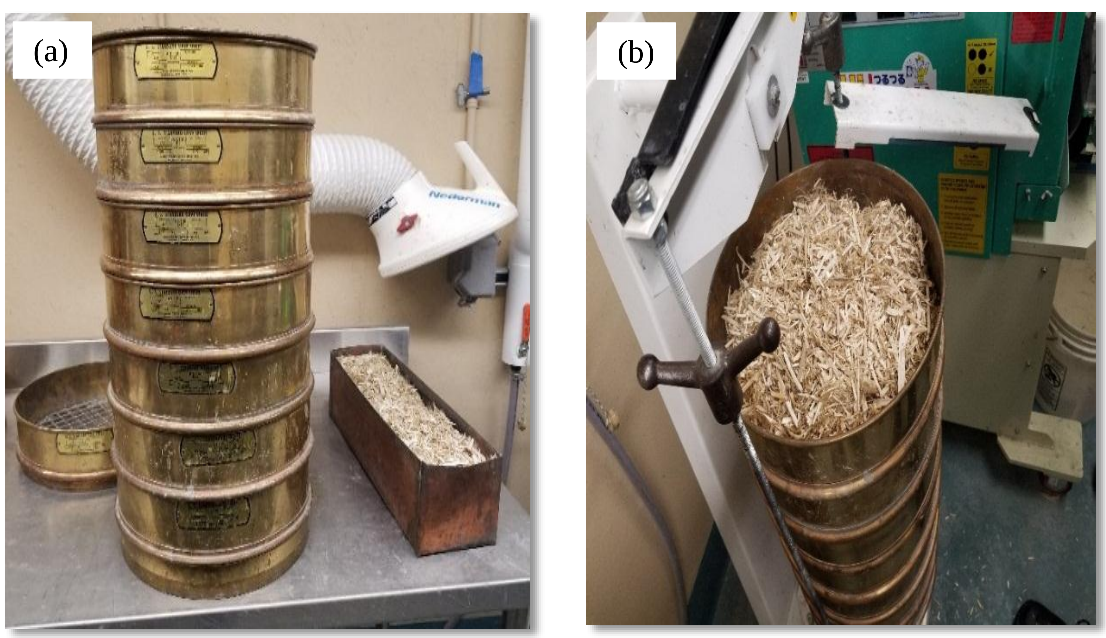


Figure 3: Mechanical sieve test: (a) sieve orientation and (b) sieve shaker test setup

Additionally, microstructure image recordings were conducted on hemp hurd particles using FEI Quanta 650 FEG Scanning Electron Microscope (SEM) at the Manitoba Institute of Materials (MIM), University of Manitoba. Scanning of the hemp hurds were conducted at low-vacuum mode 10 to 130 Pa by placing them at the electron microscope to obtain the microstructural imaging. The microstructure analysis of hemp hurd illustrated in Figure 4 (a), (b), (c), and (d) shows the cellular porous nature of hemp hurd particles, including non-uniform elliptical shape pores present only in part of the walls of vessels. The purpose of this image recording was to visualize the porous nature of hemp hurd. Numerous existing studies also reported that hemp hurds contains an extensive amount of hydraulic pores that enables absorption and retention of liquid flow (Walker et al., 2014; Arnaud, 2008).

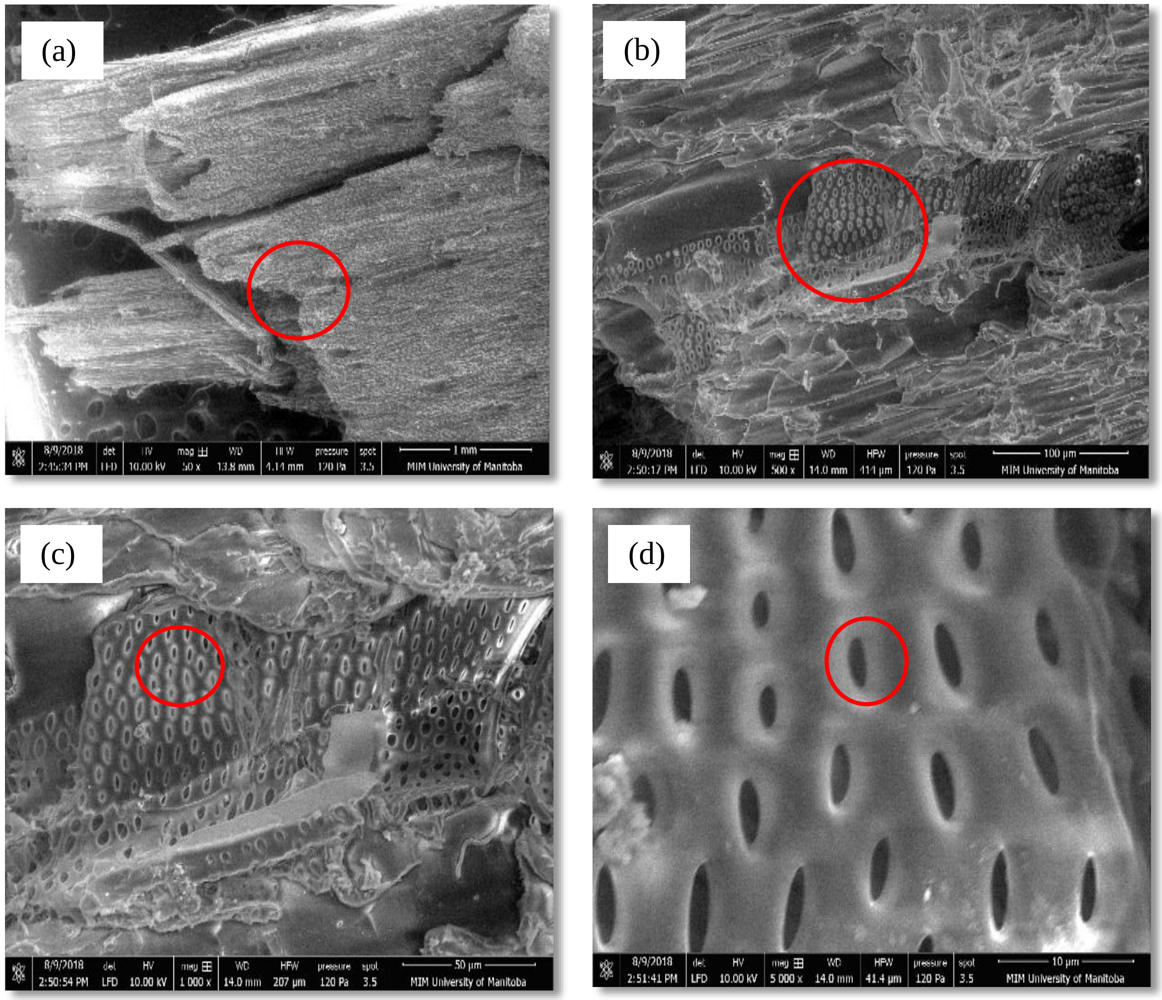


Figure 4: SEM analysis of hemp hurd: (a) hemp hurd at 1 mm magnification; (b) hemp hurd at 100 µm magnification; (c) hemp hurd at 50 µm magnification; (d) hemp hurd at 10 µm magnification.

### 3.1.2 Binders

The binders used in this study included high calcium hydrated lime produced according to the ASTMC207-06 (ASTM C207, 2006) standard by Western Lime Corporation and metakaolin created following CSA A3001 and ASTM C618-12 by Whitemud Resources Inc. (CSA A3001, 2013; ASTM C618, 2012).

Hydrated lime and metakaolin are selected based on their binding properties, environmental impact, availability, and price. In this regard, hydrated lime is especially suitable for the development of hempcrete due to the following advantages. First, hydrated lime is breathable due to its high porosity and high water vapor permeability (Evrard and Herde, 2010). Second, hydrated lime has a relatively low thermal conductivity ranging from 0.65 W/mK to 0.84 W/mK in a dry state (Amziane and Arnaud, 2013). Third, it has excellent workability, high durability, and possesses autogenous healing properties (Walker & Pavia, 2010). Finally, yet importantly, hydrated lime is mold growth and pests resistant as well as easy to maintain (Amziane and Arnaud, 2013; Evrard and Herde, 2010). Moreover, because hydrated lime is obtained by calcination between 800 °C and 1200 °C as opposed to 1450 °C for the production of Portland cement, the carbon emissions of the lime production are approximately 20% less than of cement (Amziane and Arnaud, 2013; Dinh, 2014).

Metakaolin is a calcined kaolin clay that reacts with lime and forms hydrates: calcium silica hydrate (CSH) and calcium aluminosilicates. Metakaolin is particularly favorable pozzolan for hempcrete due to the several advantages. First, metakaolin has a low permeability, fast setting, and high reactivity (Walker & Pavia 2010). Furthermore, in reaction with hydrated limes, metakaolin uses the free lime present in the adhesives to form Calcium Silica Hydrates (CSH), thus adding extra durability to the mix (Whitemud Resources Inc., 2009). Moreover, metakaolin is an eco-friendly material due to the less energy-intensive production compared to cement (Magwood, 2016; Sabir et al., 2001). For instance, because of the lower calcination temperature ranging from 650 °C to 800 °C, the production of metakaolin results in approximately 55% less $CO_2$ emissions compared to Portland cement (Amziane & Arnaud, 2013).

The densities of hydrated lime and metakaolin measured in the laboratory according to ASTM C110 using a cylindrical container of 200 mm high and 100 mm in diameter were approximately 500 kg/m$^3$ and 800 kg/m$^3$, respectively (ASTM C110, 2011). Hydrated lime is an alkaline earth hydroxide where more than 90% of its weight is calcium hydroxides [$Ca(OH)_2$] and less than 1% calcium or magnesium oxides (MSDS: Pure Cal, 2009). The chemical constituents of metakaolin are 78% to 80% calcinated kaolin, and 18% to 20% quartz ($SiO_2$) (MSDS: Whitemud Resources Inc., 2009). Table 2 summarizes the physical properties of the hydrated lime and metakaolin used in this study, and Table 3 summarizes their chemical compositions.

Table 2: Physical properties of the binders

| Binders | Laboratory bulk density (Kg/m$^3$) | Sp. gravity (MSDS) (g/cc) | Color (MSDS) | Physical state |
|---|---|---|---|---|
| Hydrated lime | ~ 500 | 2.2 to 2.4 | White | Solid (Powder) |
| Metakaolin | ~ 800 | 2.6 | Off-white | Solid (Powder) |

Table 3: Chemical composition of hydrated lime and metakaolin (MSDS: Pure Cal, 2009; MSDS: Whitemud Resources Inc., 2009).

| Chemical Component | % by weight | |
|---|---|---|
| | Hydrated lime | Metakaolin |
| $Ca(OH)_2$ | >90.0 | -- |
| MgO | <2.0 | 0.65 |
| CaO | <1.0 | 0.20 |
| $SiO_2$ | -- | 61.0 |
| $Al_2O_3$ | -- | 34.0 |
| $K_2O$ | -- | 1.25 |
| $Na_2O$ | -- | 0.13 |
| $Fe_2O_3$ | -- | 1.65 |

## 3.2 Hempcrete

### 3.2.1 Hempcrete Mix Preparation

This research focuses on maximizing the hemp hurd ratio within the hempcrete mixture to improve its thermal properties while reducing its carbon footprint and price. Hence, the ratio used in the preparation of the hempcrete sample was 1:1 of hemp hurds and binders by mass with a density adequate for wall applications between 300 kg/m³ and 400 kg/m³ (Evrard, 2008; Evrard and Herde, 2005). Four mixing formulas and 7 batches were produced using various proportions of hemp hurd, binders, and water content. Hence, as summarized in Table 4, the metakaolin and hydrated lime percentages applied within the developed samples composition range from 2.17% to 15.56% and from 6% to 19.57%, respectively. The water percent vary between 55.56% and 60% depending on the batch named as LMK (lime-metakaolin), where the numerical suffix represents the ratio percentage of applied metakaolin. The water variations used in some batches, including LMK20, LMK50, and LMK70, enabled insights into the impact of water content on the thermo-physical properties of the developed hempcrete samples.

Table 4: Specimen mix ratios for testing

| Mix Formula | Batch No. | Design name | Mix ratio by weight Hemp/Lime/Metakaolin/Water | | | | Materials composition (Percentage by weight) |
|---|---|---|---|---|---|---|---|
| | | | H | L | MK | Water | |
| Lime + Metakaolin | 1 | LMK70 | 1 | 0.3 | 0.7 | 3 | 20% Hemp, 6 % Lime, 14% Metakaolin, 60% Water |
| | 2 | LMK70B | 1 | 0.3 | 0.7 | 2.5 | 22.22% Hemp, 6.67 % Lime, 15.56% Metakaolin, 55.56% Water |
| Lime + Metakaolin | 1 | LMK50 | 1 | 0.5 | 0.5 | 3 | 20% Hemp, 10 % Lime, 10% Metakaolin, 60% Water |
| | 2 | LMK50B | 1 | 0.5 | 0.5 | 2.5 | 22.22% Hemp, 11.11 % Lime, 11.11% Metakaolin, 55.56% Water |
| Lime + Metakaolin | 1 | LMK20 | 1 | 0.8 | 0.2 | 3 | 20% Hemp, 16 % Lime, 4% Metakaolin, 60% Water |
| | 2 | LMK20B | 1 | 0.8 | 0.2 | 2.5 | 22.22% Hemp, 17.78 % Lime, 4.44% Metakaolin, 55.56% Water |
| Lime + Metakaolin | 1 | LMK10 | 1 | 0.9 | 0.1 | 2.6 | 21.74% Hemp, 19.57 % Lime, 2.17% Metakaolin, 56.52% Water |

There are no standards and official procedures for mixing and preparation of hempcrete samples. Thus, as recommended by Gourlay and Arnaud (2010) and Hirst et al. (2010), the first step in the preparation of the hempcrete sample included the mixing of the binders and water to create a slurry. Consequently, as presented in Figure 5, the hemp hurd is added into the mixer pan to the slurry in two phases to ensure well mixing. Finally, the uniform distribution of hemp hurd within the sample required 12-15 minutes mixing in the mixer.

Figure 5: Hemp and binders mixing

### 3.2.2 Test Samples

Test samples for the thermal conductivity test were cast using rectangular wooden moulds (26 cm wide x 26 cm long x 5.5 cm high) presented in Figure 6. The moulds were first thoroughly cleaned and oiled up on the inner surfaces to prevent the samples from sticking at the sidewall of the box. The mixture was then placed in the one-quarter portion of the mould at a time and tamped until reaching the desired wet density. The moulds were sealed using a wooden lid at the top surface to achieve a smooth surface area. The samples were demoulded after seven days and cured at room temperature of $22 \pm 1^0$ C, with RH ~50%

until they were ready for testing (see Figure 6). In total, 14 different samples were tested to ensure the repetitiveness of the results and to investigate the relationship between the dry density and thermal conductivity. Measurement of the thermal conductivity of dry samples required oven drying at 100±5 °C until reaching constant mass (i.e., changes in weight readings of less than 0.1%).


Figure 6: Test samples for thermal conductivity measurements

## 3.3 Thermal Conductivity Test

FOX314 Heat Flow Meter Apparatus (HFMA) from the TA instrument was used to determine the thermal conductivity of the specimen. Figure 7 shows the FOX314 HFMA at W.R. McQuade Heavy Structure Laboratory, University of Manitoba. FOX314 HFMA consists of the chamber with two plates and the base with a key-pad-display section, as presented in Figure 7. The upper plate is stationary, and the lower one can move up and down by four independently controlled stepping motors. High-output transducers complying with ASTM C518 with an overall thickness of about 1 mm and made of hundreds of small thermocouples that provide high sensitivity and integration of the signals are bonded to the surfaces of both plates (ASTM C518, 2015). Type E thermocouples are bonded in the center of each transducer and positioned next to the plates' surfaces to provide accurate readings of both sample surfaces' temperatures. These thermocouples are also used to control the temperatures of the center and the periphery of the plates.

Furthermore, 24-bit Analog-to-Digital Converter (ADC) by following NIST 1450b SRM (Standard Reference Material of National Institute of Standards and Technology) converts analog signals of the thermocouples and the heat flow meters to the digital domain with 0.6μV resolution (Zarr et al., 2014). The resolution of the temperature measurements is approximately 0.01 °C (Fox 314 – TA Instruments). Both plates are equipped with state-of-the-art heating and cooling systems to control the heat flux through the sample in-between.

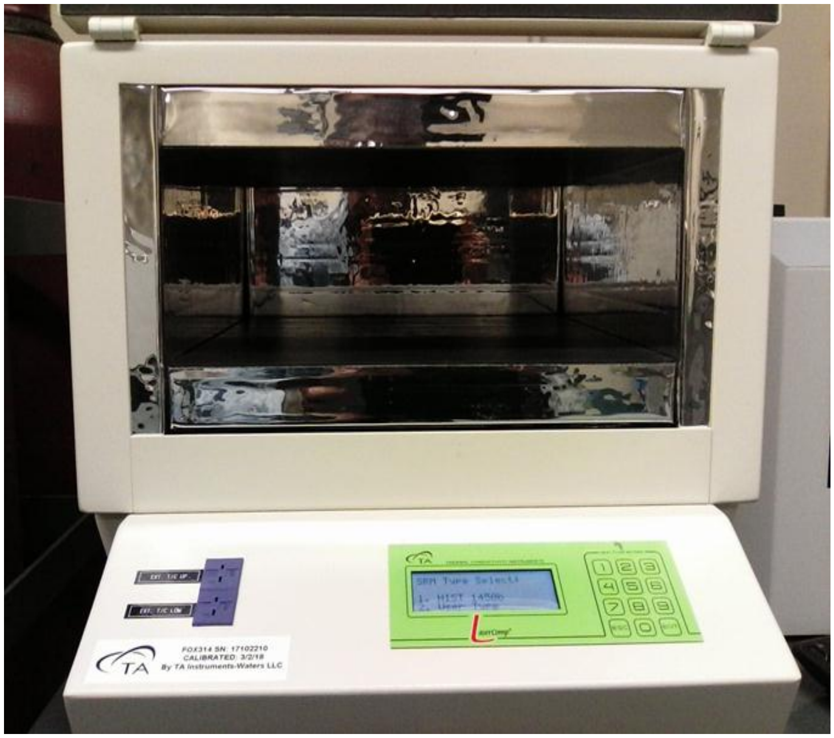


Figure 7: Fox314 Heat flow meter instrument with an opened stack

The temperature that can be set by the instrument ranges from -20 °C to 75 °C with an accuracy of ±0.01°C. Thermal conductivity measurements range from 0.005 W/mK to 0.35 W/mK for internal thermocouples and 0.001 W/mK to 2.5 W/mK for externally attached thermocouples. The HFMA follows the ASTM C518 standard for a steady-state test (ASTM C518, 2015) and creates steady one-dimensional heat flux through the sample by setting both plates at constant but different temperatures with an accuracy of ±0.03 °C. The instrument calculates the thermal conductivity of the material using Fourier’s Law of Heat Conduction, described in Equation 1, with an accuracy of approximately ±1% at a mean temperature of the plates.

$$q = k\,\frac{\Delta T}{L} = SQ\ [\frac{W}{m^2}] \qquad \dots\ \dots\ \dots\ \dots\ \dots\ (1)$$

Where $\Delta T$ is the temperature difference between upper and lower plates, S is the heat flow meter's calibration factor (W/ ($m^2$ $\mu$V)), Q is its output signal ($\mu$V), L is the sample's thickness (m), and k is thermal conductivity (W/m K).

Figure 8 shows the test samples with the attached external thermocouples at the center to the sides facing the transducers. Besides, rubber mats were used along with the samples to avoid degradation of the plate coating from rough edges of hempcrete. Initially, two rubber mats were calibrated in the device without placing the specimens. After calibration, hempcrete sample with external thermocouples attached to it was placed inside the chamber, keeping the rubber mats on top and bottom. The samples were placed in the middle of the exposed surface area inside the device chamber to keep the internal thermal sensor in the middle section. As presented in Figure 8, the sample was insulated all-around to improve the accuracy of the measurements by minimizing its edge heat losses. Finally, the sample was enclosed into the device, and thermocouples from the sample were attached to the FOX 314 exterior plug point. The 'Wintherm32' software was used following the guideline stated in the manual of FOX 314 Heat Flow Meter Apparatus.

Figure 8: Hempcrete sample prepared for testing

According to ASTM C518-15, the steady-state standard heat transmission method requires a constant temperature field inside the heat flow meter for different temperatures between the hot and cold plates. Therefore, samples were tested by choosing seven different pre-calibrated temperatures for hot and cold plates. Thus, the thermal conductivity test was carried out, keeping a constant temperature gradient 25 $^{0}$C starting from -20 $^{0}$C to a maximum of 65 $^{0}$C with a regular increment of 10 $^{0}$C. The temperature difference allowed the hempcrete sample to conduct heat from one side to the other at a constant rate that created a stable heat flux inside the chamber. The average temperatures maintained between the hot and cold plates were (-Ve) 7.35 $^{0}$C, 2.64 $^{0}$C, 12.6 $^{0}$C, 22.57 $^{0}$C, 32.53 $^{0}$C, 42.5 $^{0}$C, and 52.30 $^{0}$C. The collected data from the plates' transducers outputs consisted of 512 successive data points organized in one block and averaged to get the mean plate temperatures and heat fluxes. The averaged values at one block are compared with the average values of the previous block to check for the thermal equilibrium criteria. The test at a specific set-point is complete when a certain number of successive blocks satisfy two equilibrium criteria. First, the block average plate temperature must be equal to the earlier block average temperature within ±0.2 $^{0}$C. Second, the difference between the transducers average signal outputs of two successive blocks must be within a typical value of 50 µV, and 2% of the earlier block average.

## 3.4 Finite Element Modeling

This section describes the numerical model development of a hempcrete infill wall that was used for comparison of long-term hygrothermal performance of hempcrete infill multi-layer wall systems that satisfy the National Energy Code of Canada for Buildings. This section first describes two hempcrete wall assemblies: (1) base hempcrete infill wall-assembly 1, and (2) multilayer hempcrete infill wall-assembly 2. Then, the section gives details about the numerical design, including the geometry of the wall, material description, and initial-boundary conditions such as relative humidity, temperature, and water content. Finally, it describes the four combinations of boundary conditions (i.e., indoor and outdoor surface conditions) used in the simulations.

### 3.4.1 Description of Wall Assembly

The National Energy Code of Canada for Buildings (NECB, 2015) provides information about the minimum R-value requirements for the different climatic zone of Canada. According to code requirements, Winnipeg belongs to zone 7A (HDD 5000-5999), where the minimum R-value requirement per unit of wall is 4.76 $m^2k/W$ or R27 for above-grade wall assemblies (NECB, 2015). These recommendations were followed to define two assembly types, including (1) base monolithic wall and (2) multilayer wall. The monolithic wall is determined based on the literature review, and it is composed of a hempcrete infill sandwiched between the lime plaster layers. The multilayer wall reduces the overall thickness of the wall, and it consists of inside lime plaster, hempcrete infill, insulation, and external lime plaster.

Experimental data was used to specify the thermal conductivity of hempcrete and WUFI library to define the properties of plaster and insulation. Table 5 summarizes the physical characteristics of materials used in the numerical analysis. Based on this information, using WUFI software, it is calculated that the base wall composed of a 20 mm internal lime plaster layer, a 405 mm hempcrete section, and a 15 mm exterior lime plaster layer meets the prescribed code requirements. Similarly, the multilayer hempcrete wall made of a 20 mm internal lime plaster layer, a 140 mm hempcrete section (i.e., the width of the studs), 105 mm Rockwool insulation, and a 15 mm exterior lime plaster layer complies with the code requirements. Figure 9 illustrates, and Table 6 summarizes the composition of the modeled assembly cases. Additionally, Appendix A provides the calculations of minimum wall thickness using WUFI software.

Table 5: Material properties of hempcrete wall used in modeling

| Material | Bulk Density $kg/m^3$ | Porosity | Spec. Heat Capacity J/kg K | Thermal Conductivity W/mK | Water Vapour Diffusion Resistance Factor |
|---|---|---|---|---|---|
| Lime Plaster | 1600 | 0.3 | 850 | 0.7 | 7 |
| Hempcrete | 302 | 0.68 | 1412 | 0.08623 | 3.5 |
| Rockwool | 119 | 0.956 | 850 | 0.034 | 1.3 |

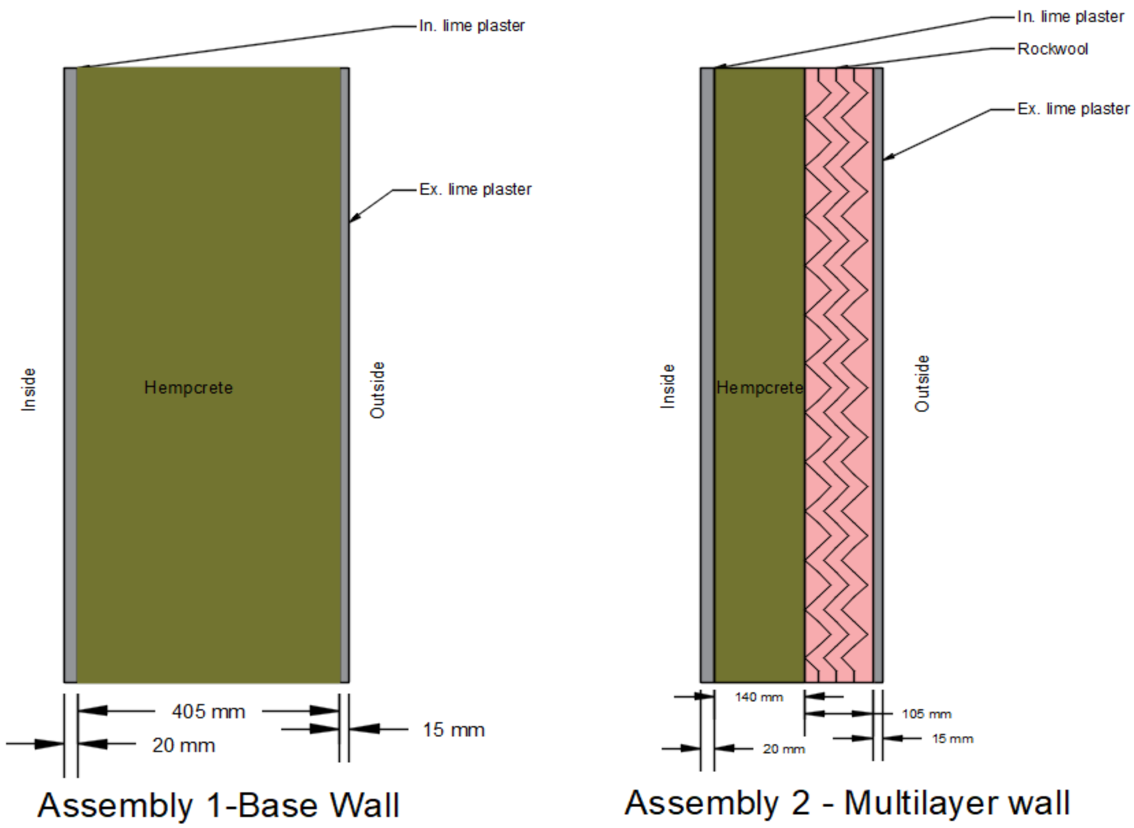


Figure 9: Base wall and multilayer wall geometry for numerical modeling

Table 6: Layers of assembly cases shown from left to right, interior to exterior

| | | | | | | | |
|---|---|---|---|---|---|---|---|
| **Assembly 1:** | | | | | | | |
| *Base wall* | Lime plaster 20 mm | + | Hempcrete 405 mm | + | Lime Plaster 15 mm | | |
| **Assembly 2:** | | | | | | | |
| *Multilayer wall* | Lime plaster 20 mm | + | Hempcrete 140 mm | + | Rockwool 105 mm | + | Lime Plaster 15 mm |

### 3.4.2 Description of Wall Geometry and Elements

The geometry of the modeling wall was plotted in WUFI®2D, keeping dimensions as described in Table 6 (see Appendix B). The cross-sectional height plotted for all the assemblies was 500 mm. Further, the WUFI finite element system automatically plots a minimum of 2 elements for each geometry section. Therefore, one element is in the X direction, and another is in the Y direction, which bears the material characteristics along the section. The accuracy of numerical solution depends on the mesh sizes of the numerical grid (Künzel, 1995). Further, the study recommended that high moisture, temperature gradient and boundary layers required to have numerical grid of few millimetres with variable mesh sizes. Therefore, the modeling considered a minimum of 2 elements in the X-Y direction along with the maximum of 90 elements in the X direction and 60 in the Y direction for all assemblies. After the initial analysis, the numerical grid system detected the total number of elements 68 in X and 45 in the Y direction for all sections. In X direction, the size (width) of the elements ranged from 0.59 mm to 36.4 mm and in Y direction they ranged between 3.2 mm to 27.4 mm. Each of these 68 elements represents the elemental characteristics at X direction and 45 in the Y direction within the geometry that has varying sizes of meshes.

### 3.4.3 Boundary Conditions

Before starting the modeling, WUFI software requires defining the initial boundary condition of the materials to redirect the content into its starting value and observe the flow cycle throughout the year. Table 7 shows the initial boundary conditions applied to the materials. The initial boundary condition of the materials determined and imported from the WUFI library and literature (WUFI.ca; Dhakal et al., 2017)

Table 7: Initial boundary conditions for the materials

| Material | Temperature ($^0$C) | Water Content (kg/m$^3$) | Relative Humidity (%) |
|---|---|---|---|
| Lime Plaster | | 30 | |
| Hempcrete | 20 | 29 | 80 |
| Rockwool | | 0.82 | |

Next, WUFI software requires defining surface boundary conditions to analyze the model for specific indoor and outdoor environmental conditions. The WUFI weather database provides various external and internal boundary conditions that differ regarding the location and severity. In this regard, four scenarios that combine two external and two internal boundary conditions were developed and applied to both wall assemblies. The two external boundary conditions include the Cold Year, which represents a typical cold year in Winnipeg, and ASHRAE Year 1, which represents the most severe years concerning moisture damage out of a measured ten year period. Two internal conditions include the High Moisture Load, which considers high moisture load and low temperature, and ASHRAE 160: Cold Year, which assumes medium moisture load and high temperature. It should also be noted that symmetric components transfer heat and moisture across the symmetry axis.

Therefore, the top and bottom surfaces of the modeled wall assemblies are treated as an adiabatic or impermeable boundary. Table 8 summarizes the four developed scenarios, and Appendix C provides temperature and humidity charts of all selected internal and external boundary conditions.

Table 8: Indoor and outdoor environmental boundary conditions

<table>
<tr><th>Scenarios</th><th>Outdoor Conditions</th><th colspan="2">Indoor Conditions</th></tr>
<tr><td>Scenario 1</td><td rowspan="2">Cold Year<br><br>Maximum temp. = 33.9$^0$C<br>Minimum temp. = -45$^0$C<br>Mean temp. = 1.2$^0$C<br><br>Maximum RH= 100%<br>Minimum RH= 19%<br>Mean RH=73.1%</td><td>High Moisture Load<br>Maximum temp. = 22$^0$C<br>Minimum temp. = 20$^0$C<br>Mean temp. = 21$^0$C</td><td><br>Maximum RH = 60%<br>Minimum RH = 50%<br>Mean RH = 55%</td></tr>
<tr><td>Scenario 2</td><td>ASHRAE 160: Cold Year<br>Maximum temp. = 31$^0$C<br>Min temp. = 21 $^0$C<br>Mean temp. = 26$^0$C</td><td><br>Maximum RH = 70%<br>Minimum RH = 21%,<br>Mean RH= 45%</td></tr>
<tr><td>Scenario 3</td><td rowspan="2">ASHRAE Year 1<br><br>Maximum temp. = 32.2$^0$C<br>Minimum temp. = -40$^0$C<br>Mean temp. = 2.3$^0$C<br><br>Max RH= 100%<br>Min RH= 12%<br>Mean RH=74.4%</td><td>High Moisture Load<br>Maximum temp. = 22$^0$C<br>Minimum temp. = 20$^0$C<br>Mean temp. = 21$^0$C</td><td><br>Maximum RH = 60%<br>Minimum RH = 50%<br>Mean RH = 55%</td></tr>
<tr><td>Scenario 4</td><td>ASHRAE 160: Cold Year<br>Maximum temp. = 31$^0$C<br>Min temp. = 21 $^0$C<br>Mean temp. = 26$^0$C</td><td><br>Maximum RH = 70%<br>Minimum RH = 21%,<br>Mean RH= 45%</td></tr>
</table>

The numerical analysis was performed in two stages. First, all four scenarios are applied to the base and multilayer walls for five consecutive years, ranging from 1$^{st}$ June 2014 to 31$^{st}$ May 2019. The output variables include water content, relative humidity, temperature, isopleths, and heat flow.

# 4 Results and Discussion

## 4.1 Chapter Outline

This chapter provides the results and findings of the experimental and modeling analyses. It starts with a description and comparison of the physical properties of hemp hurd, such as bulk density, moisture content, and particle size distribution. Then, it describes the dry density of hempcrete samples. The chapter further provides the thermal conductivity test results of hempcrete obtained through the experimental measurements using a heat flow meter instrument. Next, it presents and discusses the results of a hygrothermal numerical study about condensation and mold risk of two wall assemblies' base wall – assembly 1, and multilayer wall – assembly 2 performed in finite element software WUFI®. Analysis and discussion of the numerical heat flow results of the developed wall models close the chapter.

## 4.2 Hemp Hurd

### 4.2.1 Bulk Density and Moisture Content

The bulk density of the hemp hurd was measured in the laboratory: (1) before oven-drying at average room temperature 20–25 $^{\circ}$C and RH of 35–45%, and (2) after oven-drying for 24 hours at 105 $^{\circ}$C. The bulk density of hemp hurd recorded at room temperature before oven-drying was 114.6 kg/m$^3$. The bulk density of hemp aggregates depends on several factors: the origin of production, size distribution, fiber/dust particles, moisture content, and compaction type (Evrard, 2008; Page et al., 2017; Rahim et al., 2016; Hirst, 2013).

Table 9 presents the bulk density of the hemp hurd reported in the literature. It can be seen that the hemp hurd used in this study has a bulk density that is comparable to the values reported in the literature.

Table 9: Bulk density of hemp hurd from literature

| Literature | Bulk density (kg/m$^3$) |
|---|---|
| Arnaud and Gourlay (2012) | 115 |
| Dinh (2014) | 110.9 ± 0.7 |
| Evrard (2008) | 52–162 |
| Dhakal (2016) | 125.42 |
| Cerezo (2005) | 130 |
| Nguyen (2010) | 102.83 |
| Rahim et al. (2016) | 125 |
| Nozahic (2012) | 114.2 ± 2.3 |
| Page et al. (2017) | 110 |
| Williams et al. (2018) | 119–129 |

Amziane et al. (2017) reported that the bulk density of hemp hurd linked to the inter-particular porosity of the particles, which results in differences in density calculation. Also, the differences in the measurement of bulk density depend on particle size distribution that increases when the size of particles is small (Niyigena et al., 2018). Further, they reported that large particles are difficult to rearrange, which increases the number of empty spaces, leading to a lower density. This study recorded a similar observation that the hemp hurd used was easy to rearrange due to its average small size (2.36 to 4.75 mm), which reduces the empty spaces, leading to a higher density.

The dry density of hemp hurd recorded after oven-drying was 105 kg/m$^3$. Equation (2) was used to calculate moisture content, where *m1* is the original mass of the hemp hurd in the container (in kg) before oven-drying, and *m2* is mass of the same hemp hurd in the container (in kg) measured after oven-drying.

$$Moisture\ content\ (\%) = \frac{m1-m2}{m1} x\ 100 \quad \ldots\ldots\ldots\ldots\ldots\ldots\ldots\ldots\ldots\ldots\ldots\ldots\ldots\ldots\ (2)$$

As anticipated, moisture content reduced after oven-drying to approximately 8.4%. Table 10 shows that the calculated moisture content of 8.4% is slightly lower compared to the moisture contents of other studies that range between 10% and 13.3%. A possible explanation can be found in the storing conditions (See Table 10). For instance, in this study, the hurd was stored in a space that has approximately 15% lower RH compared to the RH reported in other studies. Other reasons could include fiber content and particle sizes. In this regard, Niyigena et al. (2018) reported that the fibers are non-absorbed or inert in water. Therefore, hemp hurds containing fewer fibers have more moisture content. Visual inspection of the hemp hurd used in this study showed a significant amount of fiber.

Table 10: Comparison of moisture content in hemp hurd

| Literature | Moisture content (%) | Storage conditions |
|---|---|---|
| Current study | 8.4 | 20–25 ºC and RH 35–45% |
| Garnier (2000) | 10–12 | 20–21 ºC and RH 50–60% |
| Gourlay (2008) | 11 | 20 ºC and RH 50–60% |
| De Bruijn et al. (2009) | 13.3 | - |

## 4.2.2 Particle Size Distribution

Hemp hurds should be graded according to particle size to allow consistency in hemp characterization. There are two methods for particle size distribution: (1) mechanical sieve analysis (Amziane et al., 2017; Dinh, 2014; Pinkos, 2011), and (2) image analysis (Page et al., 2017; Amziane et al., 2017; Nguyen et al., 2009; Williams et al., 2018). According to the literature, it is difficult to detect small particles and fibers in the image analysis, hence hindering the results (Nozahic et al., 2012; Dinh, 2014). Because the hemp hurd used in this study had a lot of fiber (~40%) in its constituents, the mechanical sieve analysis was performed using batches of 100g and 200g for grading. Table 11 summarizes the results of the mechanical sieving test by showing the mass of raw hemp hurds retained on each sieve. As presented, no. 8 sieve (2.36 mm sieve opening) retained 55.95 g hemp particles out of 100-g sample size, and 107.81g hemp particles out of a 200-g sample size. These results suggest that more than 50% of hemp particles are larger than 2.36 mm in length and width.

Furthermore, Table 12 presents the average percentage of raw hemp materials passing through different sieve grades. Most hemp particles, more than 99%, pass through 19 mm, 16 mm, 12.5 mm, and 9.5 mm sieves. Also, the passing percentage decreases with the 2.36-mm sieve: approximately 88% of 100 g samples and 77.55% of 200 g samples pass through it.

Table 11: Mass of hemp hurds retained in each sieve

| SL No. | Mesh | Sieve Grade (mm) | Retained mass (g) Sample size 100 g | Retained mass (g) Sample size 200 g |
|---|---|---|---|---|
| 1 | ¾ in | 19 | 0.16 | 0.05 |
| 2 | 5/8 in | 16 | 0.15 | 0.04 |
| 3 | ½ in | 12.5 | 0.33 | 0.69 |
| 4 | 3/8 in | 9.5 | 1.03 | 1.96 |
| 5 | ¼ in | 6.3 | 4.87 | 12.59 |
| 6 | No. 4 | 4.75 | 9.82 | 11.83 |
| 7 | No. 8 | 2.36 | 55.95 | 107.81 |
| 8 | - | Bottom pan | 28.07 | 65.74 |
| Total | | | 100.36 | 200.71 |

Fiber contents of hemp particles prevented the hurd from passing through the fine-opening sieves. Therefore, the passing percentage through the small opening (i.e., 2.36 mm, 4.75 mm) is higher for the 100-g sample size as it contains less fiber than the 200-g sample size. Figure 10 illustrates the particle size distribution curves of the hemp hurd. The particle size distribution of the hurds developed by mechanical sieving is between 2.36 and 6.3 mm. Moreover, the hemp hurd used in this study has a grading that is comparable to the range used in the literature. For example, the particle size distribution of hemp hurd produced by mechanical sieving ranged between 0.5 and 5 mm (Page et al., 2017), and also between 0.4 and 5 mm (Dinh, 2014).

Table 12: Proportion (%) of hemp hurd passing through a sieve

| Mesh | Sieve Grade (mm) | Average (%) of materials passing | |
|---|---|---|---|
| | | Sample size 100 g | Sample size 200 g |
| 1 in | 25 | 100.00 | 100.00 |
| ¾ in | 19 | 99.97 | 99.99 |
| 5/8 in | 16 | 99.95 | 99.99 |
| ½ in | 12.5 | 99.90 | 99.87 |
| 3/8 in | 9.5 | 99.72 | 99.54 |
| ¼ in | 6.3 | 98.92 | 97.45 |
| No. 4 | 4.75 | 97.28 | 95.48 |
| No. 8 | 2.36 | 87.98 | 77.55 |

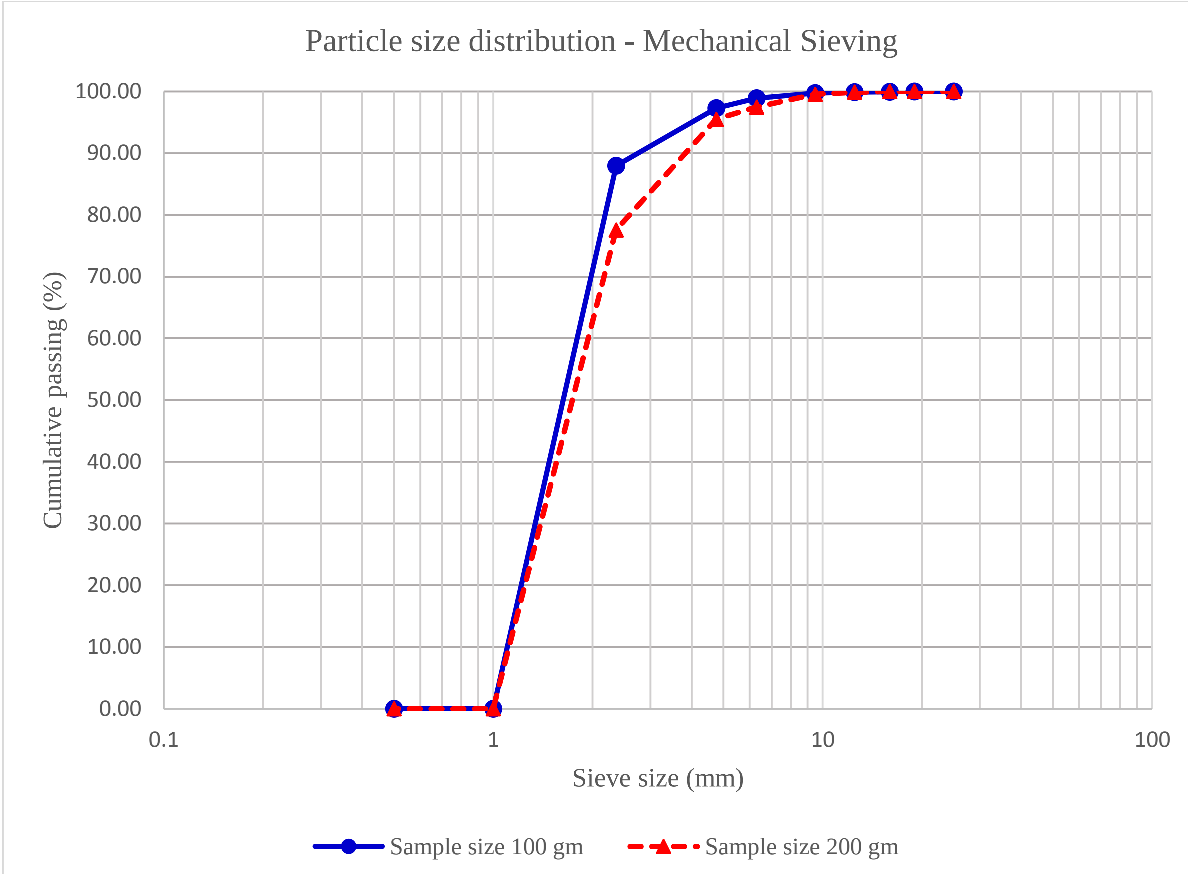


Figure 10: Particle size distribution curves of raw hemp hurd

## 4.3 Density of Hempcrete Samples

The targeted final density for hempcrete infill "wall" application was between 300 kg/m$^3$ and 350 kg/m$^3$, focusing on the maximization of hemp hurd ratio within the hempcrete mixture to improve its thermal properties. Therefore, the wet density of the hempcrete samples ranged from approximately 450 kg/m$^3$ to 600 kg/m$^3$. Table 13 summarizes the dry densities of different hempcrete samples recorded on the testing day, and Figure 11 compares their average dry densities. The densities of hempcrete samples produced in this study show excellent consistency with a standard deviation of less than 6. In this regard, the average density of all samples is 306.13 kg/m$^3$ with an accuracy ±5%. The dry densities of all the produced samples range between 298.55 kg/m$^3$ and 318.05 kg/m$^3$, with most densities falling between 300 kg/m$^3$ and 310 kg/m$^3$. The lowest average density has an LMK70 sample, and the highest has an LMK10 sample. The differences in the samples' density are mainly due to the variation in the compaction level.

Table 13: Dry density of samples on the day of thermal conductivity testing

| Design mix | Water (kg) | Dry density (kg/m$^3$) | | |
|---|---|---|---|---|
| | | Batch 1 | Batch 2 | Batch 3 |
| LMK70 | 3 | - | 298.55 | 300.84 |
| LMK70B | 2.5 | 301.58 | - | - |
| LMK50 | 3 | - | 302.57 | 301.90 |
| LMK50B | 2.5 | 303.85 | - | - |
| LMK20 | 3 | - | 305.36 | 304.52 |
| LMK20B | 2.5 | 307.85 | - | - |
| LMK10 | 2.6 | 318.05 | 316.03 | 312.45 |

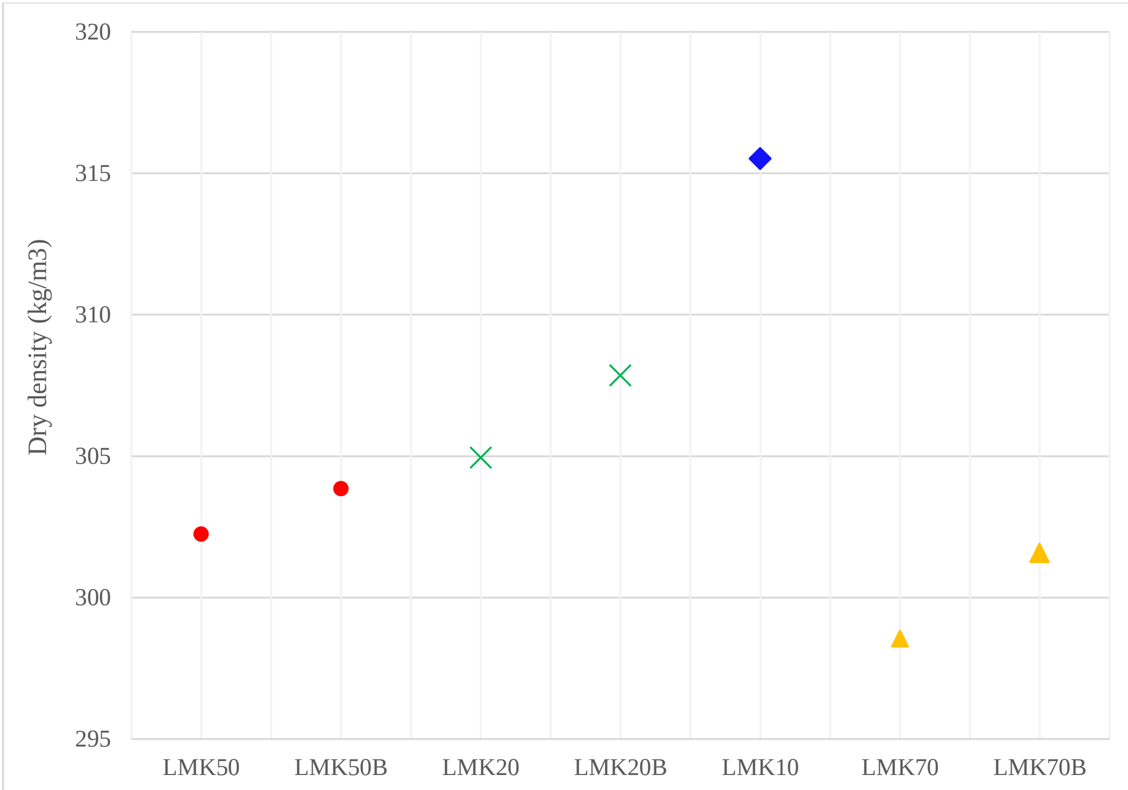


Figure 11: Average density of samples prepared for the thermal conductivity test

Moreover, the hempcrete samples produced in this study for wall applications have densities comparable to the literature presented in Table 14, which shows that the dry density of the "wall" hempcrete ranges from 250 kg/m³ to 550 kg/m³. Thus, Sutton et al. (2011) reported the lowest hempcrete density for wall application of 270 kg/m$^3$ and the highest density of 330 kg/m$^3$. Similarly, Shea et al. (2012) reported the lowest density of 275 kg/m$^3$ for the hempcrete wall produced using hemp hurd to binder ratio 1:1.5. Furthermore, Cérézo (2005) reported the lowest hempcrete density of 275 kg/m$^3$ and the highest density of 440 kg/m$^3$ for wall application, developed using hemp to binder ratio 1:1.5 and 1:2, respectively.

Table 14: Literature densities of hempcrete for wall application

| Author(s) | Dry density (kg/m$^3$) |
|---|---|
| Shea et al. (2012) | 275 |
| Sutton et al. (2011) | 270–330 |
| Cérézo (2005) | 275–440 |
| Amziane and Arnaud (2013) | 317–430 |
| Arnaud and Gourlay (2012) | 250 |
| Evrard (2008) | 440±20 |
| Abbott (2014) | 275 |
| Bevan and Woolley (2008) | 300–400 |
| Tran Le et al. (2010) | 413 |
| Dinh (2014) | 375–550 |
| Dhakal et al. (2017) | 233–387.8 |
| Collet and Pretot (2014) | 381 |
| Collet et al. (2013) | 430 |
| Ahlberg et al. (2014) | 220–330 |
| Sinka et al. (2018) | 210–490 |
| Pinkos (2014) | 418 |

## 4.4 Thermal Conductivity

ASTM C1045-19/ASTM C518-15 standard provides the method for testing the thermal conductivity as a function of temperature for a hempcrete sample from data taken at specified temperature differences. In this regard, Table 15 summarizes the thermal conductivity results of the hempcrete samples for all design mixes measured at different temperatures using the heat flow meter. As presented, the thermal conductivity range between 0.075 W/mK and 0.094 W/mK for the mean temperature range of 7.35-52.3 ºC. These results are comparable to the previous studies. For example, Amziane and Arnaud (2013) reported the thermal conductivity of hempcrete samples tested using guarded hot boxes at temperatures between 5 ºC and 20 ºC between 0.064 W/mK and 0.09 W/mK for densities of 220 kg/$m^3$ to 450 kg/$m^3$. Additionally, Evrard (2008) reported the thermal conductivity of hempcrete 0.115±0.006 W/mK tested by developing a temperature gradient of 10 ºC using three different mean temperatures: 18±0.2 ºC, 26±0.2 ºC, and 34±0.3 ºC. Table 15 and Figure 12 also show that the average thermal conductivity of all the samples is between 0.081 W/mK and 0.089 W/mK. The calculated standard deviation of 0.004–0.007 shows consistency in the results.

Table 15: Thermal conductivity test results of design mixes along with water content, and dry density of the samples.

| Design mix | Water (kg) | Dry density ($kg/m^3$) | Thermal conductivity (W/mK) Mean temperature Lowest –7.35 ºC | Middle 22.45 ºC | Highest 52.3 ºC | Avg. | SD |
|---|---|---|---|---|---|---|---|
| LMK70 | 3 | 300.84 | 0.0776 | 0.0836 | 0.0877 | 0.0827 | 0.005 |
| | | 298.55 | 0.0756 | 0.0826 | 0.0876 | 0.0816 | 0.006 |
| LMK70B | 2.5 | 301.58 | 0.0772 | 0.0821 | 0.0891 | 0.0831 | 0.006 |
| LMK50 | 3 | 302.57 | 0.0802 | 0.0862 | 0.0902 | 0.0852 | 0.005 |
| | | 301.90 | 0.0788 | 0.0838 | 0.0908 | 0.0848 | 0.006 |
| LMK50B | 2.5 | 303.85 | 0.0809 | 0.0853 | 0.0919 | 0.0864 | 0.0055 |
| LMK20 | 3 | 305.36 | 0.0813 | 0.0865 | 0.0933 | 0.0873 | 0.006 |
| | | 304.52 | 0.0805 | 0.0861 | 0.0935 | 0.0870 | 0.0065 |
| LMK20B | 2.5 | 307.85 | 0.0806 | 0.0866 | 0.0946 | 0.0876 | 0.007 |
| LMK10 | 2.6 | 318.05 | 0.0854 | 0.0887 | 0.0944 | 0.0899 | 0.0045 |
| | | 316.03 | 0.0839 | 0.0869 | 0.0919 | 0.0879 | 0.004 |
| | | 312.45 | 0.0817 | 0.0887 | 0.0937 | 0.0877 | 0.006 |

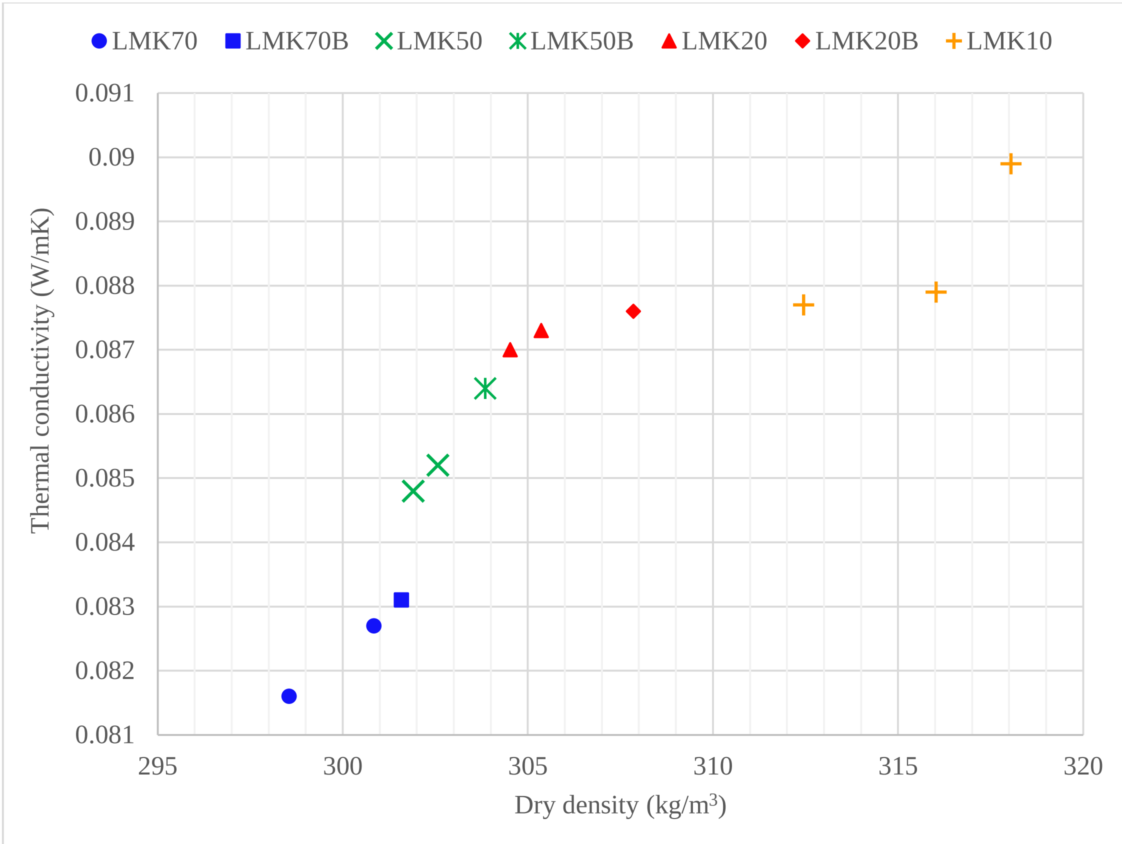


Figure 12: Thermal conductivity for different densities of hempcrete

Furthermore, the experimental results showed that thermal conductivity is a function of the density of hempcrete. Thus, the lowest density hempcrete of 298.55 kg/m$^3$ has the lowest thermal conductivity of 0.075 W/mK. In contrast, the highest density hempcrete of 318.05 kg/m$^3$ has the highest thermal conductivity of 0.094 W/mK. These findings are consistent with the previous studies presented in Table 16. For example, Arnaud and Gourlay (2012) reported thermal conductivity of 0.06 to 0.12 W/mK for density between 250 and 660 kg/m$^3$, respectively. Also, Sassoni et al. (2014) developed hempcrete samples that have the lowest thermal conductivity of 0.078 to the highest of 0.138 W/mK for densities between 330 and 640 kg/m$^3$. Dhakal et al. (2017) produced three hempcrete densities of 233, 317, and 388 kg/m$^3$ that have a linear relationship with the thermal conductivity of between 0.074 and 0.103 W/mK. Thus, with a density increase of 36% (317 kg/m$^3$) and 67% (388 kg/m$^3$), the thermal conductivity of hempcrete increased by 18.32% and 38.12%, respectively.

Table 16: Reference experimental value of thermal conductivity in literature

| Author(s) | Thermal conductivity (W/mK) | Dry density (kg/m$^3$) |
|---|---|---|
| Amziane and Arnaud (2013) | 0.082–0.105 | 317–430 |
| Arnaud and Gourlay (2012) | 0.06–0.12 | 250–660 |
| Dinh (2014) | 0.08–0.106 | 375–550 |
| Dhakal et al. (2017) | 0.074–0.103 | 233–387.8 |
| Bevan and Woolley (2008) | 0.05–0.12 | 300–400 |
| Abbot (2014) | 0.06 | 275 |
| Shea et al. (2012) | 0.06–0.09 | 275 |
| Page et al. (2017) | 0.057–0.086 | 245–400 |
| Bedliva and Isaacs (2014) | 0.065 | 275 |
| Tran Le et al. (2010) | 0.10 | 413 |
| Walker and Pavia (2014) | 0.117–0.138 | 531–627 |
| Collet and Pretot (2014) | 0.13 | 381 |
| Evrard (2008) | 0.115±0.006 | 440±20 |

The percentage of mineral pozzolan (i.e. metakaolin) has a significantly lower impact on the thermal conductivity of hempcrete compared to the density. For example, the average thermal conductivity of hempcrete in this study ranged from 0.081 W/mK to 0.089 W/mK. These findings are expected considering, on the one hand, similar thermal conductivities of the binder constituencies between 0.35 W/mK and 1.0 W/mK (Dinh, 2014), and on the other hand, the same binder to hemp ratio of the samples. Furthermore, other studies also reported similar findings. For instance, Amziane & Arnaud (2013) showed that the partial substitution of the Portland cement by metakaolin has no effect on its thermal conductivity. Moreover, Dinh (2014) suggests that the thermal conductivity of the hempcrete samples directly depends on dry density, and indirectly depends on binder nature. Similarly, Walker and Pavia (2014) produced six types of hempcrete using the commercial binder, lime binder, and metakaolin of different compositions. Their study reported a relationship between thermal conductivity and density without any significant effect of binder type.

Nevertheless, it should be mentioned that an increase in the binder content increases the thermal conductivity of the hempcrete. In this regard, studies that applied higher binder amounts reported higher thermal conductivities of the hempcrete samples. For example, Cérézo (2005) reported the thermal conductivities of 0.13 W/mK and 0.14 W/mK for hemp to binder ratios of 1:3 and 1:4, respectively.

## 4.5 Hygrothermal Performance of the Base and Multilayer Wall Assemblies

According to the DIN 4108 – 4E, WUFI® manual, and literature (Dhakal, 2016; Evrard, 2008), after several years of use, the construction should reach dynamic equilibrium, that is, similar sequences of hygrothermal conditions repeat, and the long-term water content does not change annually. If the moisture content decreases below the initial conditions, the wall assembly dries out. On the other hand, an increase in the moisture content over several years, and long-term high moisture levels may lead to the occurrence of mould, corrosion, frost damage, rotting, and increased heat losses. Because the water content depends on the thickness of the wall assembly and the layer materials, the comparison of the numerical values of the water content, and in particular, between different material types, is less relevant than long-term trends of the total water content. Furthermore, according to WUFI manual, DIN 4108 – 4E and the literature (Viitanen, 2003; Marceau et al., 2017), a component is susceptible to mold growth when relative humidity (RH) exceeds 80% (DIN 4108 – 4E, 1991). Therefore, if the RH is between 80% and 95%, the element is susceptible to mold growth, and when RH exceeds 95%, there is a danger of decay (Viitanen, 2003). In addition to high relative humidity, mold growing also requires warm temperatures, typically between 22 ºC and 35 ºC (Baughman & Arens, 1996).

Thus the impact of the water content, relative humidity, and temperature were analyzed for condensation and mold growth risks in two wall assemblies, the base wall, and the multi-layer wall (see Figure 9). Furthermore, the heat flow distributions for both wall assemblies were analyzed and discussed.

### 4.5.1 Moisture Accumulation Risks of Base and Multilayer Wall Assemblies

Figure 13 presents the average water content ($kg/m^3$) distributions of the base and multi-layer walls for four scenarios (see Table 8) from 1st June 2014 to 31st May 2019. Additionally, Table 17 summarizes the average water content in mass percent of the base and multilayer walls at the beginning and end of the simulation period.

Overall, on average, the base wall has 36% to 54% higher water content than the multilayer wall throughout the simulation period. Furthermore, the water content of the base wall ranges from 28.44 $kg/m^3$ under scenario II to 29.08 $kg/m^3$ under scenario III in 2014 and from 25.81 under scenario IV $kg/m^3$ to 30.34 $kg/m^3$ under scenario I in 2019. The water content of the multilayer wall ranges from 16.63 $kg/m^3$ under scenario II to 18.34 $kg/m^3$ under scenario III in 2014 and from 11.64 $kg/m^3$ under the scenario II to 16.86 $kg/m^3$ under the scenario III in 2019. The possible explanation for the lower water content of the multi-layer wall is its thinner layer of hempcrete infill compared to the base wall and addition of insulation layer that has a significantly lower initial water content (i.e., 0.82 $kg/m^3$) that the hempcrete (i.e., 29 $kg/m^3$).

For both wall cases, the water content decreases over time under scenarios II and IV, indicating that the assemblies dry out. At the end of the simulation period, the base wall performs the best under scenario IV and the multilayer wall under scenario II. Furthermore, the average water contents in the mass percent presented in Table 17 show that the calculated values of both wall assemblies are considerably below the practiced standard of 20 mass-percent (DIN 4108 – 4E, 1991; Dhakal, 2016). Therefore, there is no moisture accumulation in the wall assemblies under scenarios II and IV over the simulated five-year period. Table 17 also shows that the average water contents in the mass-percent of both wall assemblies under all four cases are significantly below the 20 mass-percent (DIN 4108 – 4E, 1991; Dhakal, 2016).

However, under scenarios I and III, the total average annual water content of the base wall increases, and in particular, under the scenario I in 2019, suggesting that the assembly is not drying out through time. On the other hand, the total average annual water content of the multilayer wall is gradually declining over the five years under scenarios I and III. Nevertheless, this drop in water content is not as significant as under scenarios II and IV. At the end of the simulation period, the base and multilayer wall assemblies perform the worst under cases I and III. The likely reason for all these findings is 10% lower indoor RH and 3.5 ºC to 5 ºC higher indoor air temperatures of II and IV scenarios than the average indoor RH and air temperature of cases I and III (see Table 8).

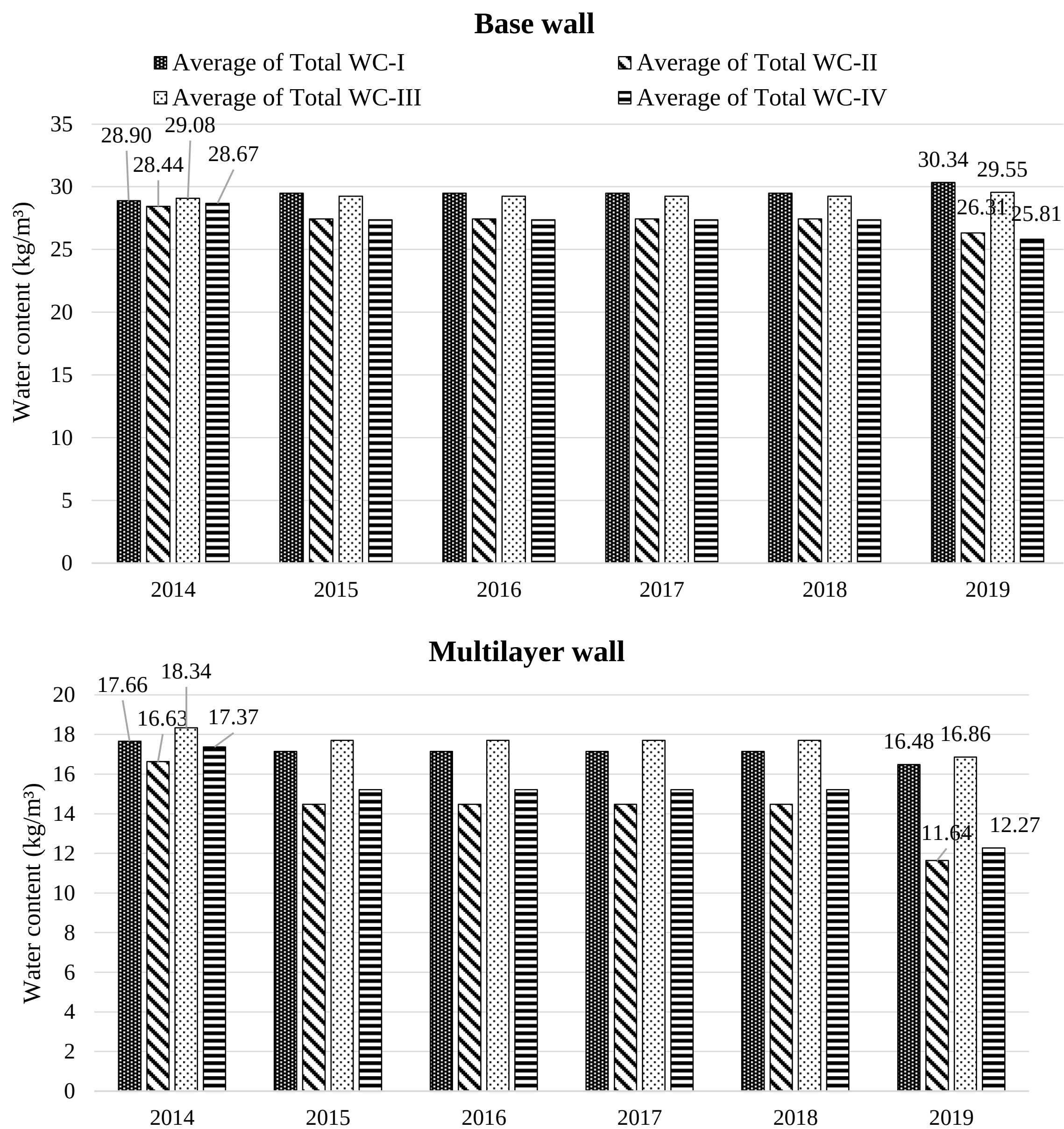


Figure 13: Average yearly water content distributions of the base wall and multilayer wall

Table 17: Average water content in the mass percent of the base and multilayer walls at the beginning and end of the simulation

| *Scenario* | **Base wall** | | **Multilayer wall** | |
|---|---|---|---|---|
| | **2014** | **2019** | **2014** | **2019** |
| | *M% - Total* | *M% - Total* | *M% - Total* | *M% - Total* |
| I | 0.8252 | 0.8664 | 0.4877 | 0.4551 |
| II | 0.8121 | 0.7513 | 0.4593 | 0.3215 |
| III | 0.8304 | 0.8438 | 0.5065 | 0.4656 |
| IV | 0.8187 | 0.7370 | 0.4797 | 0.3389 |

All these findings suggest that indoor environmental conditions, including RH and indoor air temperature, play a more critical role in the drying behavior of the base wall assembly than outdoor conditions. In particular, elevated average indoor RH has a hindering impact on drying of the base wall throughout time. For instance, although scenarios II and IV have a 10% higher maximum RH than scenarios I and III, due to their 10% lower average RH, the wall assembly performs better under cases II and IV, than under scenarios I and III.

The water content for the base hempcrete wall observed in this study is comparable to that in literature. For example, Dhakal (2016) developed a numerical modeling wall of 335 mm that reported the wall was sufficiently drying, with total water content ranging from 7.78 kg/m$^3$ to 17.57 kg/m$^3$ at the end of three years. Evrard (2008) numerically developed a hempcrete wall of 335 mm combined with a 300 mm hempcrete section and reported that water content ranged from 9.5 kg/m$^3$ to 17.6 kg/m$^3$ after 36 months.

Figure 14 presents the average monthly water content distributions of the base and multi-layer walls for four scenarios (see Table 8) from 1st June 2014 to 31st May 2019. It can be observed that the water content of both walls exhibits regular seasonal cycles under all four cases. Furthermore, the monthly average water content profiles have similar trending for both wall assemblies. For instance, both walls have maximum water content under scenarios III and IV in August and the lowest water content under scenarios II and IV in February. Also, both walls experience the most significant variations in the water content under scenarios IV and II, whereas the smallest under the scenario I, which, has the highest monthly average values of the water content for both walls. On the other hand, the monthly average water content results suggest that both walls perform the best under scenario II, which has the lowest average maximum throughout the simulation period.

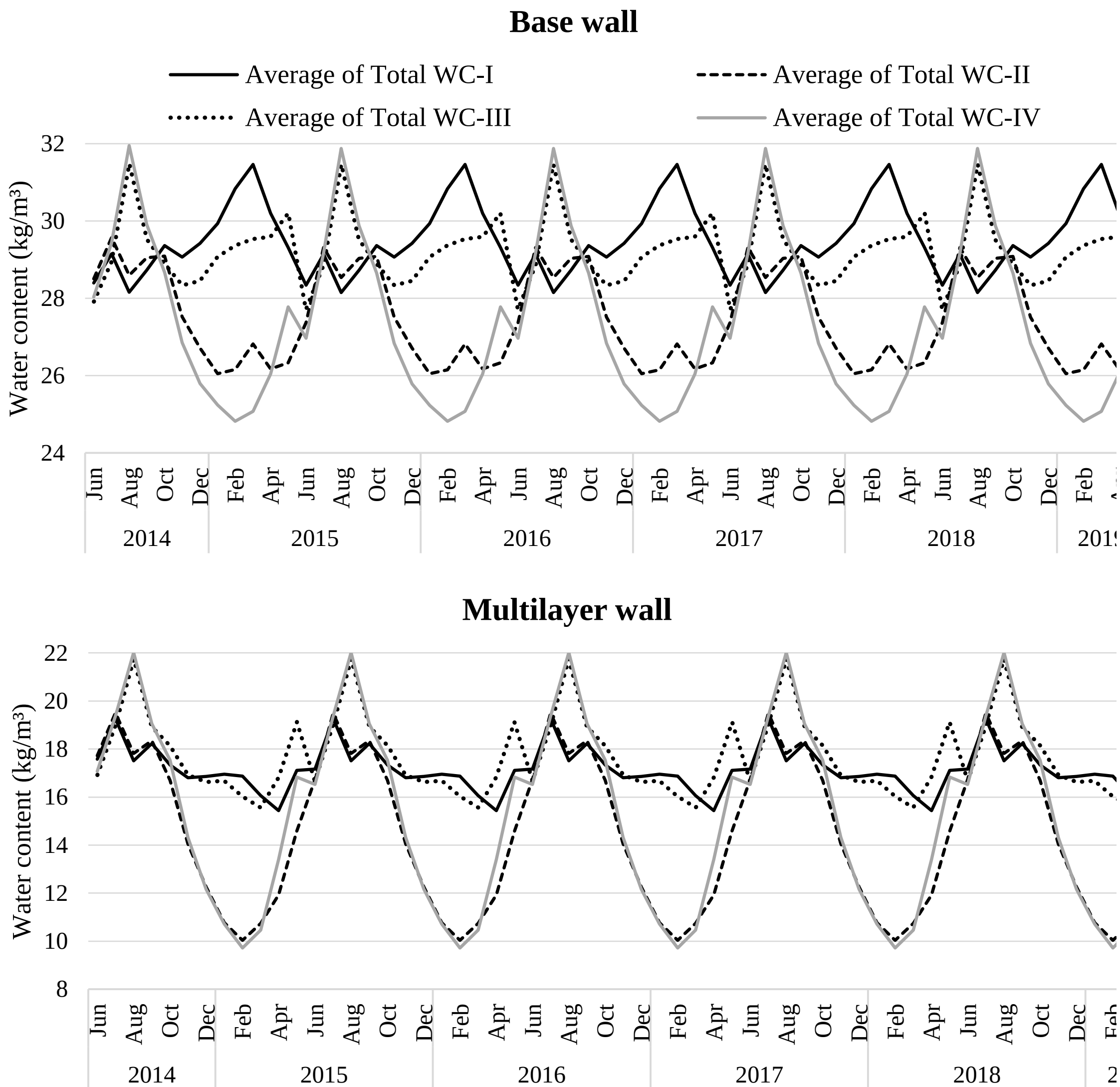


Figure 14: Average monthly water content distributions for the base and multilayer walls

Figure 15 presents the monthly average water contents of all three layers of the base wall, including exterior lime plaster, hempcrete infill, and interior plaster (see Figure 9) from 1st June 2014 to 31st May 2019. Furthermore, Figure 16 illustrates the monthly average water contents of all four layers of the multilayer wall, including exterior lime plaster, Rockwool insulation, hempcrete infill, and interior plaster (see Figure 9) from 1st June 2014 to 31st May 2019. The results suggest that outdoor and indoor conditions have a significant impact on the hygrothermal performance of the wall and especially on the layers with direct contact, including external and internal, respectively. In this regard, the outer layers of both wall assemblies had similar average monthly water content profiles among the scenarios with the same outdoor conditions. Thus, the external plaster layers of the base and multilayer walls have the highest average water content ranging between 37 kg/m$^3$ and 67 kg/m$^3$ under scenarios I and II, and between 26 kg/m$^3$ and 108 kg/m$^3$ under scenarios III and IV. Due to the lower relative humidity and higher air temperatures of the indoor compared to the outdoor environment, the inner layers of the base and multilayer walls have more moderate water contents compared to the outer layers. Therefore, the average monthly water content of the inner layer of the base wall and multilayer wall range from 19 kg/m$^3$ to 23 kg/m$^3$ under scenarios I and III, and from 9 kg/m$^3$ to 26 kg/m$^3$ under scenarios II and IV. The layers in-between the external and internal lime plasters, including the hempcrete infill and Rockwool insulation, are impacted by the position within the wall and layers in direct contact. For example, the average monthly water content profiles of the hempcrete infill of the base wall had similar patterns among scenarios with the same indoor conditions (i.e., I and III) and among those with the same outdoor conditions (i.e., II and IV). The overlapping of the average water content of the hempcrete layer between the scenarios is even higher for the multilayer wall, and the likely reason is the existence of the Rockwool insulation layer. The average water content of the insulation ranges only between 0.5 kg/m$^3$ and 1.1 kg/m$^3$ due to the considerably lower initial water content of 0.82 kg/m$^3$ compared to the lime plaster and hempcrete of 30 kg/m$^3$ and 29 kg/m$^3$, respectively. Furthermore, similarly to the exterior lime plaster layer, the monthly average water content profiles of the Rockwool insulation have similar patterns among scenarios with the same outdoor environment (i.e., III and IV) and those with the same indoor conditions (i.e., I and III).

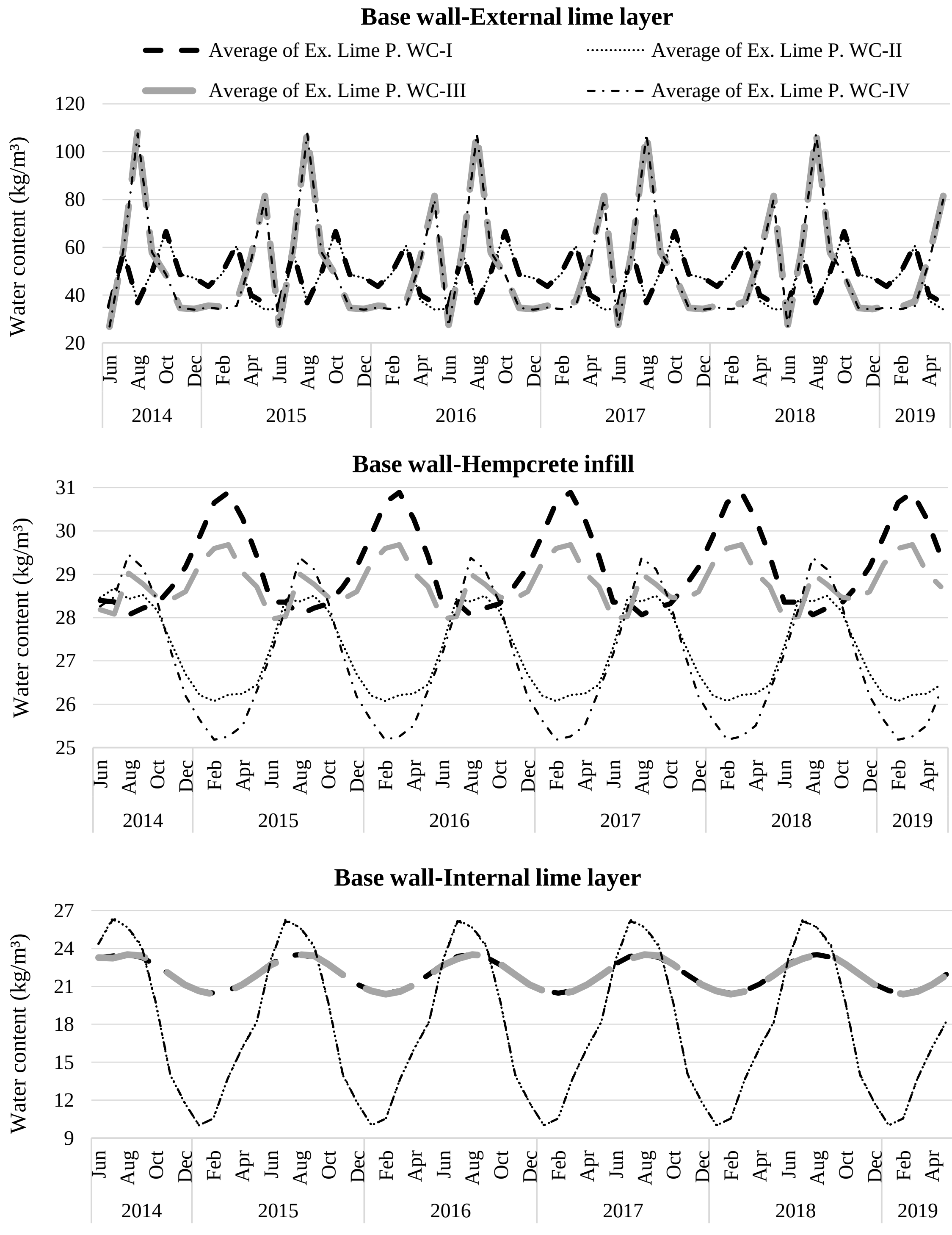

Figure 15: Average monthly water content distributions for each material of the base wall

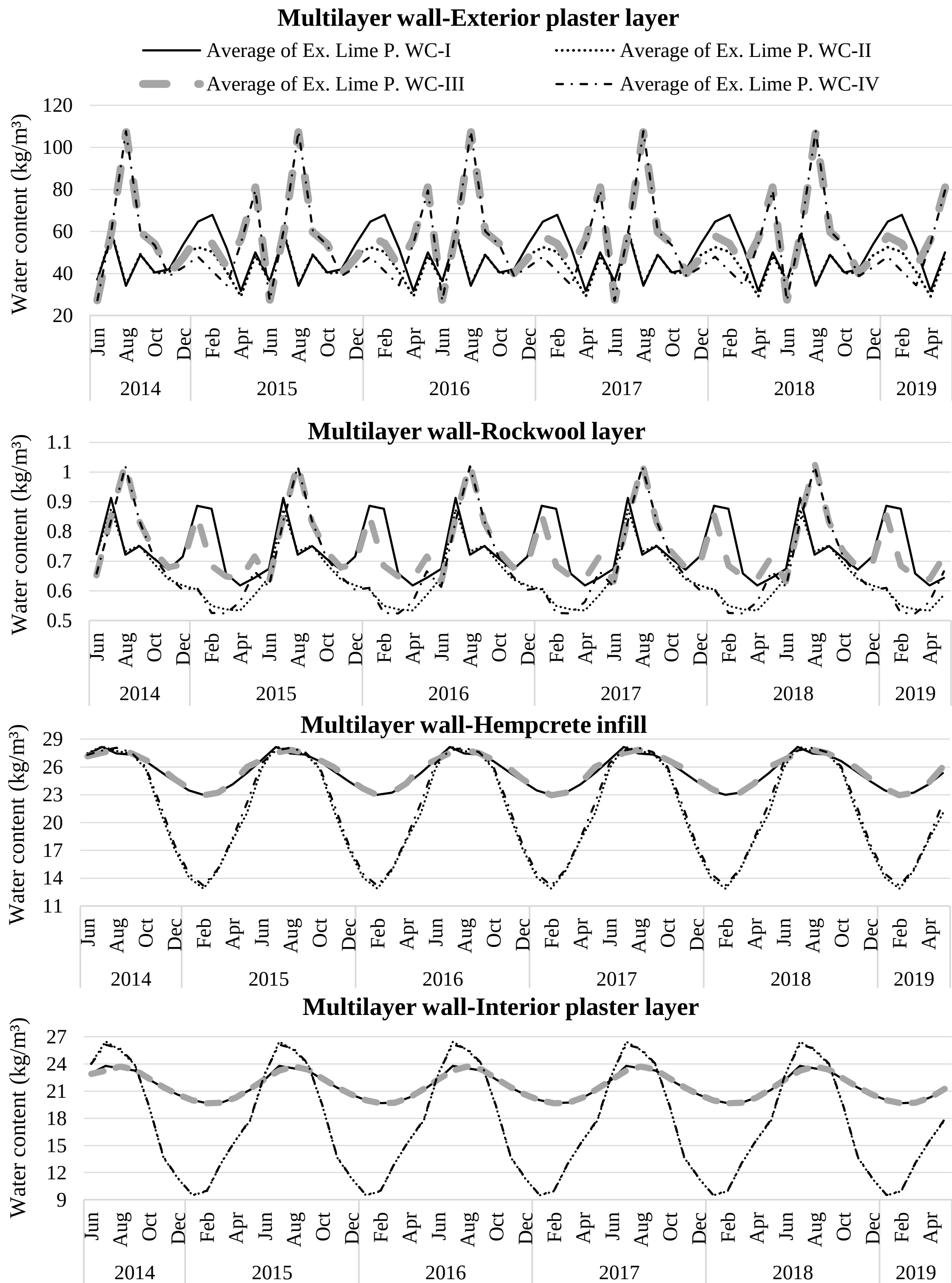


Figure 16: Average monthly water content distributions for each material of the multi-layer wall

Moreover, Table 18 compares the average, minimum, and maximum water contents in the mass percent of each layer of the base wall at the beginning and end of the simulation. Additionally, Table 19 presents the average, minimum, and maximum water contents in the mass percent of each material of the multilayer wall in 2014 and 2019. Overall, the results suggest that the average water contents in mass percent of all layers of the base and multilayer walls are significantly below the practiced standard of 20 mass-percent (DIN 4108 – 4E, 1991; Dhakal, 2016). Furthermore, the maximum water contents in mass percent of all layers are also within the prescribed limits ranging range from 1.394 $kg/m^3$ - 15.705 $kg/m^3$ for the base wall and from 0.731 $kg/m^3$ to 15.741 $kg/m^3$ for the multilayer wall. Nevertheless, under scenarios I and II, there is an increase in the average water contents in mass percent of the hempcrete layer of the base wall. These results are expected considering the increase in the water content in mass percent of the total wall assembly presented in Table 17. Furthermore, under scenario III, there is an increase in the average water contents in mass percent of the external lime plaster layer of the multilayer wall. The explanation of these results is the severe outdoor moisture conditions of ASHRAE Year 1 (see Table 8).

Table 18: Average, minimum, and maximum water contents in the mass percent of each material of the base wall at the beginning and end of the simulation

| Base wall materials | | 2014 | | | | 2019 | | | |
|---|---|---|---|---|---|---|---|---|---|
| | | ***I*** | ***II*** | ***III*** | ***IV*** | ***I*** | ***II*** | ***III*** | ***IV*** |
| ***External lime plaster (M%)*** | *Average* | 3.058 | 3.060 | 3.311 | 3.307 | 2.888 | 2.805 | 3.079 | 2.991 |
| | *Minimum* | 1.167 | 1.166 | 0.965 | 0.964 | 1.343 | 1.261 | 0.986 | 0.925 |
| | *Maximum* | 15.596 | 15.96 | 15.704 | 15.705 | 5.598 | 5.376 | 15.587 | 15.586 |
| ***Hempcrete infill (M%)*** | *Average* | 9.423 | 9.288 | 9.440 | 9.325 | 10.003 | 8.689 | 9.658 | 8.474 |
| | *Minimum* | 9.225 | 8.745 | 9.139 | 8.566 | 9.533 | 8.619 | 9.341 | 8.298 |
| | *Maximum* | 9.755 | 9.702 | 9.897 | 10.053 | 10.272 | 8.97. | 9.871 | 8.924 |
| ***Internal lime plaster (M%)*** | *Average* | 1.422 | 1.303 | 1.422 | 1.305 | 1.312 | 0.861 | 1.308 | 0.859 |
| | *Minimum* | 1.303 | 0.650 | 1.301 | 0.648 | 1.278 | 0.583 | 1.272 | 0.588 |
| | *Maximum* | 1.839 | 1.818 | 1.839 | 1.818 | 1.401 | 1.456 | 1.394 | 1.454 |

Table 19: Average, minimum, and maximum water contents in the mass percent of each material of the multilayer wall at the beginning and end of the simulation

| Multilayer wall materials | | 2014 | | | | 2019 | | | |
|---|---|---|---|---|---|---|---|---|---|
| | | ***I*** | ***II*** | ***III*** | ***IV*** | ***I*** | ***II*** | ***III*** | ***IV*** |
| ***External lime plaster (M%)*** | *Average* | 2.819 | 2.767 | 3.555 | 3.515 | 3.319 | 2.765 | 3.664 | 3.229 |
| | *Minimum* | 0.901 | 0.920 | 0.886 | 0.884 | 0.984 | 0.950 | 0.785 | 0.746 |
| | *Maximum* | 15.59 | 15.561 | 15.741 | 15.741 | 15.571 | 15.568 | 15.601 | 15.600 |
| ***Rockwool insulation (M%)*** | *Average* | 0.622 | 0.605 | 0.656 | 0.639 | 0.613 | 0.471 | 0.597 | 0.487 |
| | *Minimum* | 0.420 | 0.429 | 0.412 | 0.412 | 0.420 | 0.378 | 0.361 | 0.319 |
| | *Maximum* | 1.143 | 1.067 | 2.067 | 2.092 | 1.261 | 0.731 | 1.227 | 0.983 |
| ***Hempcrete infill (M%)*** | *Average* | 8.444 | 8.285 | 8.868 | 8.344 | 7.897 | 5.374 | 7.957 | 5.519 |
| | *Minimum* | 7.924 | 5.166 | 7.917 | 5.189 | 7.546 | 4.166 | 7.510 | 4.225 |
| | *Maximum* | 9.599 | 9.596 | 9.599 | 9.599 | 8.831 | 7.937 | 8.868 | 8.232 |
| ***Internal lime plaster (M%)*** | *Average* | 1.410 | 1.288 | 1.408 | 1.289 | 1.262 | 0.826 | 1.263 | 0.829 |
| | *Minimum* | 1.264 | 0.619 | 1.269 | 0.622 | 1.225 | 0.551 | 1.223 | 0.553 |
| | *Maximum* | 1.839 | 1.818 | 1.839 | 1.818 | 1.363 | 1.423 | 1.368 | 1.440 |

### 4.5.2 Mold Risks of Base and Multilayer Wall Assemblies

Figure 17 shows hourly relative humidity (RH) values of the base and multilayer walls in the wall cavity under four scenarios during the simulation period, from 1st June 2014 to 31 May 2019. It can be seen that RH profiles of both walls have regular patterns of seasonal fluctuation that gradually decrease over time. This behavior particularly applies to the multilayer wall, which under all scenarios, has lower RH compared to the base wall. Additionally, most of the time, both walls experience RH values below the mold risk threshold of 80%. However, under scenario I, RH values of both walls, exceed 80% during the short period, and especially of the base wall. Furthermore, the base wall experiences higher variations in RH between the scenarios compared to the multilayer wall, and both walls have more significant changes in RH under scenarios II and IV than under I and III. These findings are expected, considering the insulation of multilayer wall and significantly higher fluctuations in RH, ranging from 20% to 70%, under scenarios II and IV than the changes in RH under I and III that range from 50% to 60% (see Table 8).

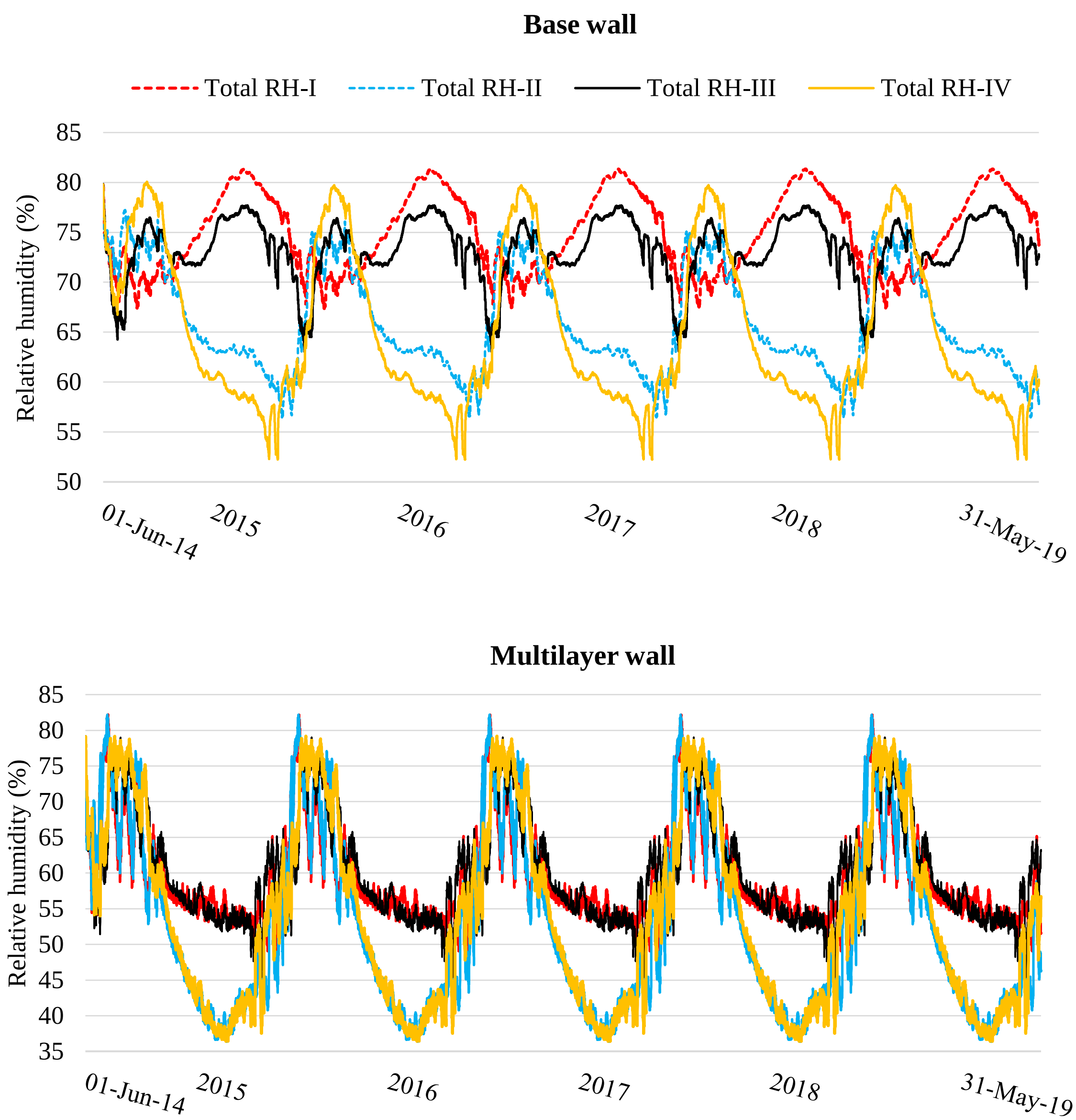


Figure 17: Hourly RH of base and multilayer walls under all scenarios

Figure 18 compares the percent frequency of the relative humidities (RH) of the base and multilayer walls under the four scenarios. These results confirm the previous finding that the multilayer wall has significantly lower RH compared to the base wall under all four scenarios over the five-year simulation period. In this regard, approximately 90-96% of the time, RH values of the multilayer wall are below the mold growth risk conditions (i.e., RH≥ 80%). These results further translate to only 0.86% to 2.05% of the time annually the multilayer wall being exposed to the mold risk conditions. Considering excellent moisture buffering features of hempcrete (Latif et al., 2015; Oumeziane et al., 2014), these findings suggest that it is unlikely that mold growth will occur in the hempcrete infill of the multi-layer wall under any of the investigated scenarios.

On the other hand, approximately 50-98% of the time, RH values of the base wall are below 80%. Similar to the previous results, the base wall performs better under scenarios II and IV than under scenarios I and III. Thus, under scenario II the base wall experiences only 2.1% of the time RH values above 80% over the five years, which translates to approximately 0.42% of the time annually. Although under scenario IV, the base wall is the longest time exposed to the low relative humidity (i.e., 34% below 65%), it has about 18% of the time RH values above 80% over the five years, which is approximately 3.65% of the time annually. The base wall performs the worst under I scenario, with about 48% of the time RH being above 80%, which is around 9.58% of the time annually. Similarly, under case III, the base wall experiences about 34% of the time RH above 80%, which is about 6.72% of the time annually.

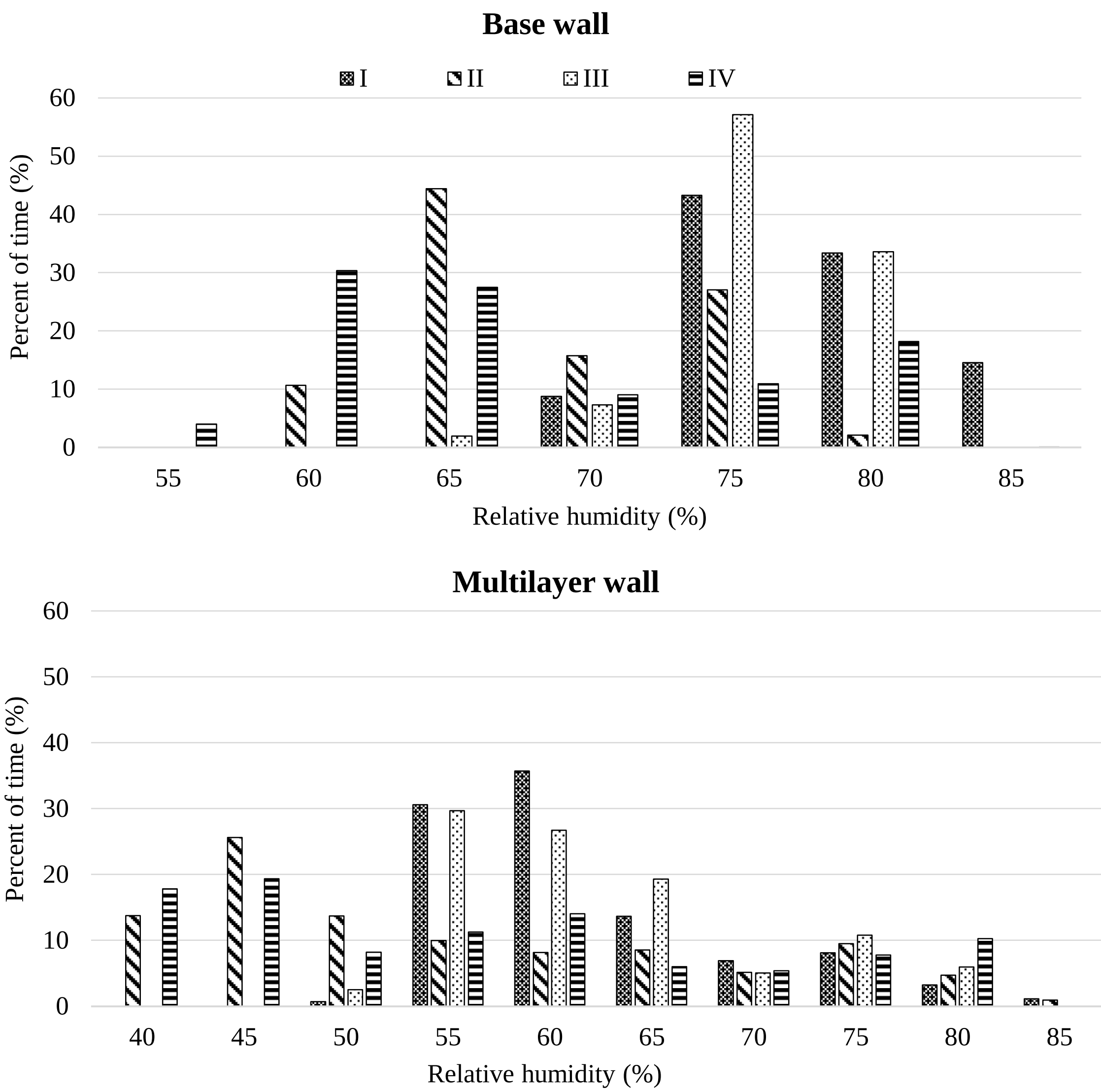


Figure 18: Percent frequency of RH of base and multilayer walls under four scenarios

Figure 19 compares the hourly RH of the hempcrete infills of the base and multilayer wall over the simulation period. Similarly to the entire assemblies, RH profiles of both hempcrete infills have regular patterns of seasonal fluctuation that gradually decrease over time, and especially in the case of the multilayer wall. Also, RH values of the hempcrete infill of the multilayer wall are below the mold growth threshold of 80% throughout the simulation under all cases. The same does not apply to the base wall, which exhibits RH values of above 80% under the scenario I.

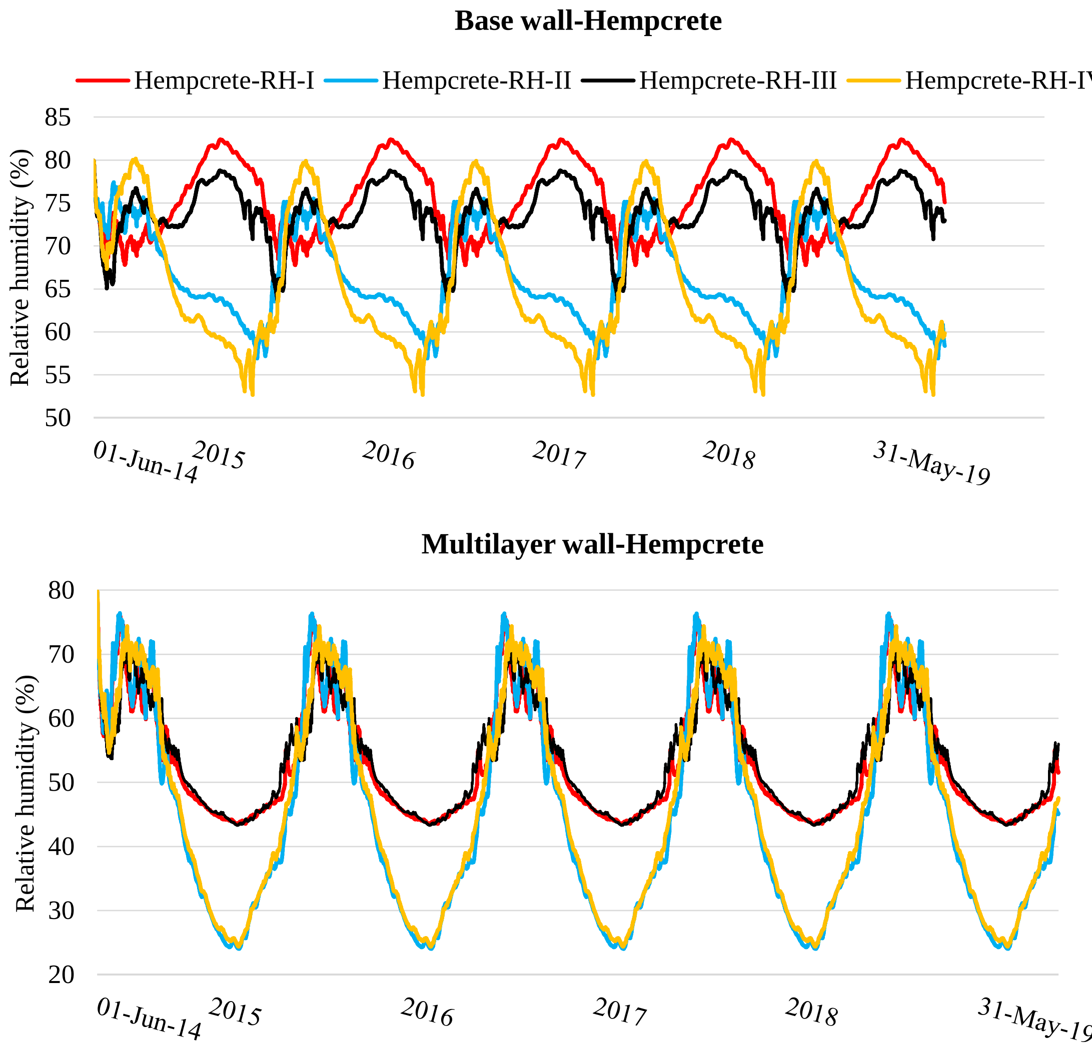


Figure 19: Hourly RH of the hempcrete infill of the base and multilayer walls under all scenarios

Figure 20 further compares the percent frequency of RH of the hempcrete infill of the base and multilayer walls under the four scenarios. Similar to the whole assembly, the hempcrete infill of the base wall is exposed significantly longer to higher RH compared to the hempcrete infill of the multilayer wall, and in particular, under scenarios I and III. Hence, about 49% and 38% of the time under scenarios I and III, respectively, the hempcrete infill of the base wall exhibits RH of 80% or higher. These results translate to about 10% and 8% of the time annually under the cases I and III, respectively. In contrast, only 2% of the time, RH of the hempcrete infill is above 80% under scenario II, which is approximately 0.46% of the time per year. Furthermore, RH of the hempcrete infill of the base wall is about 19% of the time (i.e., 4% annually) above 80% under scenario IV. These results suggest significantly higher risks of the mold growth in the hempcrete infill of the base wall under scenarios I and III. On the other hand, it substantially less likely that the mold will grow in the hempcrete infill of the base wall under the two other cases, and especially scenario II. The findings also suggest that the occurrence of mold is unlikely in the hempcrete infill of the multilayer wall.

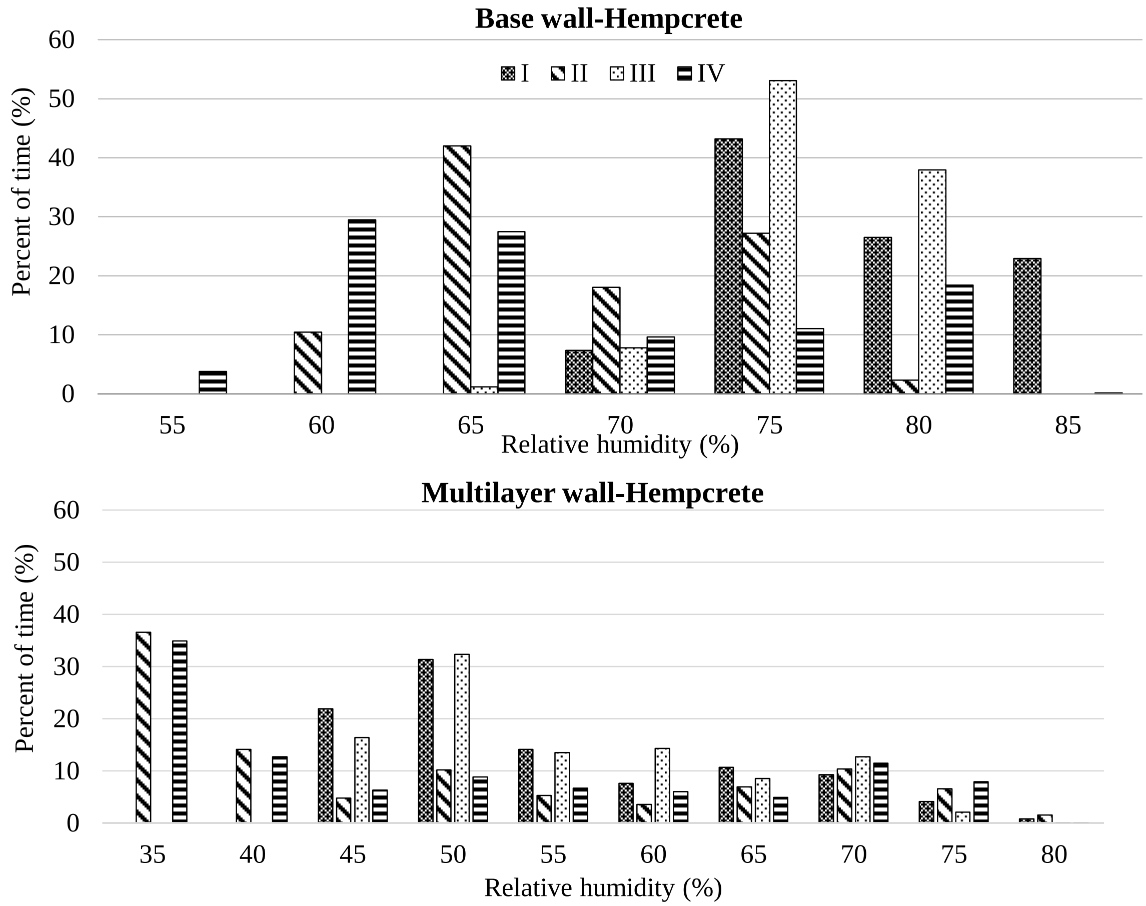


Figure 20: Percent frequency of RH of hempcrete infills of the base and multilayer walls under four scenarios

Figure 21 compares the percent frequency of temperature of the base and multilayer walls under the four scenarios. Overall, the multilayer wall is warmer under all situations compared to the base wall. Thus, the temperatures of the multilayer wall range between -2 °C to 30 °C and of the base wall they range from -4 °C to 26 °C. The explanation for these results is the addition of 10.5 cm of the insulation to the multilayer wall (see Figure 9). On the one hand, higher wall temperatures during the cold months will reduce the chance of freeze damage and provide a more comfortable indoor environment to the occupants. On the other hand, high wall temperatures during summer months, in combination with the high relative humidity, could cause mold growth and increased cooling needs.

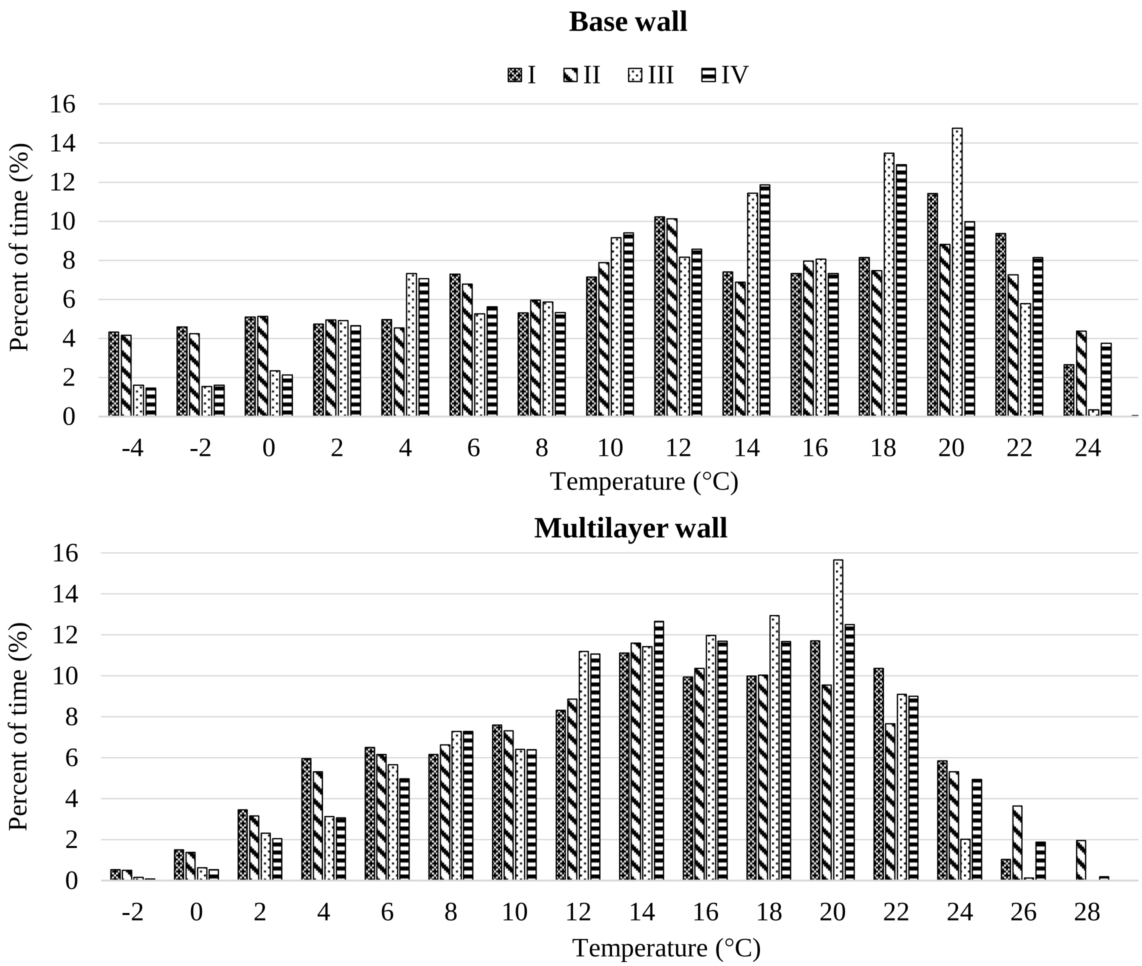


Figure 21: Percent frequency of temperature of the base and multilayer walls under four scenarios

Considering previous results about the wall temperature and RH, it is essential to understand when elevated temperatures and relative humidities occur throughout the year. In this regard, Figure 22 presents monthly average temperature and RH profiles of both wall assemblies during the simulation period under the four scenarios. Both wall assemblies experience higher average RH and temperature during the summer months under II and IV scenarios. Similar also occurs in the multilayer wall under I and III scenarios. Furthermore, both wall assemblies have somewhat higher average temperatures under scenarios II compared to other cases during the summer months. In contrast, the base wall exhibits higher average RH during the winter months and lower temperatures under I and III situations compared to the other two cases. Moreover, under I scenario, the average RH of the base wall exceeds 80% during the cold months. These results can be explained with a higher mean indoor air temperature of scenario II than those of cases I and III, as well as its higher outdoor summer temperatures than of scenarios III and IV (see Table 8).

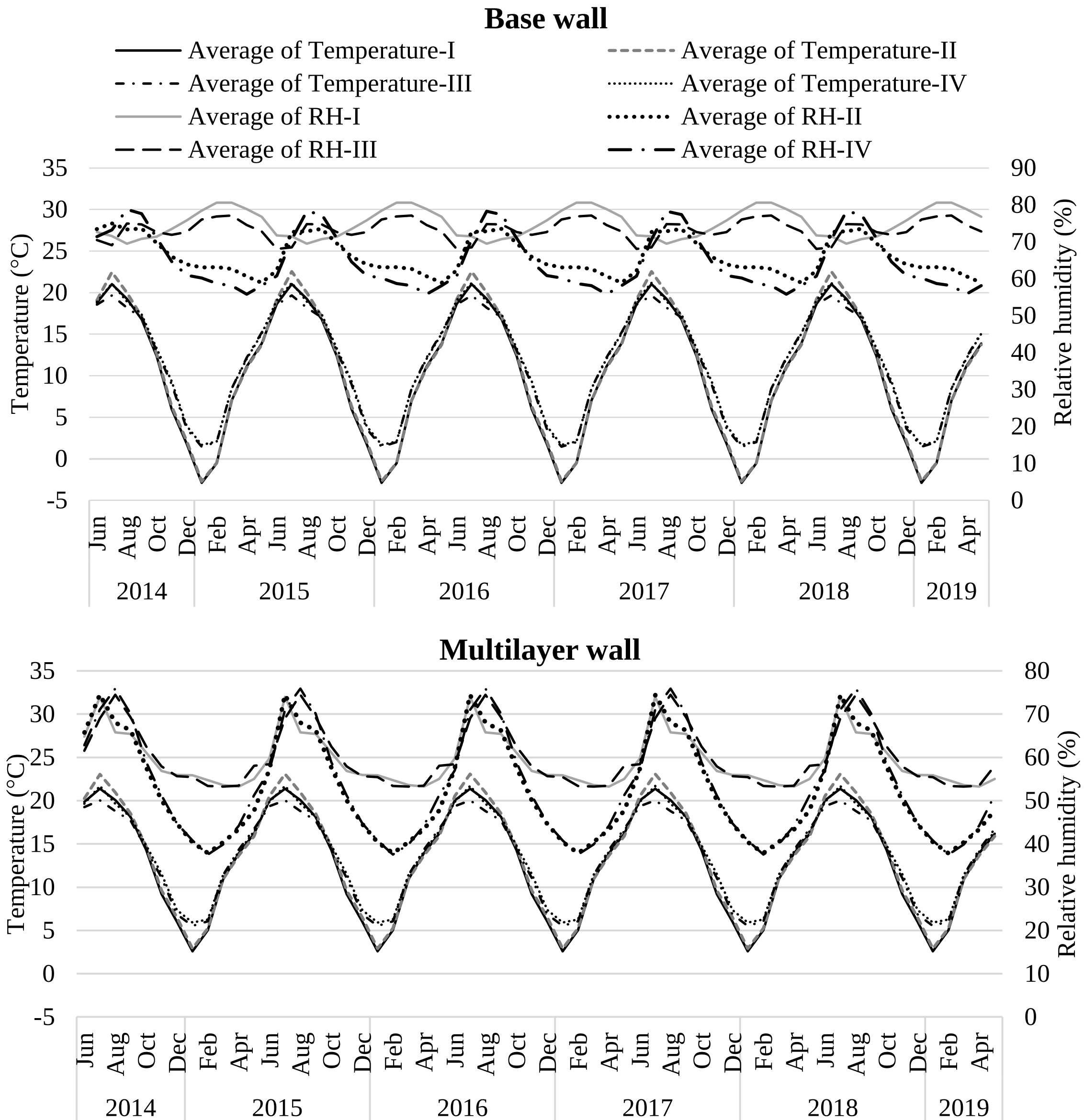


Figure 22: Monthly average RH and temperature of the base and multilayer walls under the four scenarios

The previous results show that the average RH values of both wall assemblies are below 80%, and the average temperatures are between approximately 19 °C and 21 °C during summer months. However, considering that high temperatures and RH occasionally occur in both assemblies under some of the scenarios (II and IV), and especially in the base wall, Figures 23 to 26 illustrate mold isopleths distributions on the inside surface of both wall assemblies under all four scenarios.

The mold isopleths plot the relative humidities at each time step against the simultaneous temperatures. This analysis enables the assessment of whether conditions of high temperature and high humidity occur at the same time that may create issues for some materials. In this regard, the graph shows the limiting isopleths for building materials, LIM B I and LIM B II, below which any mold growth can be safely excluded (Sedlbauer, 2001). Furthermore, LIM B I is the limit for the wallpaper and plasterboard products that are made of easily degradable materials, and LIM B II is the limit for substrates with a porous structure such as plasters, mineral building materials, and some woods. It should also be mentioned that if conditions exceed limiting isopleths for a more extended time, this only signifies that mold growth cannot be excluded, but does not necessarily imply that mold will grow. Moreover, the color of each point indicates the simulation time when that point is generated. Thus at the beginning of the calculation, the points are shown in a yellow shade, later yellow spots are progressively turning into darker shades of green, and the last points are black. This approach allows recognition of any long-term trend in the cloud of points.

The results presented in Figures 23 to 26 show that isopleths of the interior surface of both wall assemblies under all four scenarios are below both limiting lines. Furthermore, the isopleths are similar for both walls under the same scenarios. For example, the isopleths of the walls are between 18 °C and 25 °C and between 50% and 60% under scenarios I and

III. On the other hand, the isopleths of the two assemblies are between 19 °C and 32 °C and between 20% and 70% under scenarios II and IV. The explanation of these results is different indoor conditions between the cases. For instance, scenarios I and III have indoor RH between 50% and 60% and lower mean indoor air temperature of 21 °C. In contrast, scenarios II and IV have 5°C higher indoor air temperatures and more significant fluctuation in RH, ranging from 21% to 70% (see Table 8).

**Scenario I**

*Base wall* *Multilayer wall*

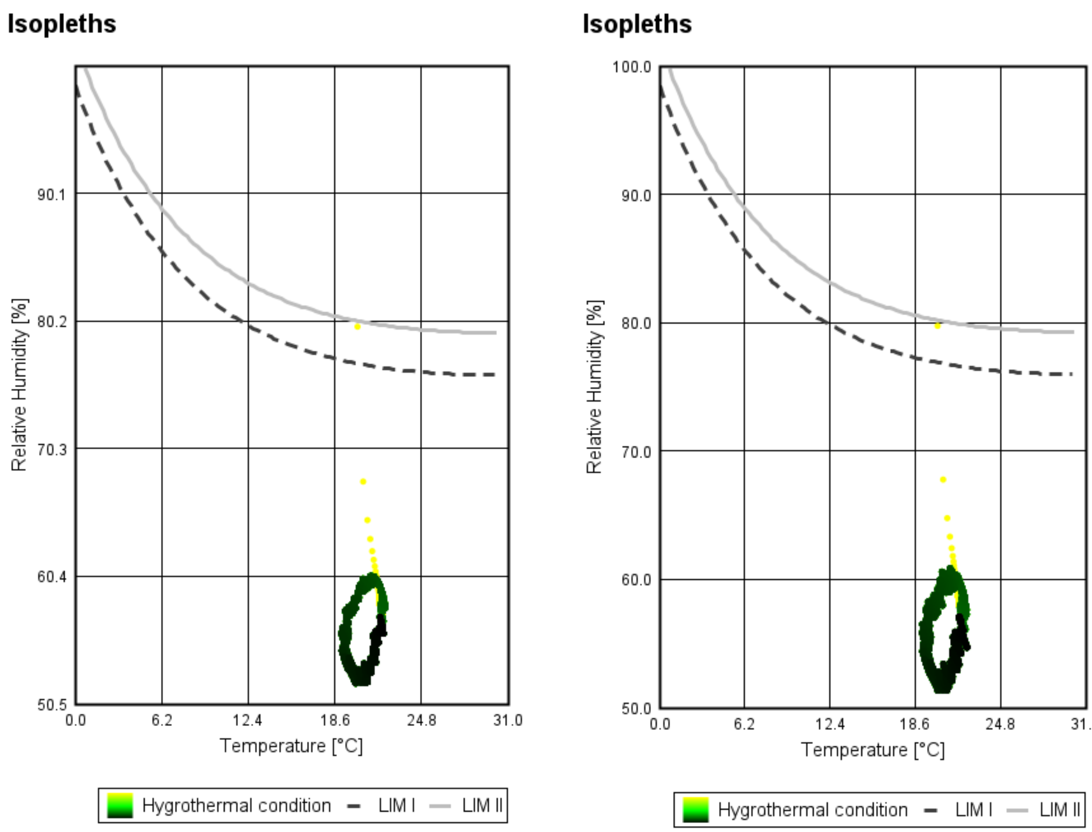


Figure 23: Isopleths of the base and multilayer walls under scenario I

**Scenario II**

*Base wall* *Multilayer wall*

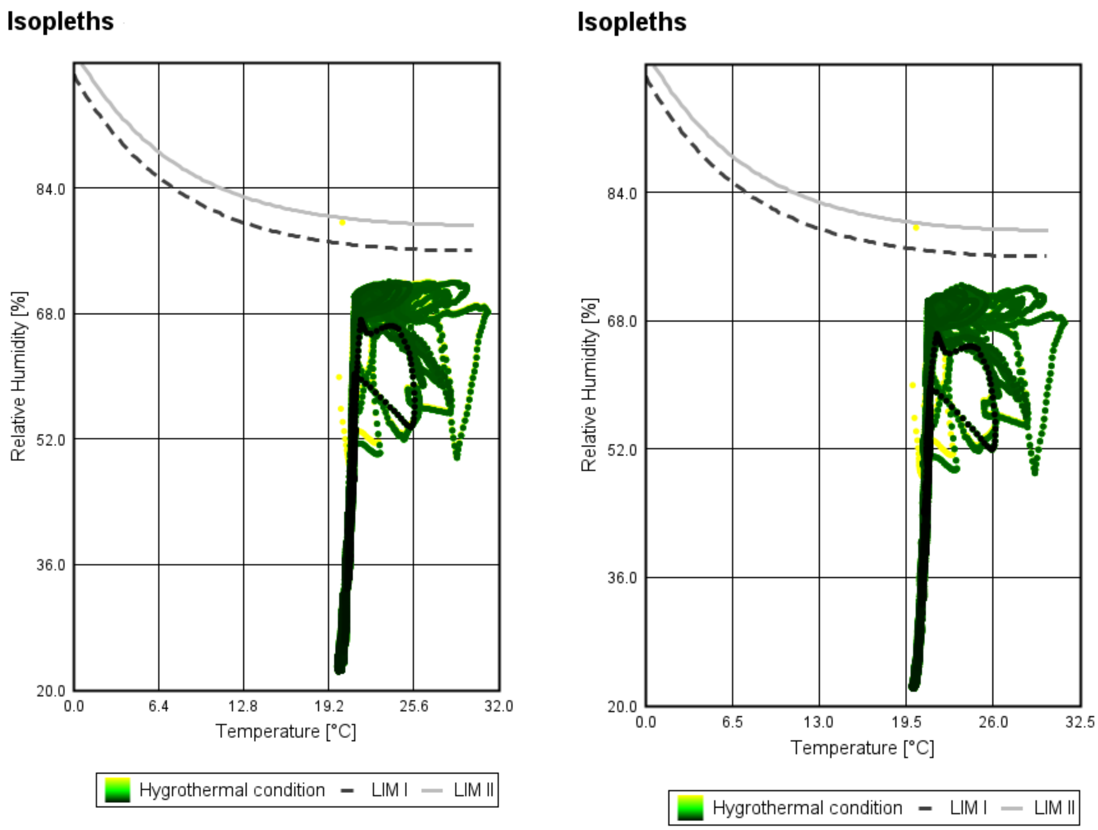


Figure 24: Isopleths of the base and multilayer walls under scenario II

**Scenario III**

*Base wall* *Multilayer wall*

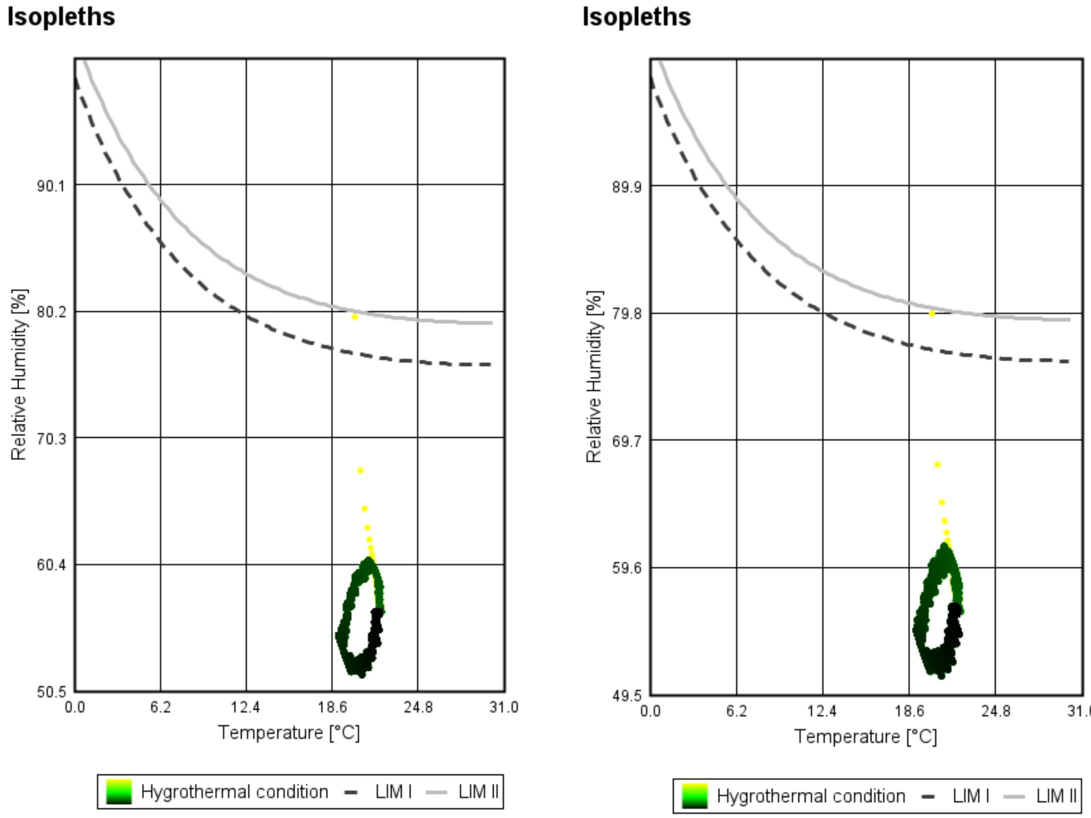


Figure 25: Isopleths of the base and multilayer walls under scenario III

**Scenario IV**

*Base wall* *Multilayer wall*

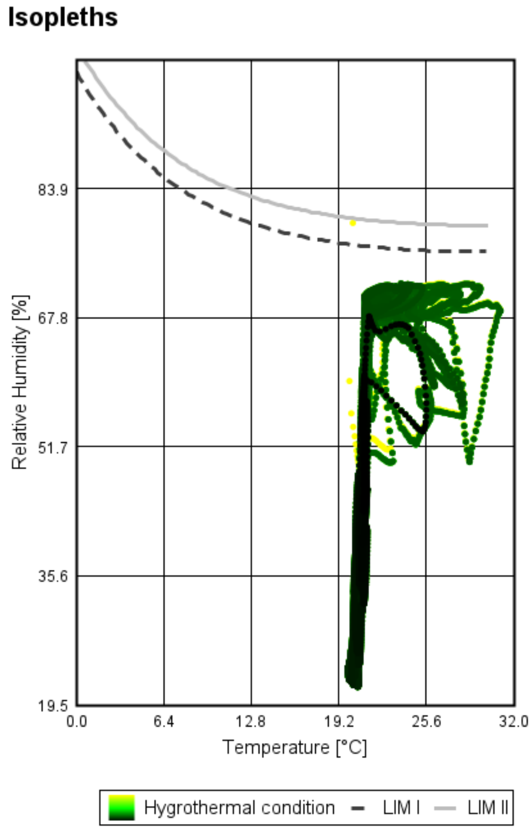


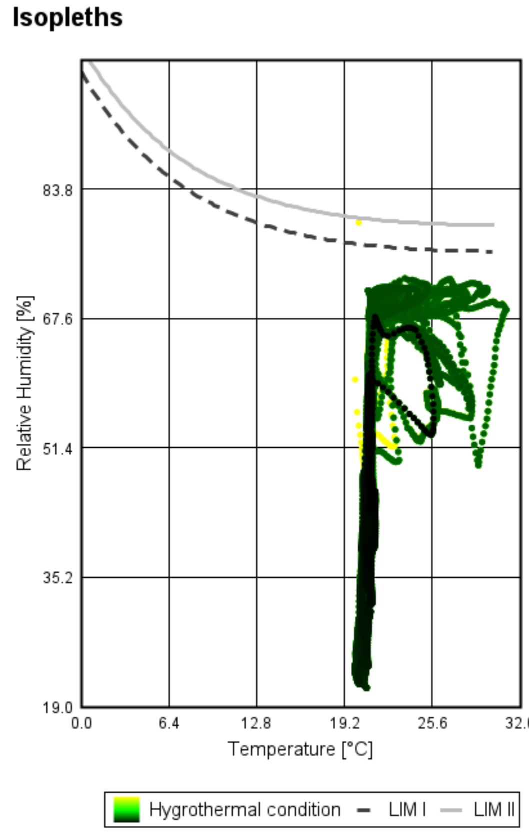


Figure 26: Isopleths of the base and multilayer walls under scenario IV

### 4.5.3 Thermal Performance of the Base and Multilayer Wall Assemblies

The final analysis of the two wall assemblies includes a comparison of their heat flows. In this regard, Figure 27 presents the total annual heat flows at the internal and external surfaces of both walls under all four scenarios during the five-year simulation period. It should be mentioned that because simulation starts on 1st June and ends on 31st May, the heat flow of the years, 2014 and 2019 are lower compared to the other years.

Overall, the multilayer wall performs better and exhibits lower annual heat flow than the base wall under all cases, and in particular, at the outside surface. The likely reason is the addition of the insulation layer with low thermal conductivity (0.034 W/mK) that reduced heat losses at the external surface of the multilayer wall. Furthermore, due to the lower outdoor air temperatures of the scenarios I and II compared to the cases III and IV (see Table 8), both walls experienced higher heat flow under I and II than III and IV scenarios. Moreover, due to the higher indoor air temperatures of cases II and IV than the other two, both walls had higher heat flow under II than I scenario and under IV than III scenario.

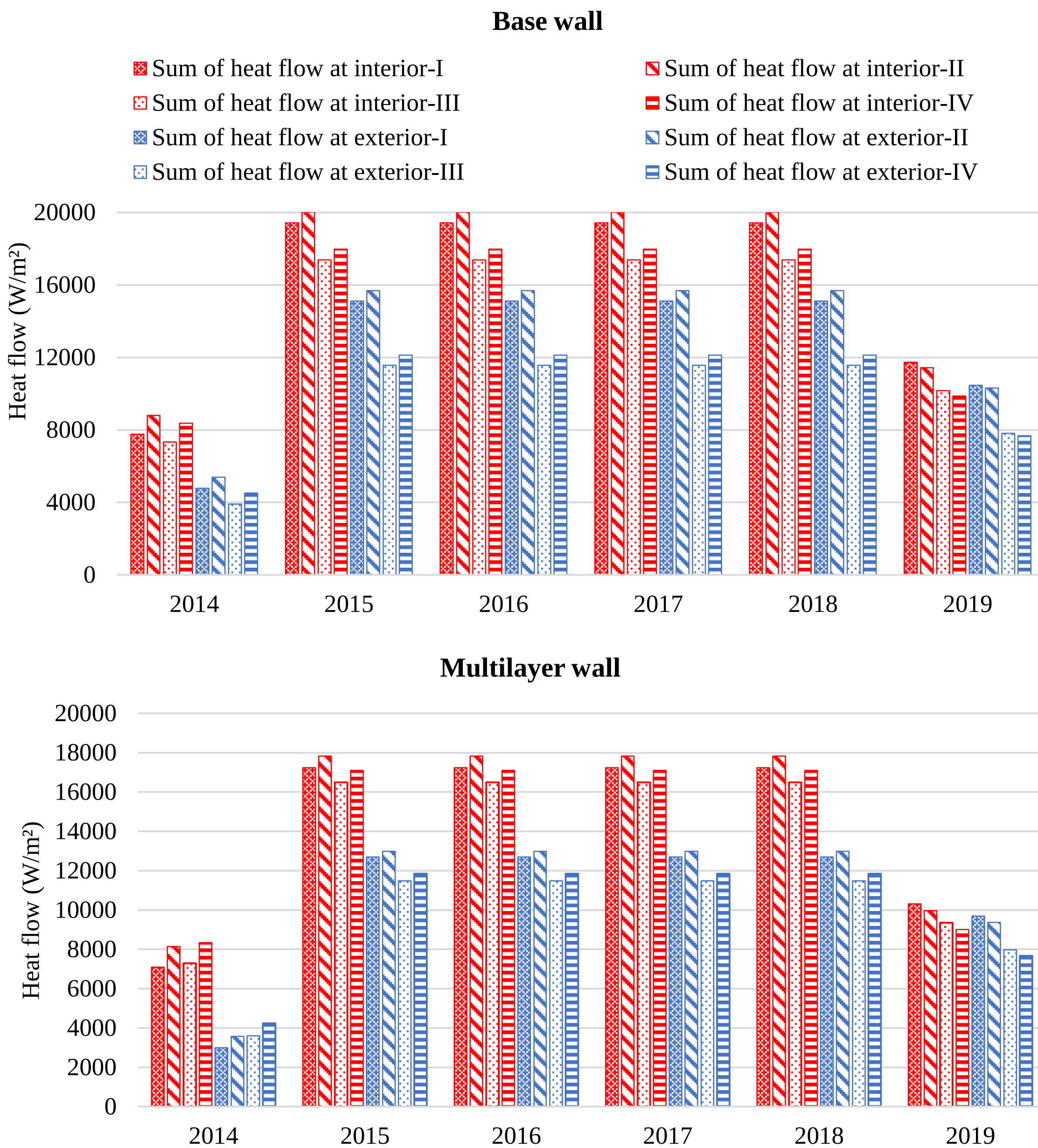


Figure 27: Annual heat flow of the base and multilayer walls under four scenarios

# 5 Conclusion and Recommendations

This research study presents the development of a hempcrete infill "wall" formula with excellent thermal properties using locally sourced materials. Thus, four different hempcrete mixes with varying concentrations of metakaolin were developed with a primary goal of maximizing the hemp hurd ratio within the hempcrete mixtures to improve their thermal properties while reducing their carbon footprint and possibly the price. Furthermore, this study also presents the finite element numerical analysis of the hygrothermal performance of the two wall assemblies, which differ in their complexity, under four design boundary conditions over five consecutive years. Therefore, this study provides new knowledge and information about the potential for the application of hempcrete under Canadian weather conditions. Hence, the results of this study are likely to be of interest to audiences in academia and industry.

## 5.1 Summary of the Main Findings

The main findings of this research project are as follows:

- The bulk density of hemp hurd recorded at room temperature before oven-drying is 114.6 kg/m$^3$, and the dry density of hemp hurd recorded after oven-drying for 24 hours at 105 ºC is 105 kg/m$^3$. Furthermore, the mechanical sieving shows that the vast majority (~99%) of the hemp hurd particles fall between sieve grades of 2.36 mm and 6.3 mm.
- The densities of hempcrete samples produced in this study show excellent consistency. Thus, the dry densities of the samples range between 298.55 kg/m$^3$ and

318.05 kg/m$^3$, with most of them falling between 300 kg/m$^3$ and 310 kg/m$^3$. Furthermore, the average density of all samples is 306.13 kg/m$^3$. The differences in the samples' density are mainly due to the variation in the compaction level.

- The thermal conductivities of the hempcrete samples range between 0.075 W/mK and 0.094 W/mK for the mean temperature range of 7.35-52.3 ºC. Furthermore, the average thermal conductivities of all the samples range from 0.081 W/mK to 0.089 W/mK. The standard deviation of 0.004–0.007 indicates consistency in the results.
- The experimental results show that thermal conductivity is a function of the density of hempcrete, and this finding is consistent with the previous studies. Thus, the lowest density hempcrete of 298.55 kg/m$^3$ has the lowest thermal conductivity of 0.075 W/mK. In contrast, the highest density hempcrete of 318.05 kg/m$^3$ has the highest thermal conductivity of 0.094 W/mK.
- On average, the base wall has 36% to 54% higher water content than the multilayer wall throughout the simulation period. The possible explanation is a thinner layer of hempcrete infill of the multilayer wall compared to the base wall and addition of insulation layer that has a significantly lower initial water content (i.e., 0.82 kg/m$^3$) than the hempcrete (i.e., 29 kg/m$^3$).
- Furthermore, the average water contents in the mass percent of both wall assemblies under all four cases are significantly below the 20 mass-percent. Moreover, the results suggest that both walls dry out under scenarios II and IV, and no water content accumulation occurs throughout the five year simulation period. At the end of the simulation period, the base and multilayer wall assemblies perform the worst under cases I and III, respectively. In this regard, under scenarios I and III, the total

average annual water content of the base wall increases, suggesting that the assembly is not drying out through time. Although the overall yearly average water content of the multilayer wall is gradually declining over the five years under scenarios I and III, this drop in the water content is not as significant as under scenarios II and IV. The likely reason for all these findings is 10% lower indoor RH and 3.5 ºC to 5 ºC higher indoor air temperatures of II and IV scenarios than the average indoor RH and air temperature of cases I and III.

- Even though most of the time, both walls experience RH values below the mold risk threshold of 80%, under I scenario, RH values of both walls, exceed 80% during the short period, and especially of the base wall. Furthermore, RH profiles of both walls have regular patterns of seasonal fluctuation that gradually decrease over time, and especially of the multilayer wall, which under all scenarios, has lower RH compared to the base wall.
- Similarly to the entire assemblies, RH profiles of both hempcrete infills had regular patterns of seasonal fluctuation that gradually decrease over time, and especially in the case of the multilayer wall. Also, RH values of the hempcrete infill of the multilayer wall were below the mold growth threshold of 80% throughout the simulation under all cases. The base wall, on the other hand, experienced RH values of above 80% under the scenario I.
- Due to the addition of 10.5 cm of the Rockwool insulation, the multilayer wall is warmer under all four scenarios compared to the base wall. In this regard, the temperatures of the multilayer wall range between -2 °C to 30 °C and of the base wall they range from -4 °C to 26 °C.

- The mold isopleths of the interior surface of both wall assemblies under all four scenarios were below both limiting lines, indicating that any risk of mold growth can be safely excluded.
- The multilayer wall performs better and exhibits lower annual heat flow than the base wall under all cases, and in particular, at the outside surface. The likely reason is the addition of the insulation layer that reduced heat losses at the external surface of the multilayer wall. Furthermore, due to the higher indoor air temperatures of cases II and IV than the other two, both walls have higher heat flow under II than I scenario and under IV than III scenario.

## 5.2 Limitations and Recommendations for Future Work

The study's limitations that point to the need for future work and investigation are as follows:

- The main limitation of this study is the lack of comparison of the modeling results against the experimentally measured data of any full-scale work. Therefore, future research should include the comprehensive onsite experiment on full-scale wall envelope and the use of collected data for the validation of developed models.
- Future research should also include additional hygrothermal experimental analyses such as investigation of the moisture buffer capacity of the developed hempcrete mixes.

- This study only used metakaolin and hydrated lime. Therefore, future work should investigate the application of different pozzolans and binder formulas. Furthermore, future work should also explore different preprocessing methods of the hemp hurd to improve the hydration of the hempcrete.
- Application of vapor barrier and different design configurations of the wall assemblies, including various insulation materials and envelope systems, should be further investigated. Furthermore, further numerical analysis is required to investigate additional combinations of indoor and outdoor boundary conditions.
- Future research should also include a detailed life cycle analysis that may advise on the affordability of the hempcrete for the construction of buildings in Manitoba and Canada as well as regarding its carbon sequestration capabilities.

# References

Abbott, T. (2014). The Limecrete Company LTD. Hempcrete Factsheet. http://limecrete.co.uk/

Amziane, S., & Arnaud, L. (2013). Bio-aggregate-based Building Materials: Applications to Hemp Concretes (1st ed.; S. Amziane & L. Arnaud, Eds.). London, UK and Hoboken, NJ, USA: ISTE Ltd and John Wiley & Sons, Inc.

Amziane, S., Collet, F., Lawrence, M., Magniont, C., Picandet, V., & Sonebi, M. (2017). Recommendation of the RILEM TC 236-BBM : characterisation testing of hemp shiv to determine the initial water content, water absorption, dry density, particle size distribution, and thermal conductivity.

Arnaud, L., & Gourlay, E. (2012). Experimental study of parameters influencing mechanical properties of hemp concretes. 28, 50–56.

ASTM C136, (2006), “Standard Test Method for Sieve Analysis of Fine and Coarse Aggregates”, ASTM International, West Conshohocken, PA, 2006.

ASTM C207, (2006), “Standard Specification for Hydrated Lime for Masonry Purposes”, ASTM International, West Conshohocken, PA.

ASTM C29, (2007), “Standard Test Method for Bulk Density (“Unit Weight”) and Voids in Aggregate”, ASTM International, West Conshohocken, PA.131

ASTM C618, (2012), “Standard Specification for Coal Fly Ash and Raw or Calcined Natural Pozzolan for Use in Concrete”, ASTM International, West Conshohocken, PA.

ASTM C110, (2011), “Standard Test Methods for Physical Testing of Quicklime, Hydrated Lime, and Limestone”, ASTM International, West Conshohocken, PA

ASTM C518, (2015), “Standard Test Method for Steady-State Thermal Transmission Properties by Means of the Heat Flow Meter Apparatus”, ASTM International, West Conshohocken, PA.

ASTM C1045, (2019), “Standard Practice for Calculating Thermal Transmission Properties Under Steady-State Conditions”, ASTM International, West Conshohocken, PA.

Baughman, A., Arens, Edward A. (1996). Indoor Humidity and Human Health - Part I: Literature Review of Health Effects of Humidity-Influenced Indoor Pollutants. Center for the Built Environment, University of California, Berkeley.

Bedliva, H., & Isaacs, N. (2014). Hempcrete – An Environmentally Friendly Material ? (October 2014). https://doi.org/10.4028/www.scientific.net/AMR.1041.83

Bejat, T., Piot, A., Jay, A., & Bessette, L. (2015). Study of two hemp concrete walls in real weather conditions. Energy Procedia, 78, 1605–1610.

Bevan, R., & Woolley, T. (2008). Hemp Lime Construction: A guide to building with hemp lime composites. IHS BRE Press.

Cazacu, C., Transilvania, U., Muntean, R., Transilvania, U., Galatanu, T., & Transilvania, U. (2016). Hemp lime technology. (February 2017), 3–9.

CAN/CSA-A3001, (2013), “Cementitious Materials for Use in Concrete”, Canadian Standards Association, Mississauga, ON.

Canadian Green Building Council (CaGBC), (2018). LEED-Canada NC version 1.0, Reference Guide: https://www.cagbc.org/

Cérézo V. (2005). Propriétés mécaniques , thermiques et acoustiques d ’ un matériau à base de particules végétales : approche expérimentale et modélisation théorique. Inst Natl Des Sci Appliquées 2005; Jun 16.

Chabannes, M., Garcia-diaz, E., Clerc, L., & Bénézet, J. (2015). Studying the hardening and mechanical performances of rice husk and hemp-based building materials cured under natural and accelerated carbonation. *Construction and Building Materials*, *94*, 105–115. https://doi.org/10.1016/j.conbuildmat.2015.06.032

Colinart, T., Lelievre, D., & Glouannec, P. (2016). Experimental and numerical analysis of the transient hygrothermal behavior of multilayered hemp concrete wall. *Energy & Buildings*, *112*, 1–11. https://doi.org/10.1016/j.enbuild.2015.11.027

Collet, F., Chamoin, J., Pretot, S., & Lanos, C. (2013). Comparison of the hygric behaviour of three hemp concretes. *Energy & Buildings*, *62*, 294–303.

Collet, F., & Pretot, S. (2014). Experimental highlight of hygrothermal phenomena in hemp concrete wall. *Building and Environment*, *82*, 459–466.

Costantine, G., Maalouf, C., Moussa, T., & Polidori, G. (2018). Experimental and numerical investigations of thermal performance of a Hemp Lime external building insulation. *Building and Environment*, *131*(December 2017), 140–153.

De Bruijn, P., & Johansson, P. (2013a). Moisture fixation and thermal properties of lime-hemp concrete. *Construction and Building Materials*, *47*, 1235–1242.

De Bruijn, P., & Johansson, P. (2013b). Moisture fixation and thermal properties of lime-hemp concrete. *Construction and Building Materials*, *47*, 1235–1242.

Dhakal, U. (2016). The Effect of Different Mix Proportions on the Hygrothermal Performance of Hempcrete in the Canadian Context (Vol. 2003).

Dhakal, U., Berardi, U., Gorgolewski, M., & Richman, R. (2017). Hygrothermal performance of hempcrete for Ontario ( Canada ) buildings. Journal of Cleaner Production, 142, 3655–3664.

Dinh, T. M. (2014). Contribution au développement de béton de chanvre préfabriqué utilisant un liant pouzzolanique innovant [Contribution to the development of precast hempcrete using innovative pozzolanic binder].

DIN 4108 - 4E: 1991, Thermal Insulation in Buildings; Characteristic Values Relating to Thermal Insulation and Protection against Moisture, German Institute for Standardisation (Deutsches Institut für Normung).

Elfordy, S., Lucas, F., Tancret, F., Scudeller, Y., & Goudet, L. (2008). Mechanical and thermal properties of lime and hemp concrete ("hempcrete") manufactured by a projection process. *Construction and Building Materials*, *22*(10), 2116–2123.

Environment and Climate Change Canada - Climate Change - Canada's Emission Trends 2014. (2019). Retrieved September 16, 2019.

Evrard, A. (2008). Transient hygrothermal behavior of Lime-Hemp Materials Ecole Polytechnique de Louvain Unité d ' Architecture Transient hygrothermal behaviour of Lime-Hemp Materials Thèse présentée en vue de l ' obtention du doctorat en Sciences de l ' Ingénieur par Co.

Evrard, A., & Herde, A. De. (2005). Bioclimatic envelopes made of lime and hemp concrete. Proceeding of CISBAT - Renewables in a Changing Climate - Innovation in Building Envelopes and Environmental Systems, 1-5, Lausanne, Switzerland.

Evrard, A., & Herde, A. De. (2010). Hygrothermal Performance of Lime – Hemp Wall Assemblies. Journal of Building Physics, 34(1).

Florentin, Y., Pearlmutter, D., Givoni, B., & Gal, E. (2017). A life-cycle energy and carbon analysis of hemp-lime bio-composite building materials. *Energy & Buildings*, *156*, 293–305. https://doi.org/10.1016/j.enbuild.2017.09.097

Fox 314 – TA Instruments. www.tainstruments.com

Gourlay, E. and Arnaud, L. (2010). Comportement hygrothermique des murs de béton de chanvre, in Proceedings of the Actes du congrès SFT, Le Touquet, France, pp. 25-28.

Gregor, L. (2014). Performance of Hempcrete Walls Subjected to A Standard Time - Temperature Fire Curve. Victoria University, Australia.

Hirst, E. A. J. (2013). Characterisation of Hemp-Lime As a Composite Building Material.

Hirst, E., Walker, P., Paine, K., and Yates, T. (2010). Characterisation of Low Density Hemp-Lime Composite Building Materials under Compression Loading, Second International Conference on Sustainable Construction Materials and Technologies, Ancona, Italy.

Hussain, A., Calabria-Holley, J., Lawrence, M., & Jiang, Y. (2019). Hygrothermal and mechanical characterisation of novel hemp shiv based thermal insulation composites. *Construction and Building Materials*, *212*, 561–568.

Ingrao, C., Lo Giudice, A., Bacenetti, J., Tricase, C., Dotelli, G., Fiala, M., … Mbohwa, C. (2015). Energy and environmental assessment of industrial hemp for building applications: A review. *Renewable and Sustainable Energy Reviews*, *51*, 29–42.

Ip, K., & Miller, A. (2012). Life cycle greenhouse gas emissions of hemp – lime wall constructions in the UK. *"Resources, Conservation & Recycling," 69*, 1–9.

IPCC, 2014: Climate Change 2014: Mitigation of Climate Change. Contribution of Working Group III to the Fifth Assessment Report of the Intergovernmental Panel on Climate Change [Edenhofer, O., Pichs Madruga, R., Sokona, Y., Farahani, E., Kadner, S., Seyboth, K., Adler, A., Baum, I., Brunner, S., Eickemeier, P., Kriemann, B., Savolainen, J., Schlömer, S., Von Stechow, C., Zwickel, T., and Minx, J. C. (eds.)]. Cambridge University Press, Cambridge, United Kingdom and New York, NY, USA.

Jami, T., Karade, S. R., & Singh, L. P. (2019). A review of the properties of hemp concrete for green building applications. *Journal of Cleaner Production*, *239*, 117852. https://doi.org/10.1016/j.jclepro.2019.117852

Künzel, H. M. (1995). Simultaneous Heat and Moisture Transport in Building Components; One and two-dimensional calculation using simple parameters. Fraunhofer Institute of Building Physics.

Latif, E., Anca, M., Tucker, S., Chitral, D., & John, D. (2015). Hygrothermal performance of wood-hemp insulation in timber frame wall panels with and without a vapour barrier. *Building and Environment*, *92*, 122–134.

Latif, E., Lawrence, M., Shea, A., & Walker, P. (2015). Moisture buffer potential of experimental wall assemblies incorporating formulated hemp-lime. *Building and Environment*, *93*, 199–209. https://doi.org/10.1016/j.buildenv.2015.07.011

Maalouf, C., Ingrao, C., Scrucca, F., Moussa, T., Bourdot, A., Tricase, C., Asdrubali, F. (2018). An energy and carbon footprint assessment upon the usage of hemp- lime concrete and recycled-PET façades for office facilities in France and Italy. *Journal of Cleaner Production*, *170*, 1640–1653. https://doi.org/10.1016/j.jclepro.2016.10.111

Magwood, C. (2016). Essential Hempcrete Construction: The Complete Step-by-Step Guide. New Society Publishers.

Marceau, S., Glé, P., Guéguen-minerbe, M., Gourlay, E., Moscardelli, S., Nour, I., & Amziane, S. (2017). Influence of accelerated aging on the properties of hemp concretes. *Construction and Building Materials*, *139*, 524–530.

Material Safety Data Sheet: Pure Cal-High Calcium Hydrated Lime (Calcium Hydroxide). (1999).

Motori, A., Manzi, S., Montecchi, M., & Canti, M. (2012). A preliminary study of physical and mechanical properties of sustainable hemp fibers based composite materials for building insulated walls. *ECCM 2012 - Composites at Venice, Proceedings of the 15th European Conference on Composite Materials*, (June), 24–28.

Moujalled, B., Aït, Y., Moissette, S., Bart, M., Lanos, C., & Samri, D. (2018). Experimental and numerical evaluation of the hygrothermal performance of a hemp lime concrete building : A long term case study. *Building and Environment*, *136*(March), 11–27. https://doi.org/10.1016/j.buildenv.2018.03.025

Mukherjee, A. (2012). Structural Benefits of Hempcrete Infill in Timber Stud. Queen's University.

NECB. (2015). National Energy Code of Canada for Building (NECB).

Nguyen, T. T. (2010). Contribution à l'étude de la formulation et du procédé de fabrication d'éléments de construction en béton de chanvre (Doctoral dissertation, Université de Bretagne Sud).

Nguyen, T. T., Picandet, V., Amziane, S., & Baley, C. (2009). Influence of compactness and hemp hurd characteristics on the mechanical properties of lime and hemp concrete. European Journal of Environmental and Civil Engineering, 13(9), 1039-1050.

Niyigena, C., Amziane, S., & Chateauneuf, A. (2018). Multicriteria analysis demonstrating the impact of shiv on the properties of hemp concrete. 160, 211–222.

Nozahic, V., Amziane, S., Torrent, G., Saïdi, K., & De Baynast, H. (2012). Design of green concrete made of plant-derived aggregates and a pumice–lime binder. Cement and Concrete Composites, 34(2), 231-241.

Oumeziane, Y. A., Bart, M., Moissette, S., & Lanos, C. (2014). Hysteretic Behaviour and Moisture Buffering of Hemp Concrete. © Springer Science+Business Media Dordrecht 2014, 515–533.

Page, J., Sonebi, M., & Amziane, S. (2017). Design and multi-physical properties of a new hybrid hemp-flax composite material. *Construction and Building Materials*, *139*, 502–512. https://doi.org/10.1016/j.conbuildmat.2016.12.037

Piot, A., Béjat, T., Jay, A., Bessette, L., Wurtz, E., & Barnes-davin, L. (2017). Study of a hempcrete wall exposed to outdoor climate : Effects of the coating. *Construction and Building Materials*, *139*, 540–550.

PLAINS HEMP®. Plains Industrial Hemp Processing Ltd. Gilbert plain, MB, Canada. plainshemp.ca

Pretot, S., Collet, F., & Garnier, C. (2014). Life cycle assessment of a hemp concrete wall : Impact of thickness and coating. Building and Environment, 72, 223–231. https://doi.org/10.1016/j.buildenv.2013.11.010

Rahim, M., Douzane, O., Le, A. D. T., Promis, G., & Langlet, T. (2016). Characterization and comparison of hygric properties of rape straw concrete and hemp concrete. 102, 679–687. https://doi.org/10.1016/j.conbuildmat.2015.11.021

Ruggieri, G., Arrigoni, A., Pelosato, R., Meli, P., Sabbadini, S., & Dotelli, G. (2017). Life cycle assessment of natural building materials : the role of carbonation, mixture components and transport in the environmental impacts of hempcrete blocks. 149, 1051–1061. https://doi.org/10.1016/j.jclepro.2017.02.161

Sassoni, E., Manzi, S., Motori, A., Montecchi, M., & Canti, M. (2014). Novel sustainable hemp-based composites for application in the building industry: Physical, thermal and mechanical characterization. *Energy and Buildings*, *77*, 219–226.

Sedlbauer, K. (2001). Vorhersage von Schimmelpilz bildung auf und in Bauteilen, Dissertation, Uni Stuttgart.

Shea, A., Lawrence, M., & Walker, P. (2012). Hygrothermal performance of an experimental hemp – lime building. 36, 270–275.

Stanwix, W., & Sparrow, A. (2014). The Hempcrete Book: Designing and building with hemp-lime. United Kingdom: Green books.

Sutton A., Black D., Walker P. (2011). Hemp lime: an introduction to low impact building materials, in: Garston (Ed.), Establishment BR, IHS BRE Press, Wat- ford.

Tran-le, A. D., Nguyen, S., & Langlet, T. (2019). A novel anisotropic analytical model for effective thermal conductivity tensor of dry lime-hemp concrete with preferred spatial distributions. *Energy & Buildings*, *182*, 75–87.

Tran Le, A. D., Maalouf, C., Mai, T. H., Wurtz, E., & Collet, F. (2010). Transient hygrothermal behaviour of a hemp concrete building envelope. *Energy and Buildings*, *42*(10), 1797–1806. https://doi.org/10.1016/j.enbuild.2010.05.016

Tronet, P., Lecompte, T., Picandet, V., & Baley, C. (2016). Study of lime hemp concrete (LHC) - Mix design, casting process and mechanical behaviour. *Cement and Concrete Composites*, *67*, 60–72. https://doi.org/10.1016/j.cemconcomp.2015.12.004

Viitanen, H. (2003). Moisture and Bio-Deterioration Risk of Building Materials and Structures. (Table 1).

Walker, R., & Pavia, S. (2010). Behaviour and Properties of Lime-Pozzolan Pastes. 8th International Masonry Conference Dresden, 353–364. Retrieved from https://www.researchgate.net/publication/235641076_Behaviour_and_Properties_of_Lime-Pozzolan_Pastes

Walker, R., & Pavía, S. (2014). Moisture transfer and thermal properties of hemp-lime concretes. *Construction and Building Materials*, *64*, 270–276.

Walker, R., Pavia, S., & Mitchell, R. (2014). Mechanical properties and durability of hemp-lime concretes. *Construction and Building Materials*, *61*, 340–348.

Western Lime Corporation: Graymont. (2018). https://www.graymont.com/en

WHITEMUD$^{MK}$, High Reactivity Metakaolin. Whitemud Resources Inc. (2018). www.whitemudresources.com

Williams, J., Lawrence, M., & Walker, P. (2018). The influence of constituents on the properties of the bio-aggregate composite hemp-lime. *Construction and Building Materials*, *159*, 9–17. https://doi.org/10.1016/j.conbuildmat.2017.10.109

WUFI®. (2019). Wärme Und Feuchte Instationär (means heat and moisture transiency). https://wufi.de/en/

Zarr, R., Heckert, N. A., and Leigh, S. D. (2014). Retrospective Analysis of NIST Standard Reference Material 1450, Fibrous Glass Board, for Thermal Insulation Measurements. Journal of Research of the National Institute of Standards and Technology, Volume 119, http://dx.doi.org/10.6028/jres.119.012

# Appendix A: Thickness Calculation in WUFI

## 1. LMK50 – Base wall

Homogenous layers

Thermal resistance: 4.748 m²K/W (without Rsi, Rse)

Heat transfer coefficient (U-value): 0.2 W/m²K

Thickness: 0.44 m

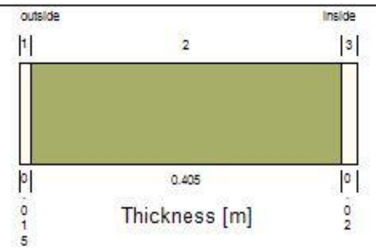


| Nr. | Material/Layer (from outside to inside) | ρ [kg/m³] | c [J/kgK] | λ [W/mK] | Thickness [m] | Color |
|---|---|---|---|---|---|---|
| 1 | Lime Plaster (stucco, A-value: 3.0 kg/m2h0.5) | 1600 | 850 | 0.7 | 0.015 | |
| 2 | Hempcrete | 302 | 1412 | 0.0862 | 0.405 | |
| 3 | Lime Plaster (stucco, A-value: 3.0 kg/m2h0.5) | 1600 | 850 | 0.7 | 0.02 | |

| Nr. | Material / Layer (from outside to inside) | λ [W/mK] | Thickness [m] |
|---|---|---|---|
| 1 | Lime Plaster (stucco, A-value: 3.0 kg/m2h0.5) | 0.7 | 0.015 |
| 2 | Hempcrete | 0.0862 | 0.405 |
| 3 | Lime Plaster (stucco, A-value: 3.0 kg/m2h0.5) | 0.7 | 0.02 |

## 2. LMK20 – Base wall

Homogenous layers

Thermal resistance: 4.751 m²K/W (without Rsi, Rse)

Heat transfer coefficient (U-value): 0.2 W/m²K

Thickness: 0.444 m

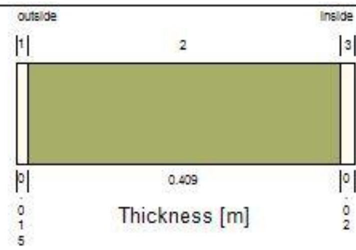


| Nr. | Material/Layer (from outside to inside) | ρ [kg/m³] | c [J/kgK] | λ [W/mK] | Thickness [m] | Color |
|---|---|---|---|---|---|---|
| 1 | Lime Plaster (stucco, A-value: 3.0 kg/m2h0.5) | 1600 | 850 | 0.7 | 0.015 | |
| 2 | Hempcrete | 314 | 1412 | 0.087 | 0.409 | |
| 3 | Lime Plaster (stucco, A-value: 3.0 kg/m2h0.5) | 1600 | 850 | 0.7 | 0.02 | |

| Nr. | Material / Layer (from outside to inside) | λ [W/mK] | Thickness [m] |
|---|---|---|---|
| 1 | Lime Plaster (stucco, A-value: 3.0 kg/m2h0.5) | 0.7 | 0.015 |
| 2 | Hempcrete | 0.0870 | 0.409 |
| 3 | Lime Plaster (stucco, A-value: 3.0 kg/m2h0.5) | 0.7 | 0.02 |

## 3. LMK10 – Base wall

Homogenous layers

Thermal resistance: 4.763 m²K/W (without Rsi, Rse)

Heat transfer coefficient (U-value): 0.199 W/m²K

Thickness: 0.445 m

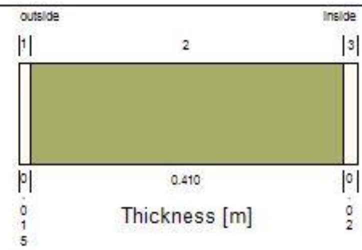


| Nr. | Material/Layer (from outside to inside) | ρ [kg/m³] | c [J/kgK] | λ [W/mK] | Thickness [m] | Color |
|---|---|---|---|---|---|---|
| 1 | Lime Plaster (stucco, A-value: 3.0 kg/m2h0.5) | 1600 | 850 | 0.7 | 0.015 | |
| 2 | Hempcrete | 314 | 1412 | 0.087 | 0.41 | |
| 3 | Lime Plaster (stucco, A-value: 3.0 kg/m2h0.5) | 1600 | 850 | 0.7 | 0.02 | |

| Nr. | Material / Layer (from outside to inside) | λ [W/mK] | Thickness [m] |
|---|---|---|---|
| 1 | Lime Plaster (stucco, A-value: 3.0 kg/m2h0.5) | 0.7 | 0.015 |
| 2 | Hempcrete | 0.087 | 0.410 |
| 3 | Lime Plaster (stucco, A-value: 3.0 kg/m2h0.5) | 0.7 | 0.02 |

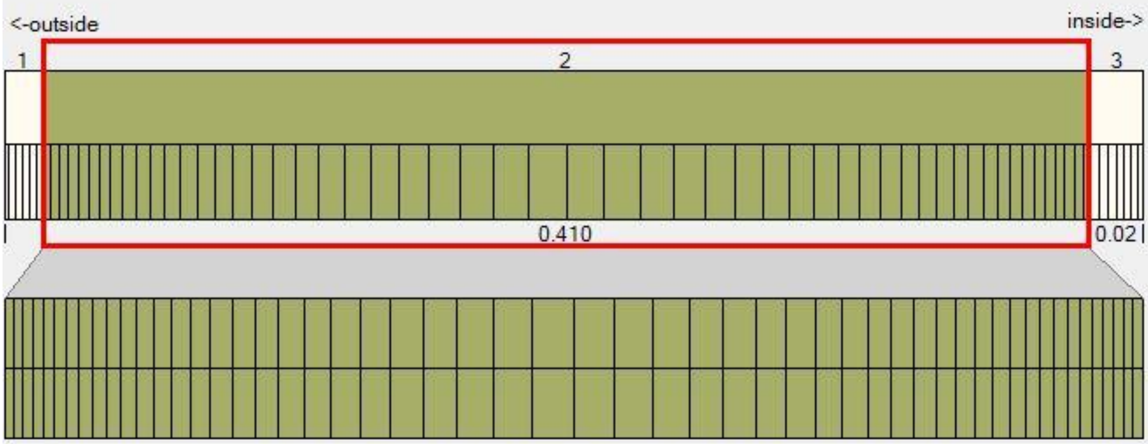

# 4. LMK70 – Base wall

Homogenous layers

Thermal resistance: 4.741 m²K/W (without Rsi, Rse)

Heat transfer coefficient (U-value): 0.2 W/m²K

Thickness: 0.415 m

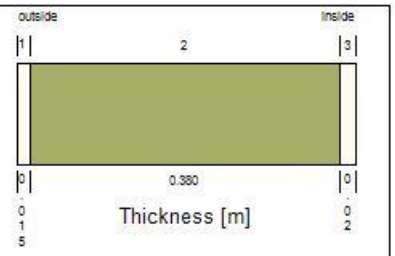


| Nr. | Material/Layer (from outside to inside) | ρ [kg/m³] | c [J/kgK] | λ [W/mK] | Thickness [m] | Color |
|---|---|---|---|---|---|---|
| 1 | Lime Plaster (stucco, A-value: 3.0 kg/m2h0.5) | 1600 | 850 | 0.7 | 0.015 | |
| 2 | Hempcrete | 301 | 1412 | 0.081 | 0.38 | |
| 3 | Lime Plaster (stucco, A-value: 3.0 kg/m2h0.5) | 1600 | 850 | 0.7 | 0.02 | |

| Nr. | Material / Layer (from outside to inside) | λ [W/mK] | Thickness [m] |
|---|---|---|---|
| 1 | Lime Plaster (stucco, A-value: 3.0 kg/m2h0.5) | 0.7 | 0.015 |
| 2 | Hempcrete | 0.081 | 0.380 |
| 3 | Lime Plaster (stucco, A-value: 3.0 kg/m2h0.5) | 0.7 | 0.02 |

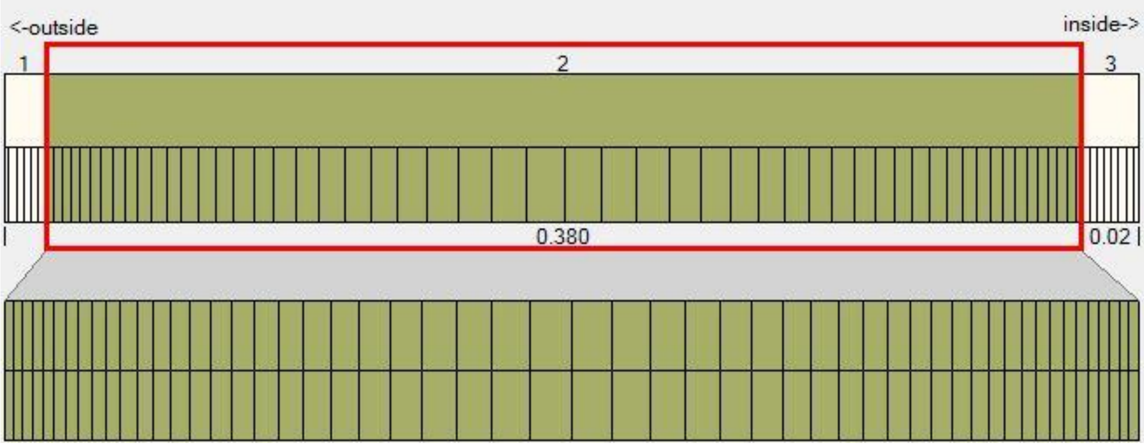

## 5. LMK50 – Multilayer wall

Homogenous layers

Thermal resistance: 4.762 m²K/W (without Rsi, Rse)

Heat transfer coefficient (U-value): 0.199 W/m²K

Thickness: 0.28 m

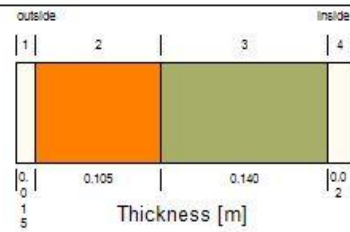


| Nr. | Material/Layer (from outside to inside) | ρ [kg/m³] | c [J/kgK] | λ [W/mK] | Thickness [m] | Color |
|---|---|---|---|---|---|---|
| 1 | Lime Plaster (stucco, A-value: 3.0 kg/m2h0.5) | 1600 | 850 | 0.7 | 0.015 | |
| 2 | Rockwool | 119 | 850 | 0.034 | 0.105 | |
| 3 | Hempcrete | 302 | 1412 | 0.0862 | 0.14 | |
| 4 | Lime Plaster (stucco, A-value: 3.0 kg/m2h0.5) | 1600 | 850 | 0.7 | 0.02 | |

| Nr. | Material / Layer (from outside to inside) | λ [W/mK] | Thickness [m] |
|---|---|---|---|
| 1 | Lime Plaster (stucco, A-value: 3.0 kg/m2h0.5) | 0.7 | 0.015 |
| 2 | Rockwool | 0.034 | 0.105 |
| 3 | Hempcrete | 0.0862 | 0.140 |
| 4 | Lime Plaster (stucco, A-value: 3.0 kg/m2h0.5) | 0.7 | 0.02 |

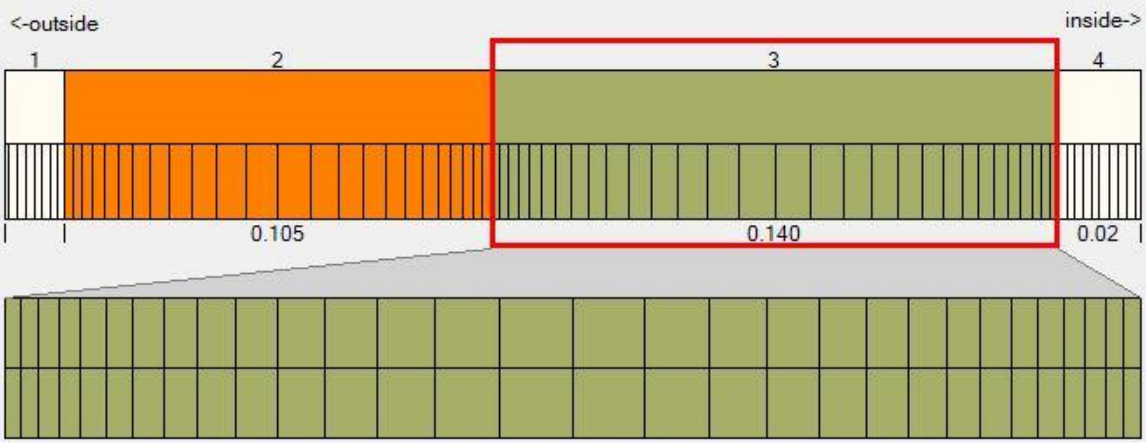

## 6. LMK20 – Multilayer wall

Homogenous layers

Thermal resistance: 4.762 m²K/W (without Rsi, Rse)

Heat transfer coefficient (U-value): 0.199 W/m²K

Thickness: 0.281 m

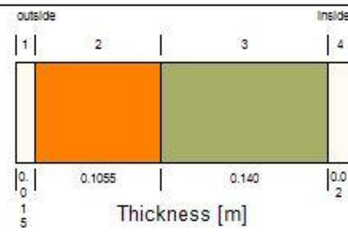


| Nr. | Material/Layer (from outside to inside) | ρ [kg/m³] | c [J/kgK] | λ [W/mK] | Thickness [m] | Color |
|---|---|---|---|---|---|---|
| 1 | Lime Plaster (stucco, A-value: 3.0 kg/m2h0.5) | 1600 | 850 | 0.7 | 0.015 | |
| 2 | Rockwool | 119 | 850 | 0.034 | 0.106 | |
| 3 | Hempcrete | 305 | 1412 | 0.087 | 0.14 | |
| 4 | Lime Plaster (stucco, A-value: 3.0 kg/m2h0.5) | 1600 | 850 | 0.7 | 0.02 | |

| Nr. | Material / Layer (from outside to inside) | λ [W/mK] | Thickness [m] |
|---|---|---|---|
| 1 | Lime Plaster (stucco, A-value: 3.0 kg/m2h0.5) | 0.7 | 0.015 |
| 2 | Rockwool | 0.034 | 0.1055 |
| 3 | Hempcrete | 0.0870 | 0.140 |
| 4 | Lime Plaster (stucco, A-value: 3.0 kg/m2h0.5) | 0.7 | 0.02 |

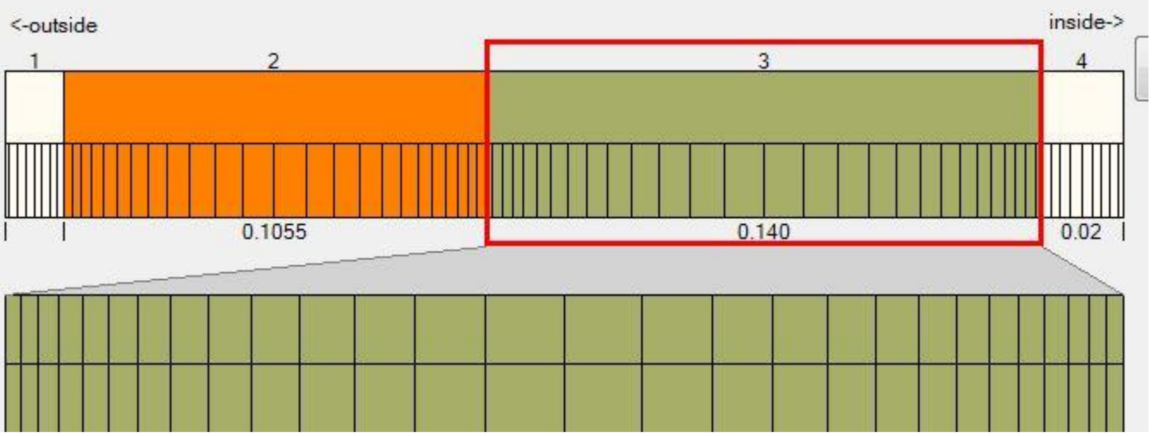

# 7. LMK10 – Multilayer wall

Homogenous layers

Thermal resistance: 4.777 m²K/W (without Rsi, Rse)

Heat transfer coefficient (U-value): 0.199 W/m²K

Thickness: 0.281 m

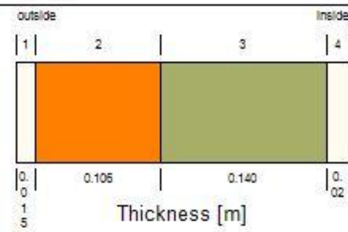


| Nr. | Material/Layer (from outside to inside) | ρ [kg/m³] | c [J/kgK] | λ [W/mK] | Thickness [m] | Color |
|---|---|---|---|---|---|---|
| 1 | Lime Plaster (stucco, A-value: 3.0 kg/m2h0.5) | 1600 | 850 | 0.7 | 0.015 | |
| 2 | Rockwool | 119 | 850 | 0.034 | 0.106 | |
| 3 | Hempcrete | 314 | 1412 | 0.087 | 0.14 | |
| 4 | Lime Plaster (stucco, A-value: 3.0 kg/m2h0.5) | 1600 | 850 | 0.7 | 0.02 | |

| Nr. | Material / Layer (from outside to inside) | λ [W/mK] | Thickness [m] |
|---|---|---|---|
| 1 | Lime Plaster (stucco, A-value: 3.0 kg/m2h0.5) | 0.7 | 0.015 |
| 2 | Rockwool | 0.034 | 0.106 |
| 3 | Hempcrete | 0.087 | 0.140 |
| 4 | Lime Plaster (stucco, A-value: 3.0 kg/m2h0.5) | 0.7 | 0.02 |

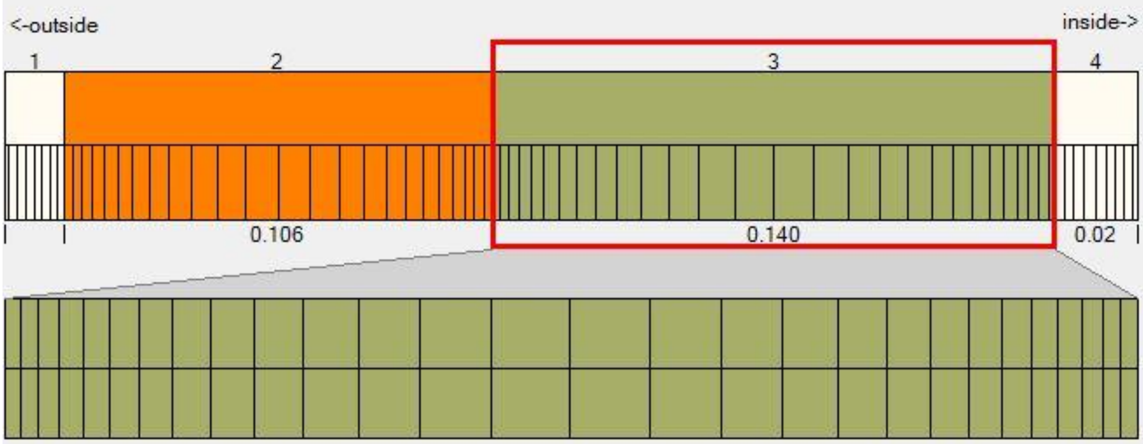

## 8. LMK70 – Multilayer wall

Homogenous layers

Thermal resistance: 4.72 m²K/W (without Rsi, Rse)

Heat transfer coefficient (U-value): 0.201 W/m²K

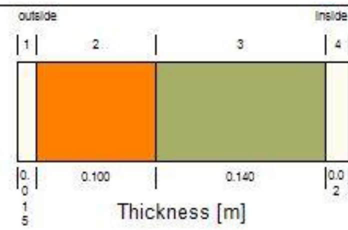


Thickness: 0.275 m

| Nr. | Material/Layer (from outside to inside) | ρ [kg/m³] | c [J/kgK] | λ [W/mK] | Thickness [m] | Color |
|---|---|---|---|---|---|---|
| 1 | Lime Plaster (stucco, A-value: 3.0 kg/m2h0.5) | 1600 | 850 | 0.7 | 0.015 | |
| 2 | Rockwool | 119 | 850 | 0.034 | 0.1 | |
| 3 | Hempcrete | 301 | 1412 | 0.081 | 0.14 | |
| 4 | Lime Plaster (stucco, A-value: 3.0 kg/m2h0.5) | 1600 | 850 | 0.7 | 0.02 | |

| Nr. | Material / Layer (from outside to inside) | λ [W/mK] | Thickness [m] |
|---|---|---|---|
| 1 | Lime Plaster (stucco, A-value: 3.0 kg/m2h0.5) | 0.7 | 0.015 |
| 2 | Rockwool | 0.034 | 0.100 |
| 3 | Hempcrete | 0.081 | 0.140 |
| 4 | Lime Plaster (stucco, A-value: 3.0 kg/m2h0.5) | 0.7 | 0.02 |

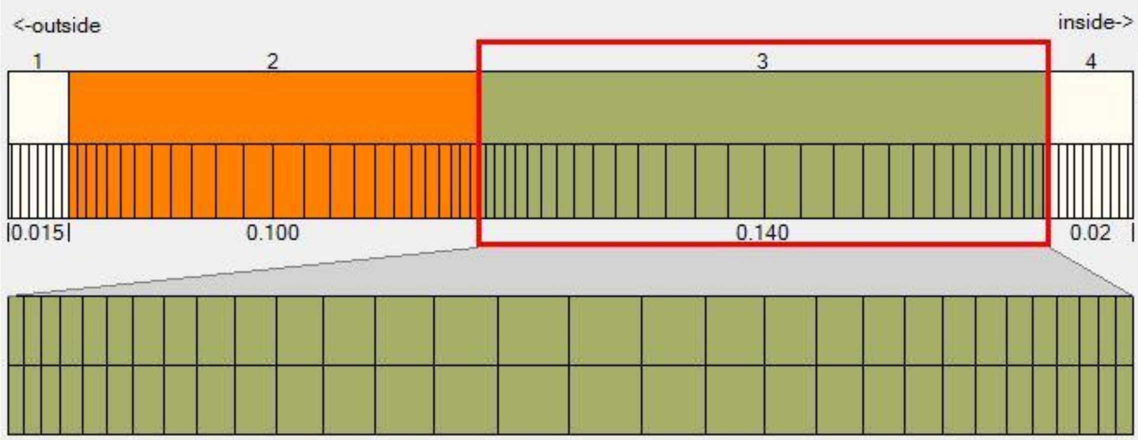

## Physical Properties of Materials Used in WUFI

### 1. Thermal conductivity functions

A. Hempcrete

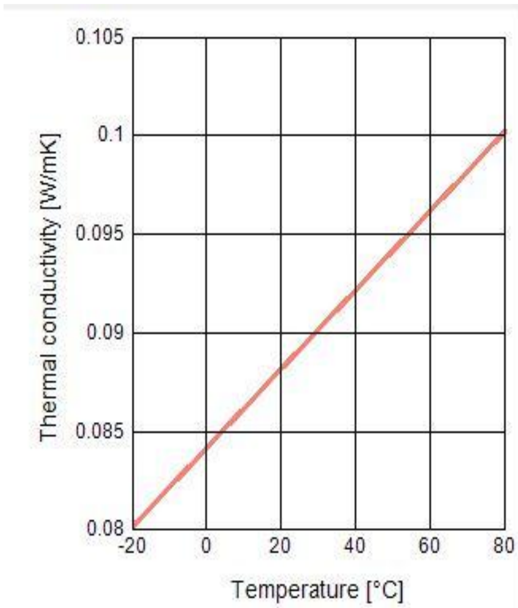


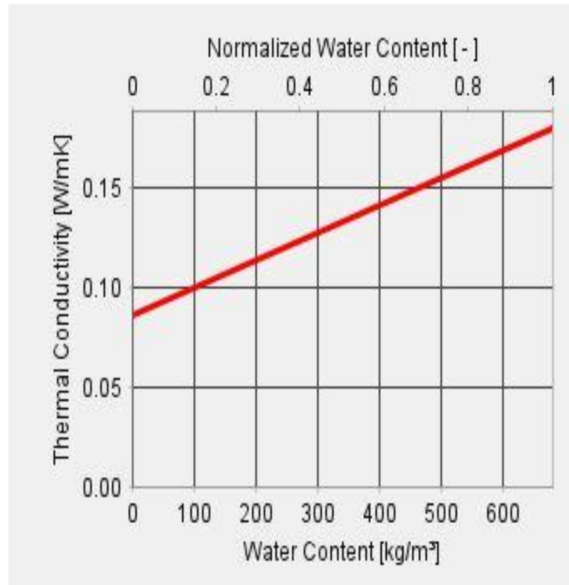


B. Lime plaster

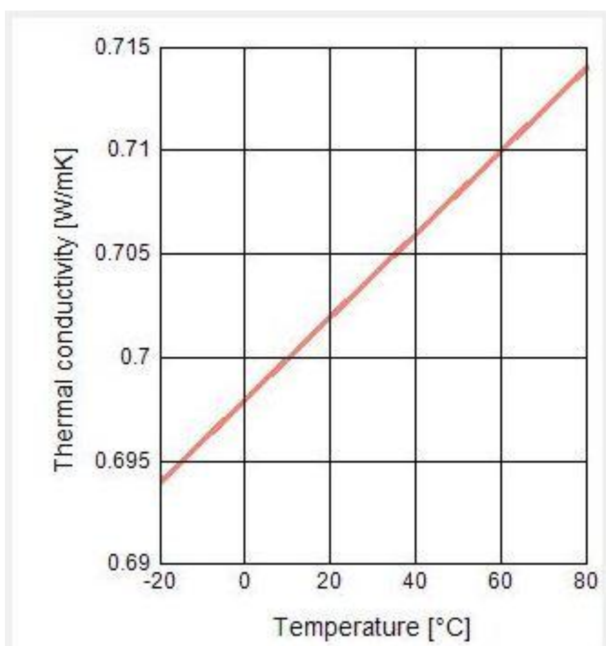

C. Rock wool

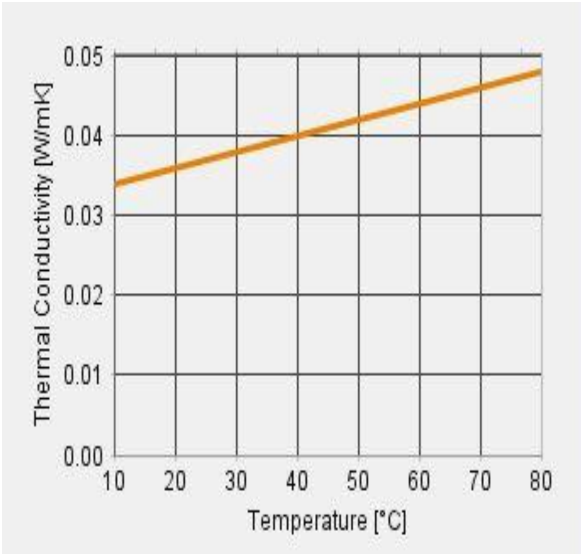


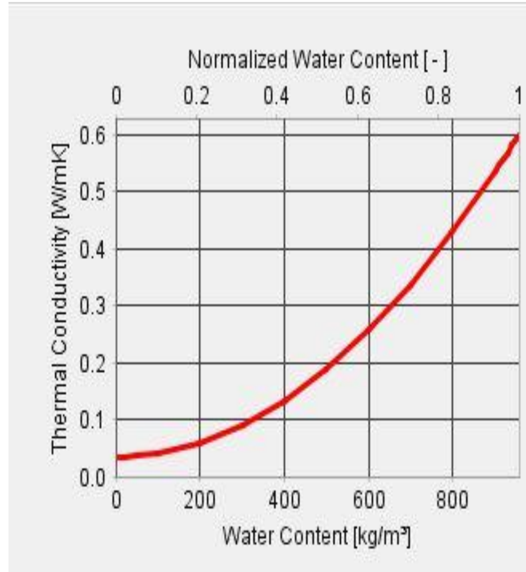


## 2. Moisture storage functions

A. Hempcrete

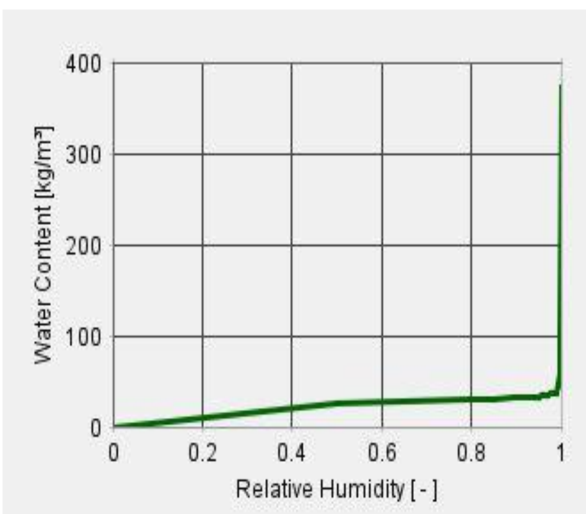


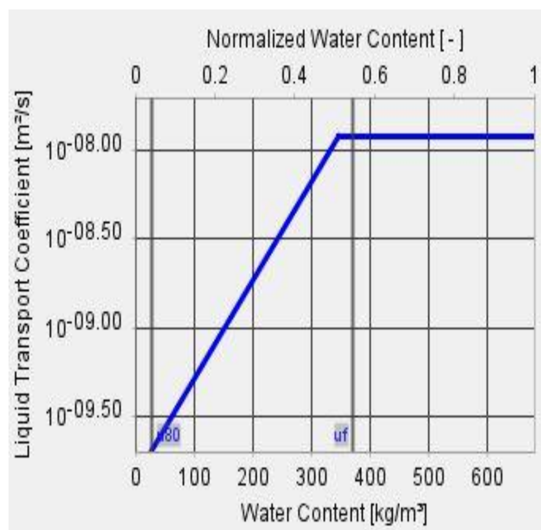

B. Lime plaster

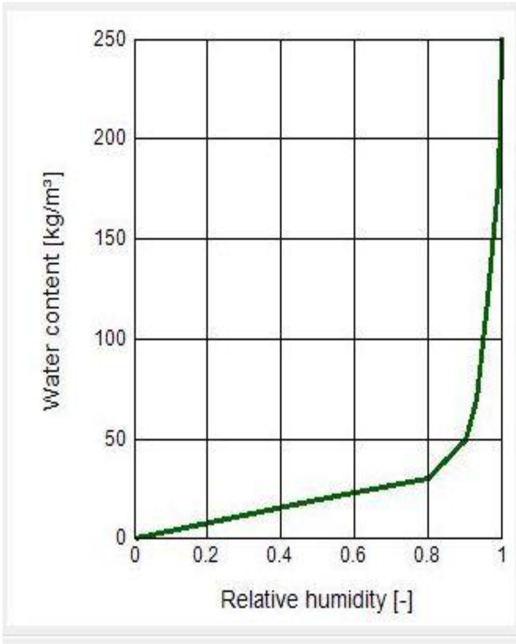


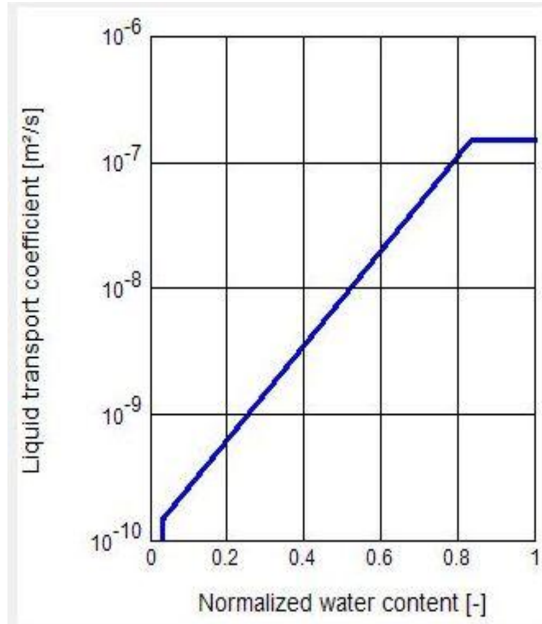


C. Rockwool

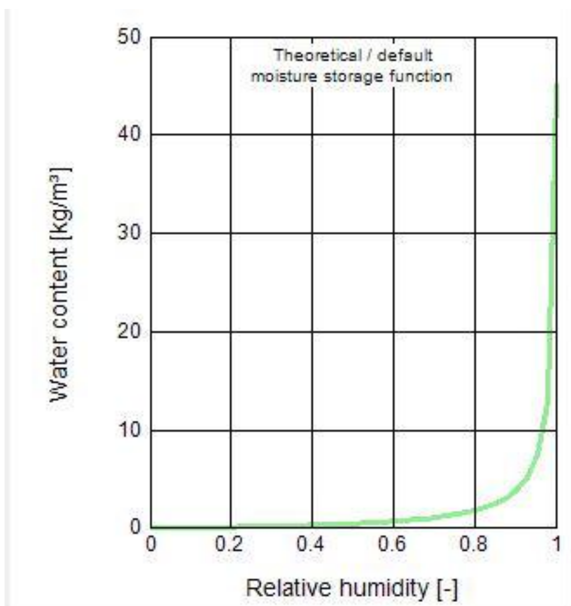

# Appendix B: Programming Code for Numerical Modeling in WUFI

## 1. Assembly 1 – Base wall

```
/r{%Macro for rectangle. Parameter: width height left bottom
newpath
name
moveto
dup 0 exch rlineto
exch 0 rlineto
0 exch neg rlineto
closepath
} def
0 0 0 setrgbcolor
/mm{1 mul}def%Macro for dimension mm
/cm{10 mul}def%Macro for dimension cm

20 mm 500 mm 0 mm 120 mm (In. lime-plaster) r stroke
405 mm 500 mm 20 mm 120 mm (Hempcrete) r stroke
15 mm 500 mm 425 mm 120 mm (Ex. lime-plaster) r stroke
```

## 2. Assembly 2 – Multilayer wall

```
/r{%Macro for rectangle. Parameter: width height left bottom
newpath
name
moveto
dup 0 exch rlineto
exch 0 rlineto
0 exch neg rlineto
closepath
```

```
} def
0 0 0 setrgbcolor
/mm{1 mul}def%Macro for dimension mm
/cm{10 mul}def%Macro for dimension cm

20 mm 500 mm 0 mm 120 mm (In. lime-plaster) r stroke
140 mm 500 mm 20 mm 120 mm (Hempcrete) r stroke
105 mm 500 mm 160 mm 120 mm (Rockwool) r stroke
15 mm 500 mm 265 mm 120 mm (Ex. lime-plaster) r stroke
```

# Appendix C: Indoor and Outdoor Boundary Conditions

## 1. Indoor Conditions

a) High Moisture Load (Scenario 1 and 3)

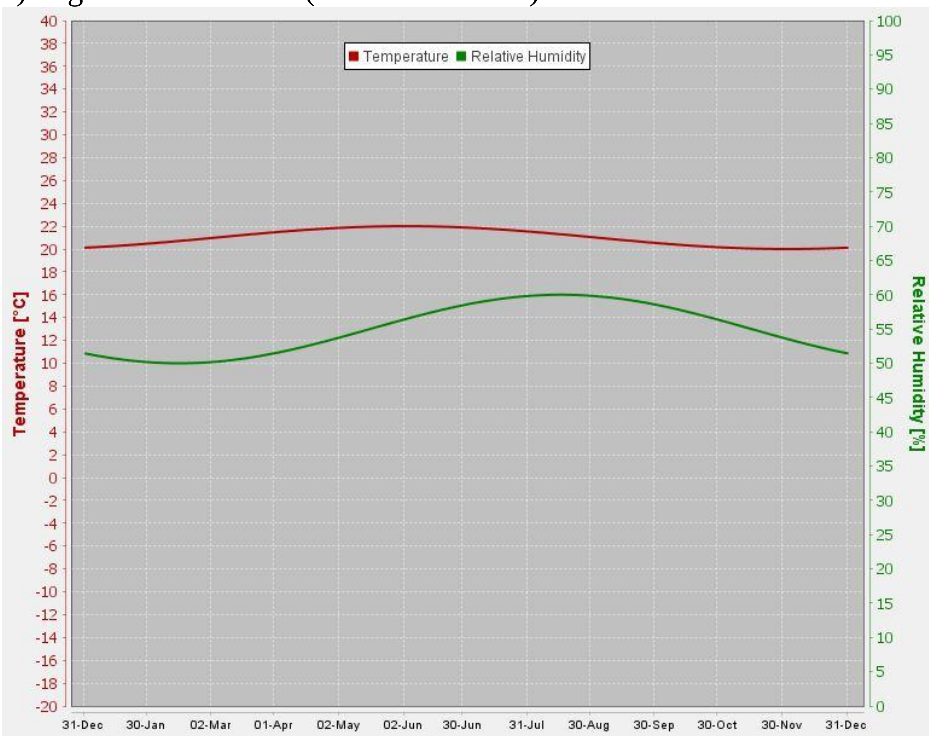


b) ASHRAE 160: Cold Year (Scenario 2 and 4)

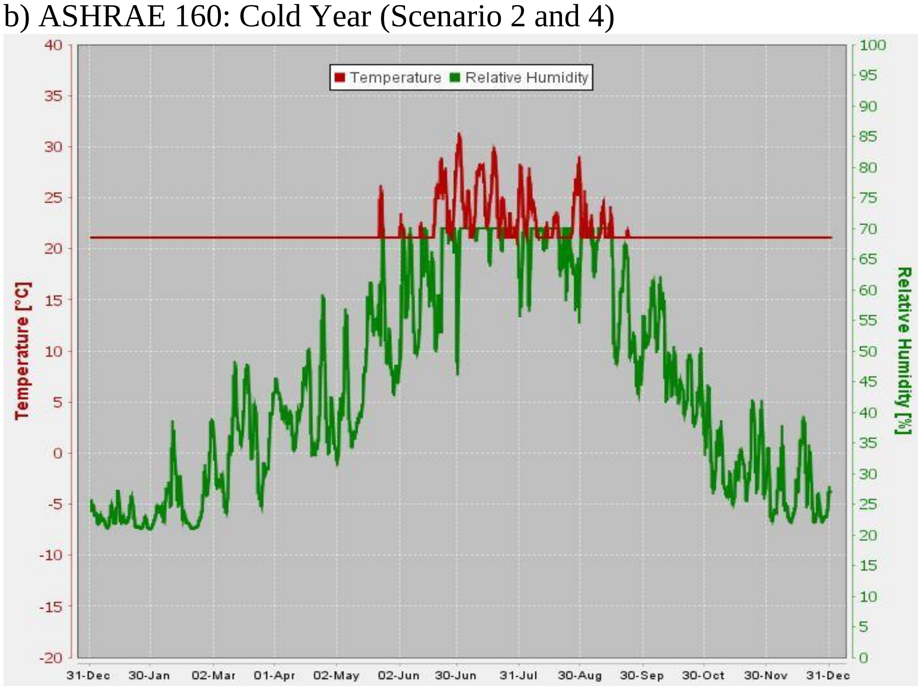

## 2. Outdoor Conditions

a) Cold year (Scenario 1 and 2)

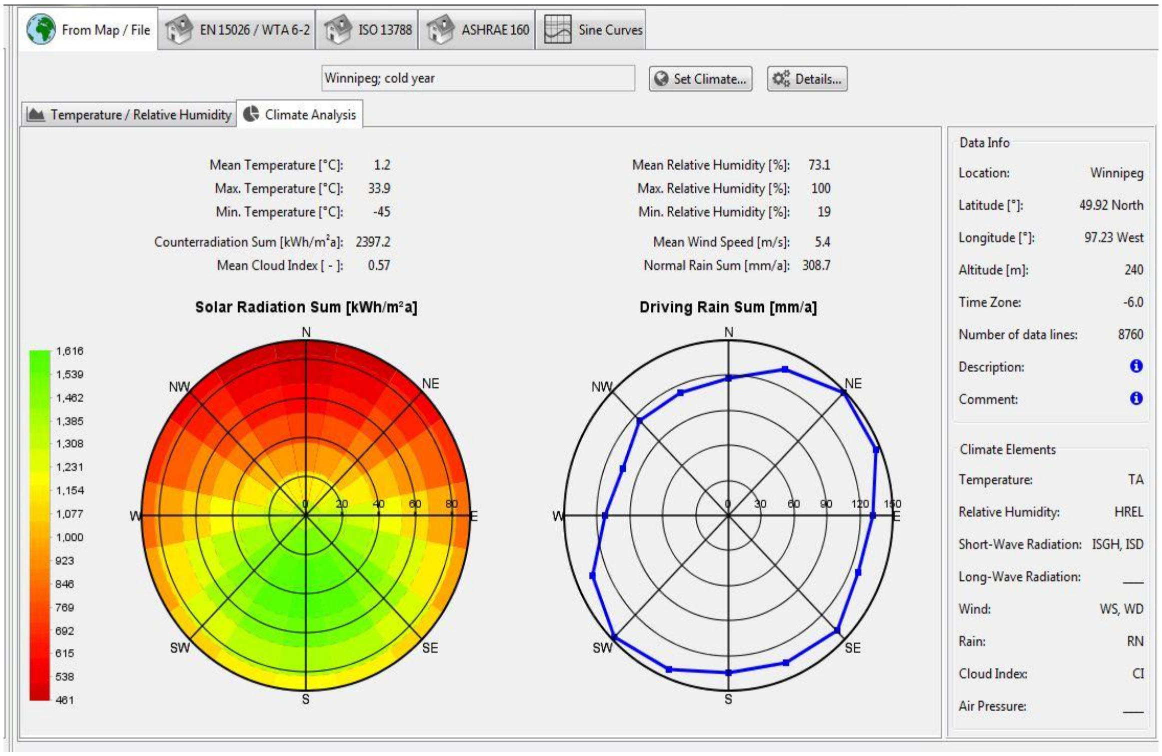


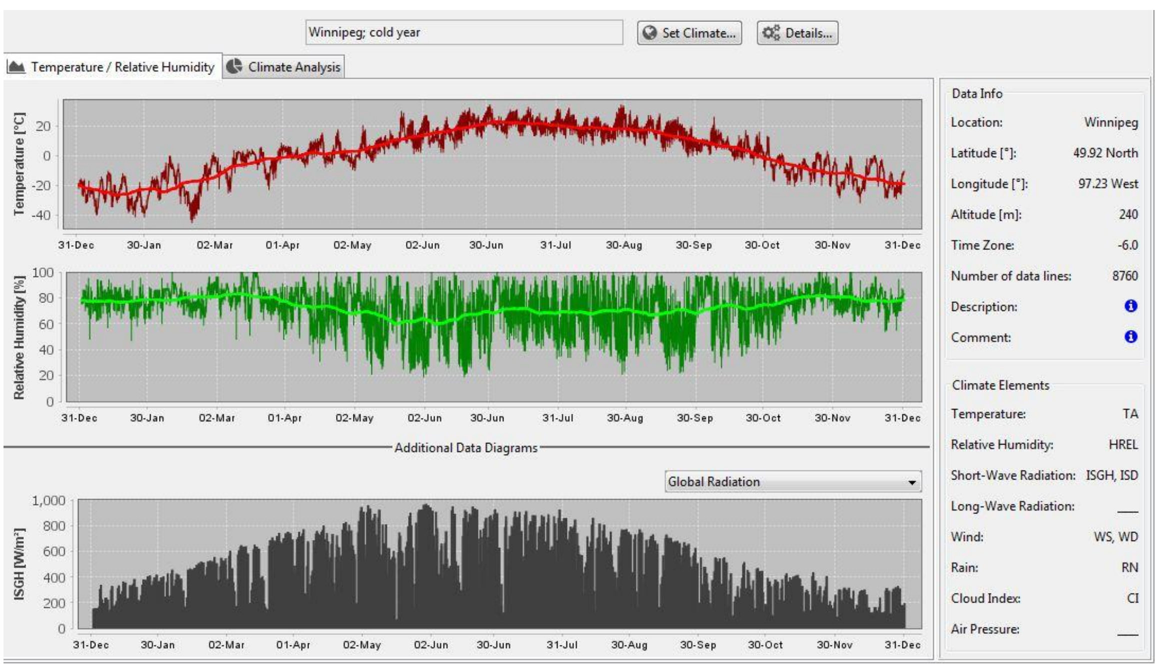

b) ASHRAE Year 1 (Scenario 3 and 4)